

Dresden Integrated Center for Applied Physics and Photonic Materials (IAPP)

Institut für Angewandte Physik

Fachrichtung Physik

Fakultät Mathematik und Naturwissenschaften

Light trapping substrates and electrodes for flexible organic photovoltaics

Dissertation

zur Erlangung des akademischen Grades

Doctor of Philosophy

vorgelegt von

Yoonseok Park

geboren am 17.04.1980 in Seoul, Korea

Dresden 2016

Eingereicht am 21.11.2016

1. Gutachter: Prof. Dr. Karl Leo

2. Gutachter: Prof. Dr. Stefan Mannsfeld

Betreuer: Prof. Dr. Koen Vandewal

Verteidigt am 20. 02. 2017

민소야, 너없이는 아무것도 못했을까야

고마워 이제 난 완전 니꺼야.



“Mein Papa zur Schule” 10th Nov. 2016, Seojean Park

Abstract

Organic solar cells are one of the most promising candidates for future solar power generation. They are thin and lightweight with several additional advantages such as scalability, environmental sustainability and low cost for processing and installation. However, the low charge carrier mobility of the absorbing material for organic solar cells requires thin absorber layers, limiting photon harvesting and the overall power conversion efficiency. Several attempts, e.g., periodically patterned structures and scattering layers have been tried to enhance the absorption of thin-film solar cells as light trapping elements. However, much effort is required to introduce light trapping structures to conventional rigid metal oxide electrodes and glass substrate. For instance, almost 13 hours are required to fabricate micro structures of 1 m² area on glass, in contrast, 1 minute on PET using a same laser set-up and an additional scattering layers are demanded for providing light trapping effects to solar cells.

In the last years, flexibility is emerging as the one of the major advantages of organic solar cells. To realize flexibility of solar cells, the classically used glass substrates and ITO electrodes are too brittle. Therefore, polymer materials are promising candidates to replace them as flexible electrodes and substrates. In this thesis, the highly transparent conducting polymer, PEDOT:PSS and PET equipped with an AlO_x encapsulation layer are used as electrode and substrate, respectively. Besides the flexibility, additional light trapping elements, e.g. scattering particles, nano- and microstructures can be easily applied to the polymer materials since they have the potential for easier shaping and processing.

In this study, we apply different light trapping and in-coupling approaches to organic solar cells. First, PET substrates are structured with a direct laser interference patterning system, which is a powerful and scalable one-step technique for patterning polymers. Almost 80 % of the light is diffracted by these patterned PET substrates and thereby the light path in the absorption layer is increased. Optical display films, commercially developed to be used as back light units of liquid crystal displays are also examined as light trapping substrates and exhibit similar enhancement as patterned PET. Moreover, since PEDOT:PSS is prepared by a solution-based process, TiO₂

nanoparticles are added as light scattering elements to the PEDOT:PSS electrodes. Consequently, those electrodes provide a dual function as electrical contact and light trapping element. Finally, 2- or 3-dimensional nanostructures are printed by a nano-imprinting technique onto the surface of PEDOT:PSS with PDMS stamps. By controlling the temperature and the time of PEDOT:PSS during an annealing step, nanostructures are transferred from PDMS masks to PEDOT:PSS.

To evaluate the effects of light trapping for all above mentioned approaches, flexible organic solar cells are produced by vacuum evaporation using blends of DCV5T-Me and C₆₀ as absorber layer. The substrates are optically characterized using UV-vis spectrometer and goniometer measurements. The topography of the samples is measured by atomic force microscopy, scanning microscopy and optical microscopy. Bending tests with various radii are performed to test the flexibility of the substrates.

In summary, light trapping effects are successfully implemented in the electrodes and substrates for OPVs, giving efficiency improvements of up to 16 %. The light trapping mechanisms in our approaches are extensively discussed in this thesis.

Kurzdarstellung

Organische Photovoltaik ist einer der vielversprechendsten Kandidaten für die zukünftige Solarstromgewinnung auf flexiblen Substraten. Um diese Flexibilität zu ermöglichen, sind herkömmliche Glassubstrate mit ITO-Elektroden zu spröde. Ein vielversprechender Kandidat, um sowohl flexible Elektroden als auch flexible Substrate herzustellen, sind Polymere, da diese sehr biegsam und leicht zu verarbeiten sind. Deshalb wird in dieser Arbeit das hoch transparente, leitfähige Polymer PEDOT:PSS als Elektrode und PET (mit einer AlO_x Verkapselungsschicht) als Substrat untersucht. Aufgrund der guten Prozessierbarkeit der Polymere konnten wir zusätzlich zu den eigentlichen Funktionen des Substrates und der Elektrode noch den Mechanismus des Lichteinfangs hinzufügen.

Zusätzlich zu ihrer Flexibilität haben organische Solarzellen noch weitere Vorteile: sie sind dünn, leicht, skalierbar und verursachen vergleichsweise geringe Kosten für Herstellung und Installation. Ein Nachteil organischer Solarzellen ist die vergleichsweise geringe Ladungsträgerbeweglichkeit der Absorbermaterialien, welche oft die Schichtdicke der Absorbermaterialien begrenzt. Dies hat weniger absorbierte Photonen, weniger Stromdichte und somit einen geringeren Wirkungsgrad zur Folge. In den letzten Jahren wurden periodisch strukturierte Substrate und streuende Schichten als Lichteinfangelemente eingesetzt, um den Wirkungsgrad organischer Solarzellen mit dünnen Absorberschichten zu erhöhen. Gestaltungsregeln für solche Lichteinfangelemente sind noch weitestgehend unbekannt. Im Rahmen dieser Arbeit strukturieren wir PET Substrate mit einem direkten Laserinterferenzsystem, welches ein leistungsfähiges, skalierbares Einschnittverfahren zur Polymerstrukturierung ist. Da PEDOT:PSS aus der Lösung prozessiert wird, können wir weiterhin Nanopartikel hinzufügen, die der Elektrode zusätzlich noch lichtstreuende Eigenschaften geben. Außerdem können 2- bzw. 3-dimensionale Nanostrukturen leicht mithilfe einer Stempeltechnik eingeprägt werden.

Um die Effekte des Lichteinfangs, welcher durch die oben genannten Methoden erzeugt wird, zu untersuchen, werden flexible organische Solarzellen mittels Vakuumverdampfung prozessiert. DCV5T-Me und C_{60} bilden dabei die photoaktive Schicht. Somit werden die Licht fangenden Eigenschaften dieser flexiblen Solarzellen ausgenutzt und ausführlich in der Arbeit diskutiert.

Abstract (Korean)

제목: 유연한 유기태양전지를 위한 빛 가두기 기능을 가진 전극 및 기판에 관한 연구

유기태양전지는 쉽게 휘어질 수 있는 유연성을 장점으로 가지있어 차세대 에너지 개발 산업에서 가장 주목되고 있는 기술이다. 기존태양전지에 사용되는 유리기판과 금속산화물 전극재료는 유연한 유기소자를 구현하기에는 상대적으로 취성이 높아 유연소자에 적용되기 어려운 문제점을 가지고 있다. 이를 극복하기 위해 유연한 고분자 재료를 전극 및 기판에 적용하는 연구가 진행되어 왔다. 본연구에서는 높은 전기전도성을 가진 투명 고분자 재료, Poly(3,4-ethylenedioxythiophene):poly(styrenesulfonate) (PEDOT:PSS)와 산화 알루미늄 막(AlO_x)이 봉지재로 증착되어있는 polyethylene terephthalate (PET)가 각각 전극 및 기판재료로 사용되었다. 고분자 재료는 앞에서 말한 유연성 함께 기존 유리기판, 산화물 전극과 비교하여 상대적으로 가공이 용이한 장점을 가지고 있다. 이에 따라 본 연구에서는 기판, 전극 본질의 기능과 함께 빛 가두기 기능(Light trapping)을 가진 고분자 기판, 전극 물질이 연구되고 논의 되었다.

유기태양전지는 유연성뿐 아니라 가볍고 얇으며 저비용으로 공정, 설치가 가능한 장점을 가지고 있다. 하지만 흡수물질의 낮은 이동도에 의하여 태양전지소자에 들어온 빛이 모두 흡수될 수 있는 충분한 두께의 흡수층을 만들기 어렵다. 빛 가두기 기능은 이러한 얇은 흡수층에 광경로를 증가시켜 더 많은 빛이 흡수되어 전기를 생산할 수 있게 도와주는 기능이다. 본연구에서는 레이저를 사용하여 PET 기판의 표면에 미세 구조를 가공하여 기판으로 사용하였고, 미세 구조를 최적화하는 연구를 진행하였다. 또한 기존 평판디스플레이에 사용되는 광학필름을 기판으로 적용하는 실험을 진행하였다. 이와 더불어 액상 공정인 PEDOT:PSS 재료와 광분산 효과를 가지는 산란입자를 섞어 광 가두기 전극을 개발하였으며, 나노인쇄 기술을 사용하여 나노단위의 구조를 PEDOT:PSS 전극표면에 구현하여 소자에 적용하였다. 이러한 기술들을 검증하기 위하여 본 연구소(IAPP)를 통해 소개, 연구된 DCV5T-Me와 C_{60} 재료를 흡수 물질로 사용하여 유기 태양전지가 제작되었고 평가되었다.

Table of Contents

Abstract	7
Kurzdarstellung	9
Abstract (Korean)	11
Table of Contents.....	13
Publications	17
1. Introduction	19
2. Basics of organic semiconductors	23
2.1 Organic semiconductors.....	23
2.1.1 Conjugated π system	24
2.1.2 Optical properties	26
2.1.3 Charge carrier transport.....	27
2.2 Organic photovoltaics (OPV).....	29
2.2.1 Working principle.....	29
2.2.2 Heterojunction p-i-n concepts	31
2.2.3 Characteristics of OPVs	32
3. Optics in organic photovoltaics.....	37
3.1 Optical models for light trapping.....	38
3.1.1 Fundamentals of light trapping.....	38
3.1.2 Limitations to Lambertian light trapping	39
3.2 Practical implementations of light trapping.....	41

3.2.1	Periodically patterned grating	42
3.2.2	Scattering layer	45
4.	Experimental	49
4.1	Materials	49
4.2	Sample preparation	51
4.2.1	Preparation of electrodes (PEDOT:PSS).....	51
4.2.2	Preparation of OPV devices	52
4.3	Sample Characterization.....	55
5.	Light trapping substrates	59
5.1	Motivation	59
5.2	Patterned PET substrates by laser structuring	61
5.2.1	Patterned PET films as substrates	61
5.2.2	Optical properties of the patterned PET substrates	62
5.2.3	Photovoltaic characteristics of devices.....	66
5.2.4	Summary	67
5.3	Display film for LCD as substrate	69
5.3.1	Display films as substrates	69
5.3.2	Optical properties of the display films	71
5.3.3	Photovoltaic characteristics of devices.....	71
5.3.4	Summary	74
6.	Light trapping electrodes	75
6.1	Motivation	75
6.2	TiO₂ nano-particles embedded in PEDOT:PSS.....	76
6.2.1	Preparation of light scattering electrodes	77
6.2.2	Characterization of scattering effect in devices	79

6.2.3	Summary	84
6.3	Nano imprinted PEDOT:PSS	85
6.3.1	Preparations for nano-imprinted PEDOT:PSS	85
6.3.2	Characterization of a nano-imprinted PEDOT:PSS	87
6.3.3	Summary	89
7.	Conclusions and Outlook.....	91
7.1	Conclusions.....	91
7.2	Outlook	93
8.	Appendix	95
	Bibliography	95
	Table of figures	103
	Table of tables	109
	Acknowledgement.....	111
	Erklärung	113

Publications

Peer reviewed articles

1. Yoonseok Park, Frederik Nehm, Lars Müller-Meskamp, Koen Vandewal, and Karl Leo, Optical display film as flexible and light trapping substrate for organic photovoltaics, *Optics Express* **24**(10) A974-A980 (2016)
2. Yoonseok Park, Ludwig Bormann, Lars Müller-Meskamp, Koen Vandewal, and Karl Leo, Efficient flexible organic photovoltaics using silver nanowires and polymer based transparent electrodes, *Organic Electronics* **36** 68-72 (2016)
3. Yoonseok Park, Lars Müller-Meskamp, Koen Vandewal, and Karl Leo, PEDOT:PSS with embedded TiO₂ nanoparticles as light trapping electrode for organic photovoltaics, *Applied Physics Letters* **108** 253302 (2016)
4. Yoonseok Park, Jana Berger, Lars Müller-Meskamp, Koen Vandewal, Andrés F. Lasagni and Karl Leo, Flexible and light trapping substrate for organic photovoltaics, *Applied Physics Letters* **109** 093301 (2016).
5. Yoonseok Park, Jana Berger, Paul-Anton Will, Marcos Soldera, Bernhard Glatz, Lars Müller-Meskamp, Kurt Taretto, Andreas Fery, Andrés Fabián Lasagni, Koen Vandewal and Karl Leo, Light trapping for flexible organic photovoltaics, *Proc. SPIE 9942, Organic Photovoltaics XVII*, 994211 (2016).

Conference Contributions

1. Y. Park, J. Berger, L. Müller-Meskamp, K. Vandewal, A. F. Lasagni and K. Leo, Efficiency enhancement of Organic Photovoltaics (OPV) cell using laser patterned PET substrate, *11th International Conference on Organic Electronics (ICOE 2015)*, June 2015, Erlangen, Germany.
2. Y. Park, L. Müller-Meskamp, K. Leo, J. Berger and A. F. Lasagni, Light trapping in Organic Photovoltaics (OPV) cell using laser patterned substrates, *10th International Conference on Electroluminescence and Optoelectronic Devices*, August 2014, Köln, Germany.
3. Y. Park, L. Müller-Meskamp, K. Vandewal and K. Leo, Light trapping substrates and electrodes for organic photovoltaics, *SPIE Photonics Europe*, April 2016, Brussels, Belgium.
4. Y. Park, J. Berger, L. Müller-Meskamp, K. Vandewal, A. F. Lasagni and K. Leo, Light trapping for flexible organic photovoltaics, *SPIE Optics + Photonics 2016*, August 2016, San Diego, California, United States.
5. Y. Park, K. Vandewal and K. Leo, Flexible organic photovoltaics: A new challenge for light trapping, *Annual meeting of the Verein Koreanischer Naturwissenschaftler und Ingenieure in der BRD 2016*, October 2016, Essen, Germany.
6. J. Berger, M. Soldera, K. Taretto, L. Müller-Meskamp, Y. Park, C. Fuchs, K. Leo and A. F. Lasagni, Optimierung von organischen Solarzellen durch direkte Laserinterferenzstrukturierung, *Werkstoffwoche 2015*, September 2015, Dresden, Germany.
7. J. Berger, A. F. Lasagni, L. Müller-Meskamp, Y. Park, and C. Fuchs, Laser Patterning of Transparent Conducting Oxide Layers for Optical Applications, *Materials Science and Engineering (MSE) 2014*, September 2014, Darmstadt, Germany.

1. Introduction

And God said, Let there be light: and there was light. And God saw the light, that it was good. [Genesis 1:3-4]

By 2022, the German government announced that it would close all of its nuclear power plants. Eight of the seventeen operating reactors in Germany were permanently shut down following the Fukushima disaster[1]. Moreover, the Bundesrat, the upper house of Germany's parliament, passed a resolution for the elimination of vehicles powered by gasoline and diesel engines by 2030[2]. Keeping pace with this movement, we can notice that the importance of renewable energy is obvious. However, so far renewable energy sources contributes only about 17% of the world's primary energy use, mainly through traditional biomass (7.4%) and large hydropower (6.1%). The share from solar, wind, modern biomass, geothermal, and ocean energy was only 3.3% in 2009[3]. Among these renewable energy forms, solar energy has the biggest potential (about 1.0 kilowatts per square meter[4]) and has various further advantages:

1. **Clean-green energy** – No harmful toxic chemicals are produced during solar energy conversion.
2. **Low cost** – Even today, solar energy is cheaper than the electricity from electrical power grid.
3. **Nature friendly** – No need for the destruction of nature, unlike hydropower.
4. **Easy maintenance** – Solar cells have no mechanically moving parts that need to be replaced regularly.
5. **Mobility** – Solar energy can be made available almost anywhere there is sunlight.
6. **Silent and safe** – Solar cells are silent and safe thereby can be installed directly on the roof of a residence.

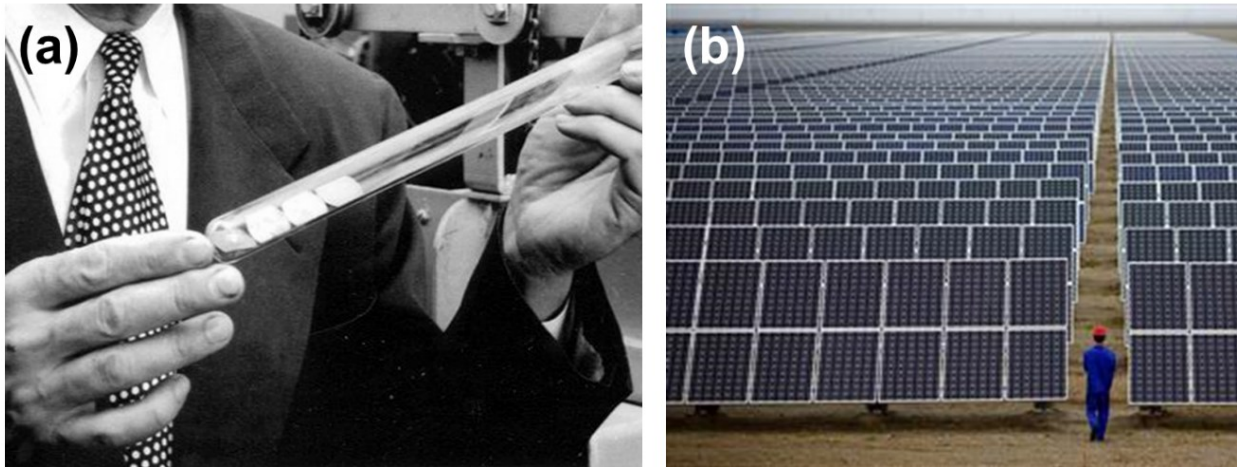


Figure 1-1 Photographs of the first solar cell that could generate significant amounts of electricity at Bell Laboratories in 1954 (a) and solar panels in the Gansu Province in China in 2015 (b). Images from AT&T Archives and REUTERS/Carlos Barria/Files.

After Bell Laboratories demonstrated the first practical silicon solar cell in 1954[5], inorganic solar panels have been installed to produce electricity as shown in Figure 1-1. Recent studies report power conversion efficiencies (PCE) of inorganic solar cells up to 46% (Soitec and Fraunhofer Institute for Solar Energy Systems (ISE))[6]. In contrast, the highest efficiency of organic solar cells achieved up to now is obtained by Heliatek with a PCE of 13.2 %[7]. Even though the performance of organic solar cells is not as high as that of inorganic ones, they have the following unique advantages:

1. **Thin, light and flexible** – Devices can be less than 1 mm thick and the weight can be less than 1 kg/m².
2. **Flexibility** – Using flexible substrate and electrode, a minimum bending radius of 10 cm can be achieved that is sufficient to be used as flexible consumer electronics.
3. **Eco-friendly** – No toxic materials are used during the fabrication process and in the end-product.
4. **Cost effective** – The cost of the materials and processing is lower than that of most inorganic solar cells.
5. **Easy to handle** – Flexibility enables fabrications by a roll-to-roll process. Moreover because of their lightweight and flexibility, installation is easy.

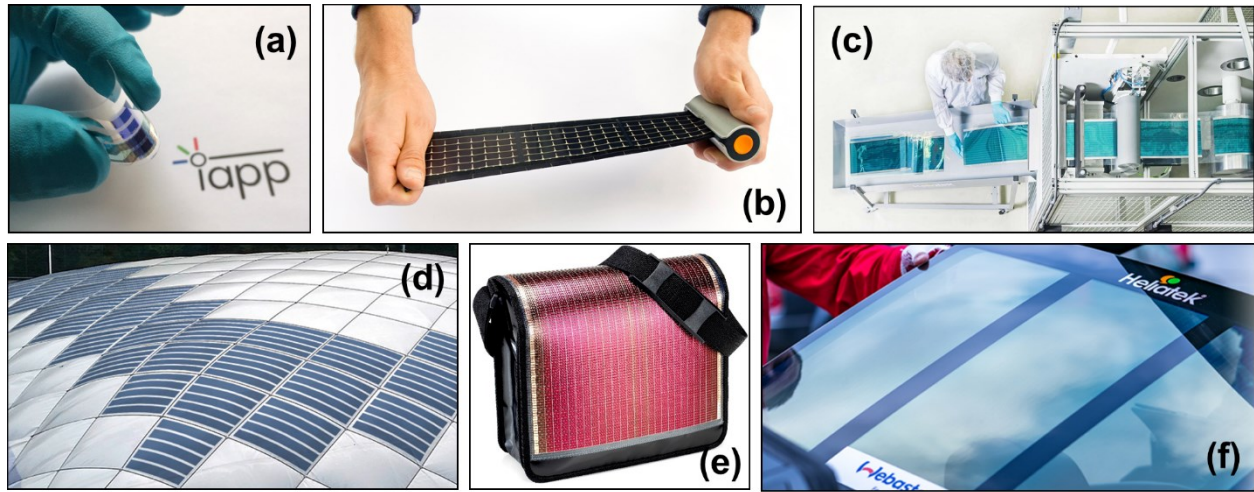


Figure 1-2 Photographs of a flexible organic solar cell from IAPP (a), a rollable solar charger (WAACS design & consultancy, Netherlands) (b), roll-to-roll process for large area (Heliatek, Germany) (c), light solar cells installed on a temporary building (Paranet-Deutschland GmbH, Germany) (d), a solar bag (element5 Daochu AG, Switzerland) (e) and a roof window with transparent solar cell for an automotive application (Heliatek & Webasto, Germany) (f)

Because of these advantages, there are attempts to bring these organic solar cells to the market in the form of mobile consumer electronics, solar chargers, bags, clothes, car rooftops and building windows (Figure 1-2). Recently, the German company Heliatek raised 80 million euro to set up a new manufacturing roll-to-roll facility[8]. They expect a capacity of one million m² p.a. of solar films when fully ramped up.

In order to set up a roll-to-roll process, flexible substrates and electrodes are required. Conventional materials are however rigid, for example glass as substrate and indium tin oxide (ITO) as electrode. These two materials are brittle, making them unsuitable to be used for flexible devices. Therefore, polymer substrates and electrodes are investigated. Besides being flexible, polymers are much easier to process and manipulate due to their relative softness as compared to glass and metal oxides. This gives the opportunity to easily introduce light trapping structures into these materials. To fabricate light trapping structures on polyethylene terephthalate (PET) substrates[9], only 1 minute is needed to prepare 1 m² area. However, over than 13 hours are required to pattern the

same area on the glass substrates[10] under same laser set-up. Moreover, the most commonly used polymer electrode, poly(3,4-ethylenedioxythiophene) polystyrene (PEDOT:PSS) is prepared using a solution based process. Therefore, PEDOT:PSS can be mixed with scattering nano-particles to produce scattering electrodes and can be easily imprinted with any structures using stamps.

This thesis investigates substrates and electrodes equipped with light trapping elements for organic solar cells. In chapter 2, organic semiconductors with a focus on their application in photovoltaics are discussed. Light management for solar cells is modelled and discussed in chapter 3. Experimental methods and materials are briefly explained in chapter 4. In the results parts of the thesis, light trapping substrates and electrodes are discussed in chapter 5 and 6, which are based on peer-reviewed publications. Finally the work is summarized in chapter 7 and future prospects are proposed in chapter 8.

2. Basics of organic semiconductors

The theory of inorganic semiconductors has been well established. In contrast, organic semiconductors have been investigated over several decades, and not all fundamental questions have been resolved. In this chapter, the basics of organic semiconductors are discussed. Of particular importance for the understanding of OPV are the conjugated π -system, optical properties, excitons, and charge transport, which are discussed at the beginning of this chapter, mainly following references[11,12]. As the second part, key parameters of OPV devices are introduced, which are important to evaluate their performance.

2.1 Organic semiconductors

Since Pochettino discovered in 1906[13] that anthracene has a photoconductive effect, the semiconducting properties of organic materials have been intensively investigated. With the advantages of flexibility[14,15], low cost[16] and biocompatibility[17–19], organic devices are promising candidates for future electronics. Organic semiconductors are different from inorganic semiconductors in many points, and one of the major differences is the relatively higher band gap (E_g) of organic semiconductors ($E_g = 1.5 - 4$ eV) as compared to typical inorganic semiconductors ($E_g = 1 - 2$ eV). This means that intrinsically, organic semiconductors are more insulating than inorganic semiconductors. To understand organic semiconductors, the conjugated π system, excitons and transport of charge carriers are covered in this section.

2.1.1 Conjugated π system

In a conjugated system, with available p-orbitals for each atom in a chain, the system can conduct charge by an extended π -system consisting of overlapping p_z orbitals. With the configuration $1s^2 2s^2 2p^2$, carbon atoms have six electrons, where the four electrons of 2s and 2p orbitals are the more loosely bound valence electrons. Due to the small energy difference between 2s and 2p orbitals, the four electrons in 2s and 2p orbitals form three hybrid sp^2 orbitals with a bonding angle of 120° within the x-y plane. The remaining p_z orbital stands perpendicular to the plane as shown in Figure 2-1(a). For a benzene molecule, σ bonds, which are the strongest type of covalent chemical bonding, are formed between the sp^2 orbitals (Figure 2-1(b)). Overlapping p_z orbitals form an extended π system. Through this delocalized π system, the electron can move, providing conductivity in organic semiconductors (Figure 2-1(c)). The overlapping p_z orbitals generate an energy gap between the new bonding (π) and anti-bonding (π^*) orbitals. This gap is in the order of a few electron volts and is much smaller than that of the σ orbitals. Due to this small energy gap between π and π^* orbitals, photon absorption can easily generate a π - π^* transition. The highest π orbital is called highest occupied molecular orbital (HOMO) and the lowest π^* orbital is called lowest unoccupied molecular orbital (LUMO) as shown in Figure 2-2. The energy gap (E_g) is given by

$$E_g = E_{LUMO} - E_{HOMO} \quad (2 - 1).$$

By increasing the spatial size of the delocalized π -system, the energy gap can be reduced[11,20]. The energy gap can be further tuned, e.g., by replacing the peripheral hydrogen atoms by side groups.

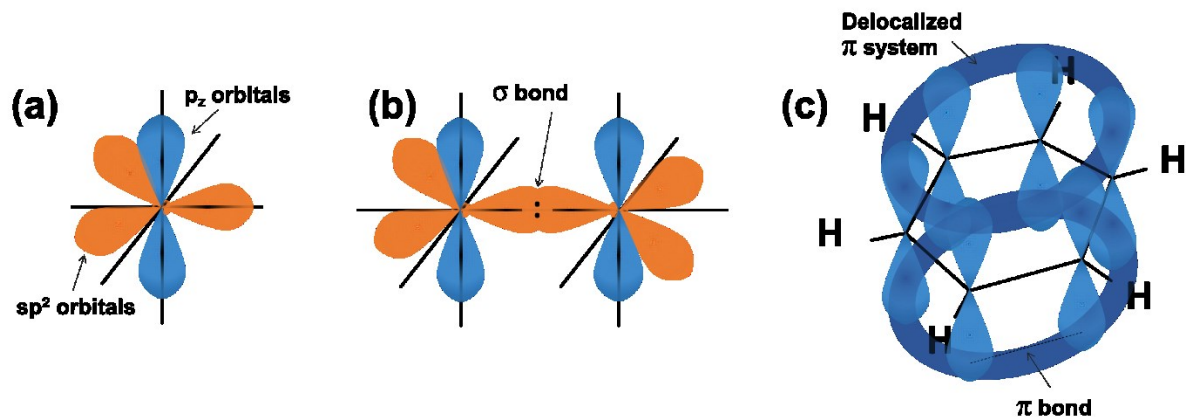


Figure 2-1 Schematics of orbitals and bonds in a conjugated carbon ring. A single sp^2 hybridized carbon atom (a), σ bond between sp^2 orbitals (b) and delocalized π system and π bonds of a benzene molecule (c).

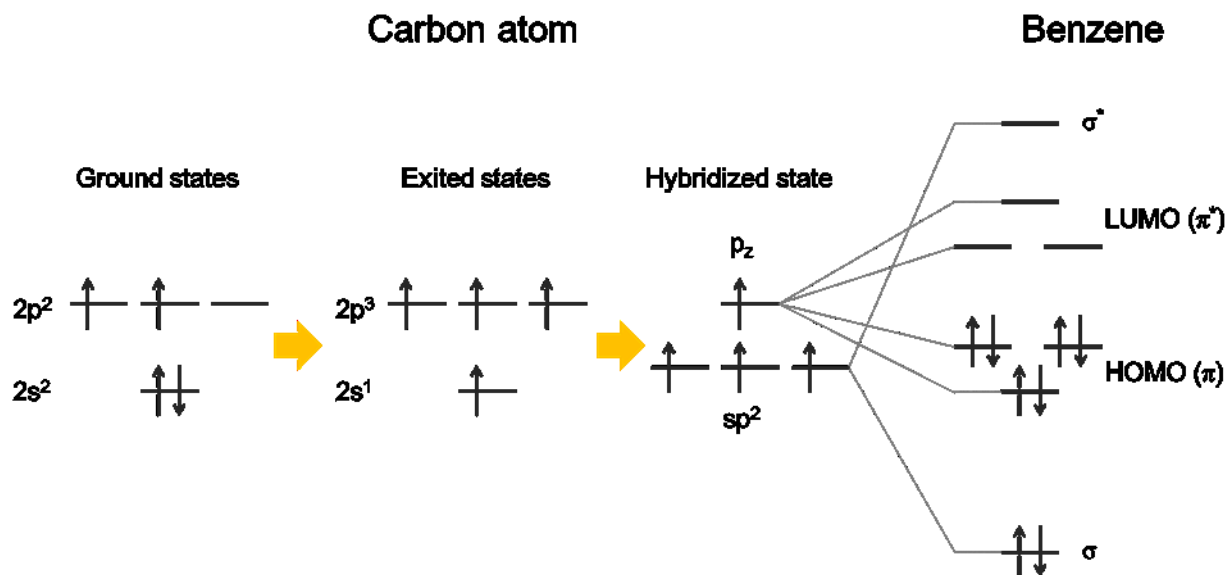


Figure 2-2 Schematics of hybridized orbitals of a carbon atom (left) and energy levels of the benzene molecule (right).

2.1.2 Optical properties

Since the van-der-Waals forces between molecules are weak, the optical properties of organic semiconductors are often similar to those of the single molecules in the gas phase. Thereby, optical interactions in the organic semiconductor can be well explained via Jablonski band diagram. The possible radiative and non-radiative transitions across the different energy states of the molecule are illustrated in Figure 2-3. S_0 is the electronic ground state. When photons have sufficient energy to excite the molecule to higher states (S_1 , S_2), the molecule can be excited by photon absorption. In return, the molecule at the S_1 state can return to S_0 by a radiative fluorescence process (time scale: 10^{-11} s – 10^{-9} s). In the ideal case, transitions from singlet S_n to triplet T_n do not take place. In organic semiconductors, an intersystem crossing from an excited S_n to T_n is sometimes observed. Similar to fluorescence, the molecule can decay from a triplet state T_n to the ground state S_0 , which is called phosphorescence (time scale: 10^{-6} s – hour)[8].

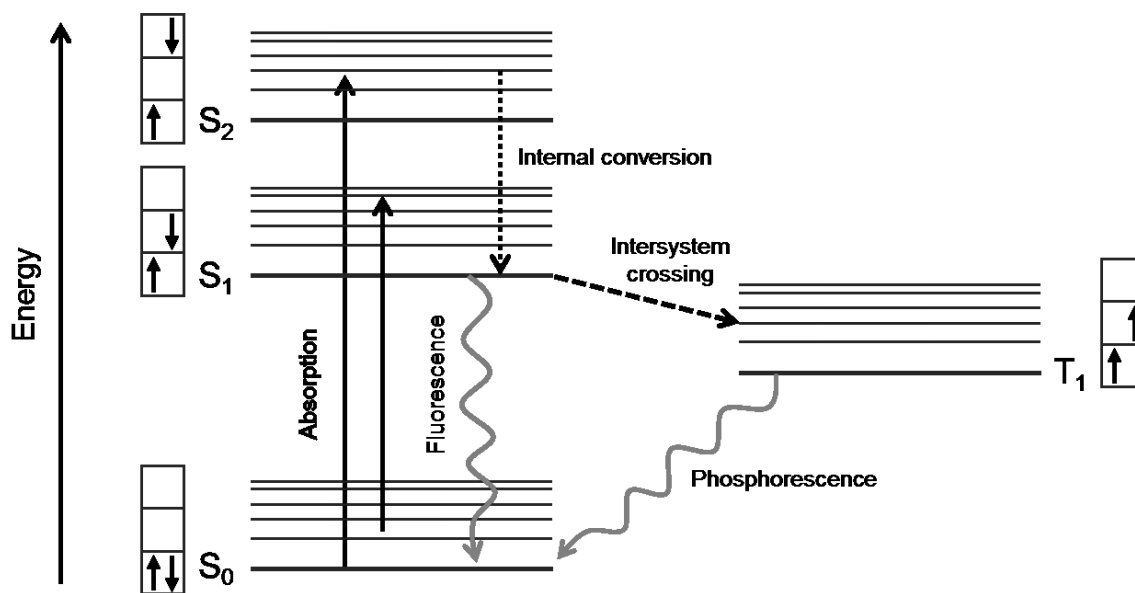


Figure 2-3 Jablonski band diagram that shows various processes of radiative and non-radiative transitions in a molecule/molecular solid (reproduced from[20]).

Although the absorption coefficient of organic semiconductors is rather high (10^5 cm^{-1} [21,22]), not all the absorbed photons can be converted to electrical current in a solar cell. This phenomenon can be explained by the existence of Frenkel excitons: a neutral and strongly bound electron-hole pair (Figure 2-4). In this case, the charge carriers are not fully separated and can recombine within a short time. Moreover, the exciton diffusion length is relatively small (3 – 90nm)[23–25]. For generating free charge carriers from Frenkel excitons, heterojunction interfaces are developed and will be discussed in the next part 2.2.

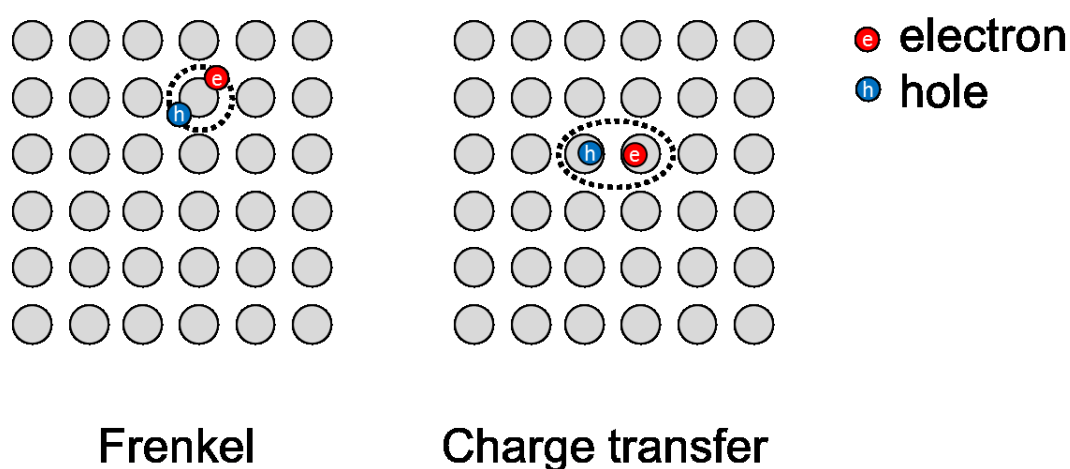


Figure 2-4 Schematics of a Frenkel exciton (left) and a charge transfer exciton (right).

2.1.3 Charge carrier transport

Organic semiconductors usually have a rather low charge carrier mobility (from $10^{-7} \text{ cm}^2/\text{Vs}$ up to $10 \text{ cm}^2/\text{Vs}$ [26–28]) as compared to inorganic semiconductors (e.g., Si $1400 \text{ cm}^2/\text{Vs}$ [29]). Moreover organic semiconductors cannot be described by the Bloch model due to their disordered nature. In contrast to band transport, hopping transport is the main mechanism for charge transport in organic semiconductors. This is schematically shown in Figure 2-5. The energetic distribution of the density of the states (DOS) is assumed to be a Gaussian distribution function $G(E)$ based on the

Bässler model. Charge carriers hop parallel to the electric field F to neighboring molecules both from lower to higher energies and vice versa. The Bässler model describes hopping transport as a thermally activated process and the mobility increases with increasing temperature. In contrast, in a perfect crystal, the mobility decreases with increasing temperature. Hereby, the mobility of disordered organic semiconductors is given by[25,30]

$$\mu(T) = \mu_0 \cdot \exp \left[- \left(\frac{2E_a}{3k_B T} \right)^2 \right] \quad (2 - 2)$$

where μ_0 is the mobility of the perfect semiconductor at infinite temperature ($T \rightarrow \infty$), E_a is an activation energy and k_B is the Boltzmann constant.

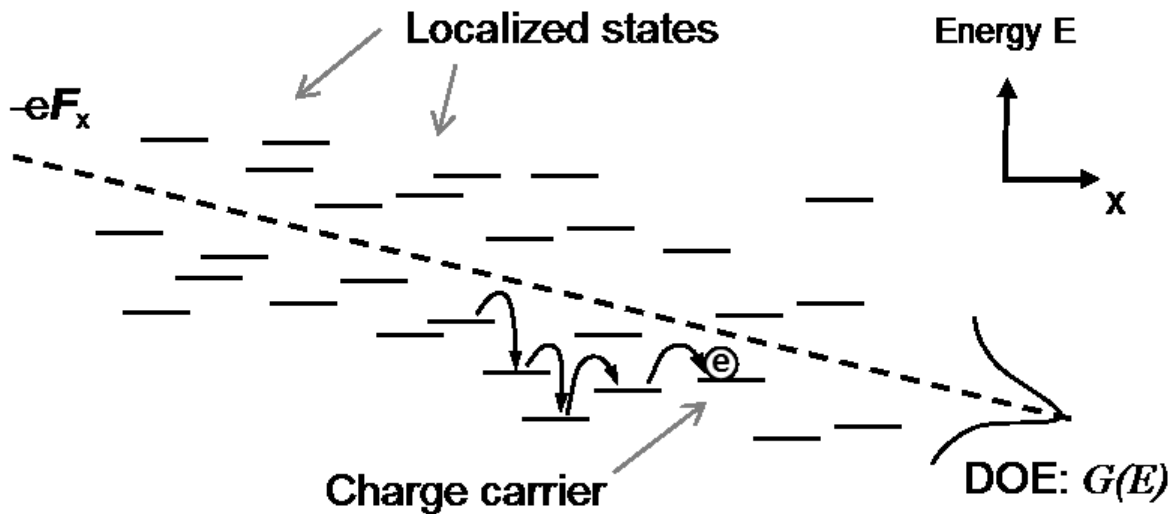


Figure 2-5 Schematic of hopping transport in a disordered organic semiconductor. Reproduced from[11].

2.2 Organic photovoltaics (OPV)

Photovoltaic effects have been explored and optimized into a technology for converting light into electricity since the 1950s by Chapin et. al.[31]. Recent studies report power conversion efficiencies (PCE) of inorganic solar cells up to 46% (Soitec and Fraunhofer Institute for Solar Energy systems (ISE))[6]. Simultaneously, organic solar cells have been investigated over the past several decades based on the fundamental photoconductive effects of the organic molecules such as acenes[20]. In 1986, Tang reported about 1 % PCE by producing single heterojunction organic photovoltaics using physical vapor deposition techniques with highly purified small molecules[32]. After that, conjugated polymers were developed[33] and nowadays many studies have been undertaken to further explore organic photovoltaics[11,23,25]. The highest efficiency achieved up to now is obtained by Heliatek with a PCE of 13.2 %[7]. In this section, the basic working principle of photovoltaic cells will be introduced. In addition to the working principle, major parameters for characterizing photovoltaic cells will be discussed.

2.2.1 Working principle

The photovoltaic effect is the conversion of the sunlight into electric power. A solar cell generates electricity when the incident light has sufficient energy to generate free charge carriers. For inorganic solar cells p-n junctions are mostly used. A p-n junction is an interface between two different types of semiconductor “p” (positive) type and “n” (negative) type. A p-type semiconductor has holes and n-type has electrons as majority charge carriers. As shown in Figure 2-6(a), an incident photon with sufficient energy can generate an exciton (a bound pair of an electron and a hole). This is also illustrated in Figure 2-3 as the transition from singlet ground state S_0 to the excited state S_n with a probability (η_{Ab}). An exciton is neutral and can only move by diffusion and is not influenced by an external electric field. Since recombination is fast, the small diffusion length (L_D in the range of 3 to 40 nm) should be considered in the design of the heterojunction[34]. The efficiency of exciton diffusion is referred to as η_{ED} . After reaching the interface between the donor and acceptor, intermolecular charge transfer generates a charge-transfer state (Figure 2-6(b)). The donor material donates the electron and this electron is accepted by acceptor materials with the efficiency of η_{CT} . The next step is charge separation. The electron

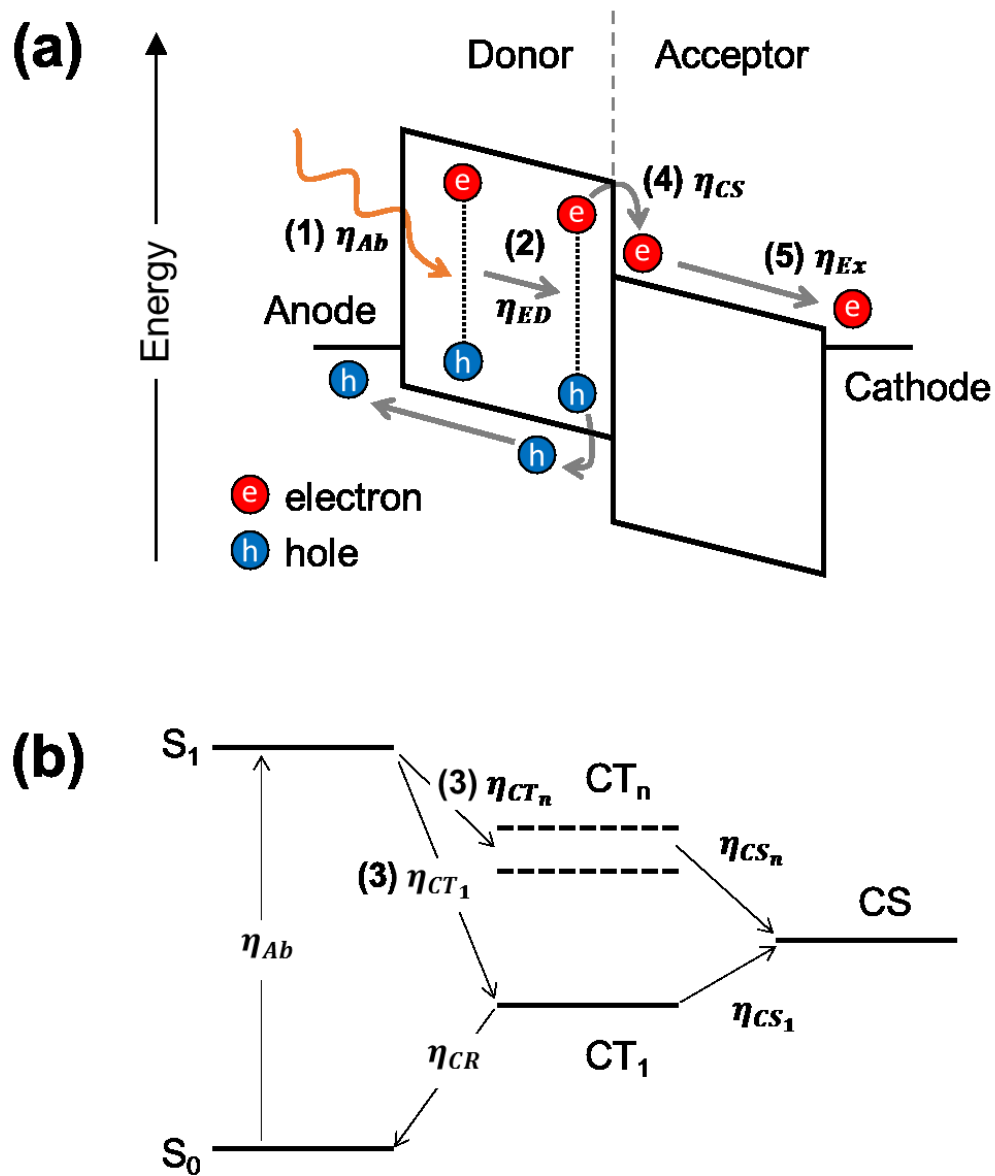


Figure 2-6 Schematic energy diagram of an organic donor-acceptor heterojunction between an anode and a cathode. Steps for converting light into electricity are illustrated: (1) absorption, (2) exciton migration, (3) charge separation, and (4) charge transport and extraction (a) and electronic state diagram which shows charge transfer, recombination and separation (b).

favors moving to the acceptor material with a lower LUMO and the hole to the donor with a higher HOMO. Charge separated states are formed with the efficiency of η_{CS} [35]. The last step for converting light into electricity is charge carrier extraction. After separation, free charge carriers are transferred to the anode and cathode, respectively, by hopping process. Therefore, high mobility materials can have higher charge extraction efficiency(η_{Ex}). The major factors which determine η_{Ex} are the HOMO and LUMO levels of both donor and acceptor materials and the work functions of the respective anode and cathode as well as the morphology of bulk heterojunction. In the state-of-the-art devices, values close to 100% are achieved for η_{Ex} by combining the proper materials and doped interfaces. Combining all the noted single step efficiencies, the external quantum efficiency (EQE) is obtained by

$$EQE = \eta_{Ab} \cdot \eta_{ED} \cdot \eta_{CT} \cdot \eta_{CS} \cdot \eta_{Ex} \quad (2 - 3).$$

The EQE is the ratio of extracted charge carriers with respect to incoming photons and it is mainly limited by η_{ED} due to the relatively short diffusion length of the excitons (L_D). If the thickness of donor and acceptor are limited to L_D , the incoming light will not be fully absorbed. To overcome this limitation, several approaches exist, which will be discussed in the following.

2.2.2 Heterojunction p-i-n concepts

In 1998, our group at IAPP applied p-i-n concepts to organic light emitting diodes[36,37] and later to organic solar cells[38,39]. As illustrated in Figure 2-8(a), a p-doped hole transport layer (HTL) and an n-doped electron transport layer (ETL) sandwich the active layers of donor and acceptor on both sides. These transport layers should have a band gap of $> 3\text{eV}$ to avoid parasitic absorption in the visible range. Additionally, the HOMO levels of HTL and donor material as well as the LUMO levels of ETL and acceptor material should be matched to prevent an accumulation of the free charges at the resulting energy barriers. Since the conductivity of the ETL and HTL can be enhanced by doping, the thicknesses of the transport layers can be adjusted to optimize the solar cell stack by placing the maximum of the optical field distribution at the position of the absorbing materials (marked as a dashed black line in Figure 2-8(a)).

Moreover, to overcome the limitation of L_D in the absorbing materials in a planar heterojunction

structure (Figure 2-7(a)), a bulk heterojunction structure as shown in Figure 2-7(b) was introduced for increasing the interfacial area between the donor and acceptor with a maximum distance of L_D between donor and acceptor. However, it has remained impossible up to now to realize such an ideal bulk heterojunction structure. Therefore, a randomly blended structure of donor and acceptor was introduced by Hiramoto et. al. and developed[33,40,41] as described in Figure 2-7(c).

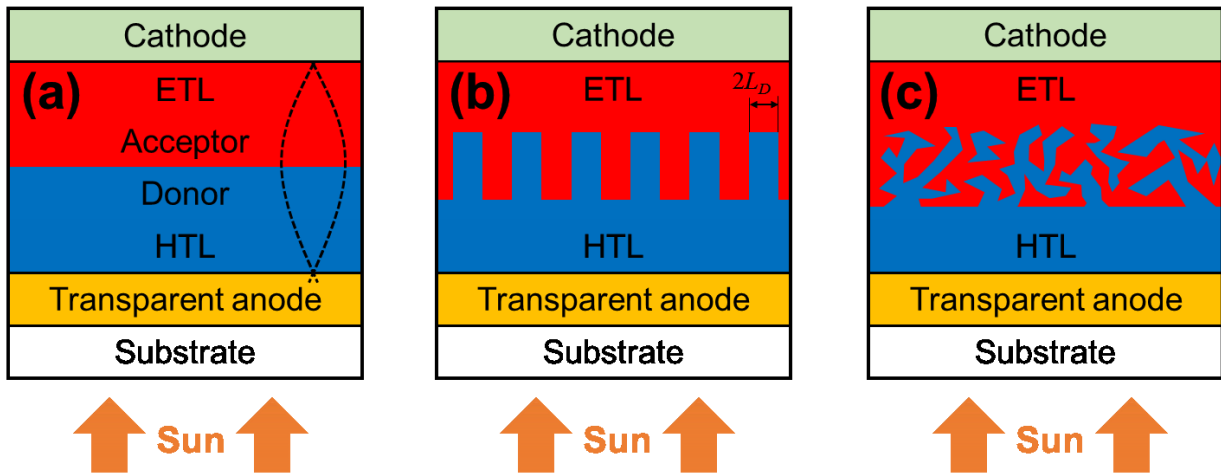


Figure 2-7 Schematics of different heterojunction *p-i-n* concepts in organic photovoltaics: planar heterojunction (a), ideal bulk heterojunction (b) real bulk heterojunction (c).

2.2.3 Characteristics of OPVs

Besides understanding the working principle of OPVs, the current-voltage characteristics of OPVs are important to evaluate devices. The current-voltage (j - V) curve of OPVs under illumination is usually recorded as shown in Figure 2-8. This j - V curve can be explained in first approximation by the Shockley equation.

$$j(V) = j_s \left[\exp\left(\frac{qV}{nk_B T}\right) - 1 \right] - j_{ph} \quad (2-4)$$

where j_s is the saturation current, n is the diode ideality factor and j_{ph} is the photocurrent density. The saturation current j_s is determined by the number of thermally generated charges, their diffusion constants and diffusion lengths. The diode ideality factor n is a constant value between 1 and 2 and j_{ph} is generated by photon absorption and charge carrier generation under illumination as explained above. The short circuit current density (j_{sc}) is the generated current density at 0 V, and equals J_{ph} . Further important factors are the open circuit voltage (V_{oc}), the fill factor (FF) and the power conversion efficiency (η). V_{oc} is the voltage when j_{sc} is 0. It can be obtained from

$$V_{oc} = \frac{nk_B T}{q} \ln \left(\frac{j_{sc}}{j_s} + 1 \right) \quad (2 - 5).$$

The power density (P) of a device is obtained by multiplying current density (j) and voltage (V), which is illustrated in Figure 2-8. The point of the $j - V$ curve with the highest P is denoted as the

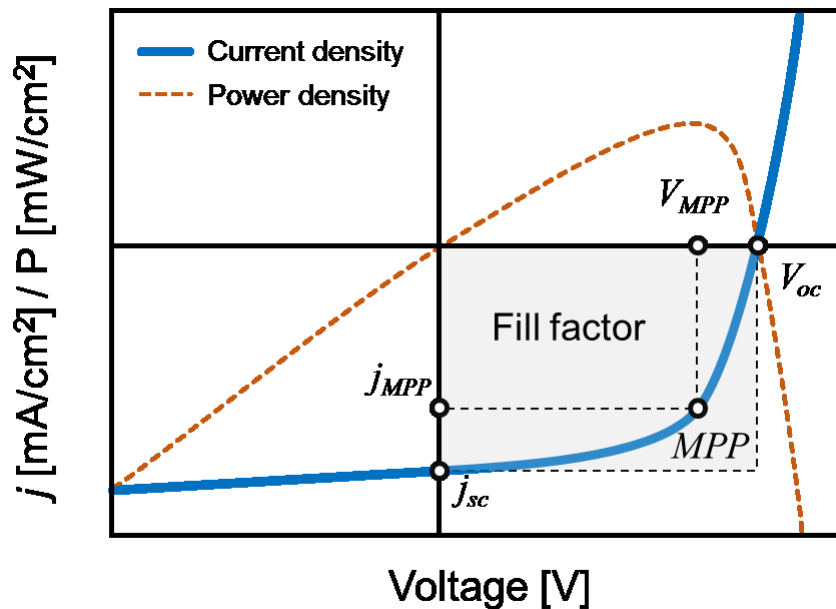


Figure 2-8 Current-voltage and power density curves of an organic solar cell with the characteristic parameters j_{sc} , V_{oc} , j_{MPP} , V_{MPP} and FF .

maximum power point (MPP), and the current density and voltage at the MPP are called j_{MPP} and V_{MPP} . The FF is defined as

$$FF = \frac{j_{MPP}V_{MPP}}{j_{sc}V_{oc}} \quad (2 - 6)$$

and indicates the ratio between the P_{MPP} and P_{ideal} ($j_{sc} \cdot V_{oc}$). The most important parameter, the power conversion efficiency (η), gives the ratio between the generated power and the incident light power, which is calculated by

$$\eta = \frac{P_{MPP}}{P_{light}} = \frac{j_{sc}V_{oc}FF}{P_{light}} \quad (2 - 7).$$

To ensure a correct measure of η , a measurement using a solar simulator with a spectrum that differs from the AM 1.5 G reference sun spectrum should be properly corrected for this mismatch. All the values of efficiencies in this thesis are mismatch corrected, of which the method is briefly explained in chapter 4.

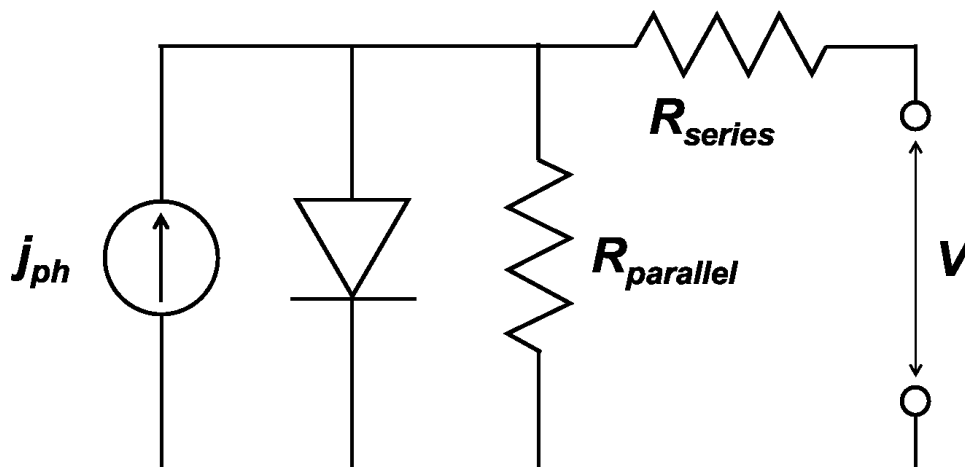


Figure 2-9 Equivalent circuit description of an OPV.

In real OPVs, the diode behavior differs from the ideal Shockley diode. They behave as the circuit described in Figure 2-9 and Shockley equation (Equation 2-4) can be modified as

$$j(V) = j_s \left[\exp \left(\frac{q(V - j(V)R_{series})}{nk_B T} \right) - 1 \right] + \frac{V - j(V)R_{series}}{R_{parallel}} - j_{ph} \quad (2 - 8)$$

where R_{series} is a series resistance and $R_{parallel}$ is a parallel resistance, which cause efficiency losses. Assuming $R_{parallel}$ as ∞ , the slope close to V_{oc} as well as FF and j_{sc} decrease with increasing R_{series} (Figure 2-10). This decrease mainly comes from a lack of conductivity of electrodes and organic layers. When R_{series} is 0, the slope close to j_{sc} increases with decreasing the $R_{parallel}$, leading to a reduction in FF and V_{oc} . In this case, local short circuits in the device, caused by rough surface or bad growth condition, is one of the main reasons that can impede lower $R_{parallel}$.

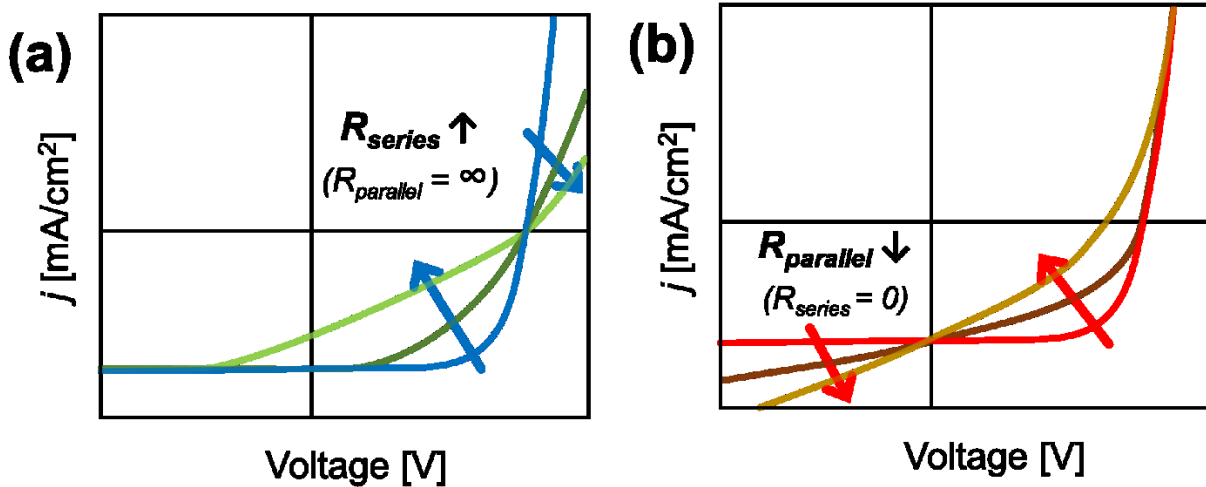


Figure 2-10 Current-voltage curve with different parallel resistances (a) and series resistances (b).

3. Optics in organic photovoltaics

When the sun illuminates a photovoltaic device, light is partly absorbed and partly reflected. In order to increase the amount of absorbed light in the device, research efforts focus on developing new materials, highly transparent electrodes, new device architectures structures and light management in the photovoltaic devices. Control of the device optics is hereby one of the most important factors to increase the photocurrent in organic photovoltaics. In this chapter, an upper limit for the fraction of absorbed light in a thin film, using Lambertian scattering and wave-guide modes by periodic structure, is introduced. Moreover, state-of-art in light trapping methods, especially periodically patterned gratings as shown in Figure 3-1 and random scattering elements, are introduced.

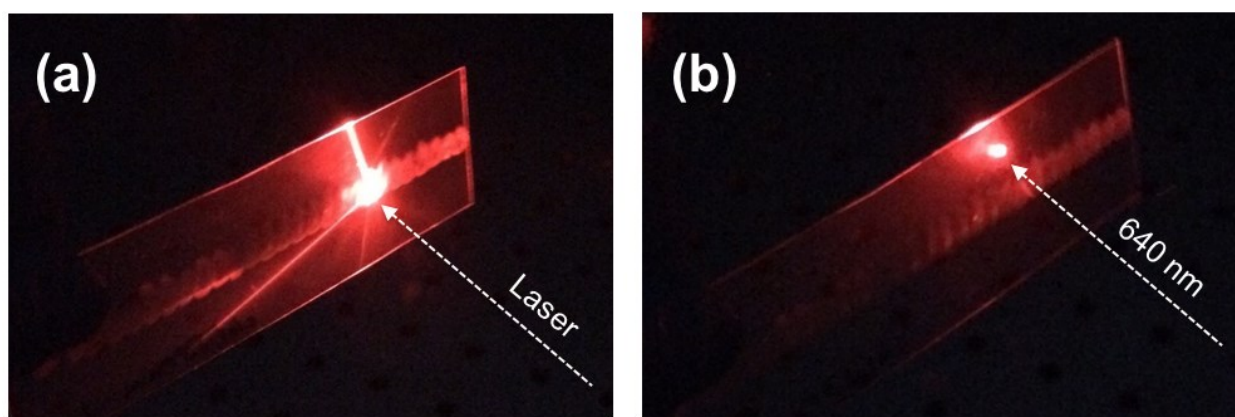


Figure 3-1 Trapped light and slightly diffused light on patterned (a) and planar (b) PET substrates with the red laser ($\lambda=640\text{nm}$).

3.1 Optical models for light trapping

In order to understand light trapping in photovoltaics, we discuss in this section some basic optical models. Starting with Lambertian scattering, we calculate how a light beam with multiple reflections passes through the absorber layer. This leads to the Yablonovitch limit for weak absorption ($\alpha(\lambda) \approx 0$) and relatively thick absorber layer ($d \gg \lambda$, d : thickness of layer). For thin films ($d \geq \lambda$), comprising grating elements, this limit needs to be modified as discussed by Yu et al. and their limit is referred in this chapter.

3.1.1 Fundamentals of light trapping

The main goal of light trapping in photovoltaic devices is to maximize the total fraction of absorbed light in the photo-active layer. Initial studies on light trapping were undertaken for the silicon based photovoltaic devices using textured surfaces as light scattering elements[42]. Internal reflection increases the average length of the light path and thereby the absorption in the absorber material, as shown in Figure 3-2. The enhanced absorption can be calculated based on geometrical optics and Lambertian light scattering[43]. Assuming that a light beam passes through an absorbing medium with l (the length of a single light pass), a fraction of the light (A_{B-L}) is absorbed and can be calculated using Beer-Lambert's law.

$$A_{B-L}(\lambda) = 1 - \exp[-\alpha(\lambda)l] \quad (3 - 1)$$

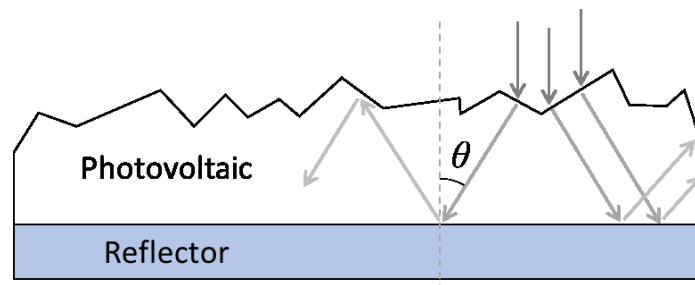


Figure 3-2 Schematic cross-section of a photovoltaic device with textured structure.

where $\alpha(\lambda)$ is the absorption coefficient of the material. Assuming a perfect mirror at the back side of the absorber and Lambertian scattering at the front interface, the length of the light path, l can be increased to

$$l = 2d \cos^{-1}(\theta) \quad (3 - 2)$$

where d is the thickness of photovoltaic device and θ is the scattering angle of the light which is changed by textured interface. Considering isotopically distributed Lambertian scattering, with the multiple reflections at the front textured interface $R_F(\lambda)$, the total absorption $A(\alpha d, \lambda)$ can be calculated by[44]

$$A(\alpha d, \lambda) = \frac{A_L(\alpha d, \lambda)}{1 - (1 - A_L(\alpha d, \lambda))R_F(\lambda)} \quad (3 - 3)$$

where all absorption by in-coupled light during 2 bounces (traveling once from the front side through the photovoltaic device and back reflector to the front interface) is given by[43]

$$A_L(\alpha d, \lambda) = 1 - \frac{\int \exp\left(-\frac{2\alpha(\lambda)l}{\cos(\theta)}\right) \cos(\theta) d\Omega}{\int \cos(\theta) d\Omega} \quad (3 - 4)$$

By these equations, we can find how much absorption enhancement is achievable, by making use of Lambertian scattering. This will be discussed in the next section.

3.1.2 Limitations to Lambertian light trapping

In the early 1980s, Yablonoitch has shown that the maximum average light path length is given by[45]

$$\bar{l}_{max} = 4 n^2 d \quad (3 - 5)$$

where n is refractive index of the absorber material. Moreover, the maximum absorption is given by

$$A(\lambda)_{max} = 1 - \exp[-\alpha(\lambda)4 n^2 d] \quad (3 - 6).$$

Following from all equations which are shown above, $A(\lambda)_{max}$ provides a maximum value of the EQE and J_{sc} . In what follows, we call the path length enhancement factor of $4 n^2$ the Yablonovitch limit. It is important to note that this limit is based on ray optics and is valid only for absorber layer thicknesses thicker than the wavelength of light ($d \gg \lambda$)[21]. Taking into account the wave nature of light, an electromagnetic limit for light trapping, with an enhancement factor of $(12 \times 4 n^2)$ has been presented by Yu et al.[46]. In their calculation, the propagation of light inside the absorber is considered as leaky waveguide modes[47]. With this light trapping concept, propagating waves are trapped in the guided modes of a photovoltaic structure with a grating with period Λ , as shown in Figure 3-3. The model is also based on the assumption of weak absorption in thin films without light trapping elements, as in Yablonovitch limit. However the model differs in the sense that the thickness of the absorber layer is smaller or equal than the wavelength of the light ($d \leq \lambda$). Incident light perpendicular to the grating is diffracted at specific angles of modes ($m = 1, 2, 3, \dots$) and the maximum absorption, A_{max} is calculated for each mode as in Figure 3-4. Furthermore, from this figure, we can deduce that A_{max} shows the maximum value when Λ is λ ($\Lambda / \lambda = 1$). A shorter periodicity (Λ) of the grating provides a longer light path and a higher absorption enhancement in photovoltaic devices at the range of $\Lambda / \lambda > 1$. However when Λ / λ is smaller than 1, A_{max} decreases.

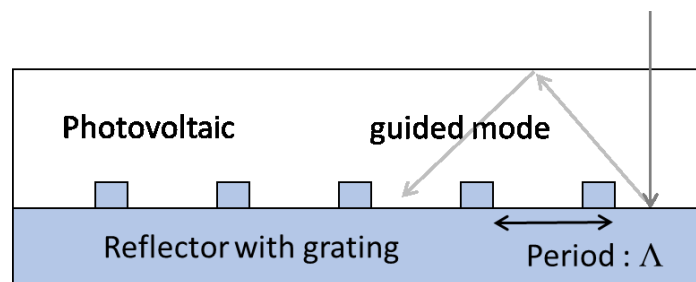


Figure 3-3 Schematic cross-section of a thin photovoltaic device with a grating on the reflector.

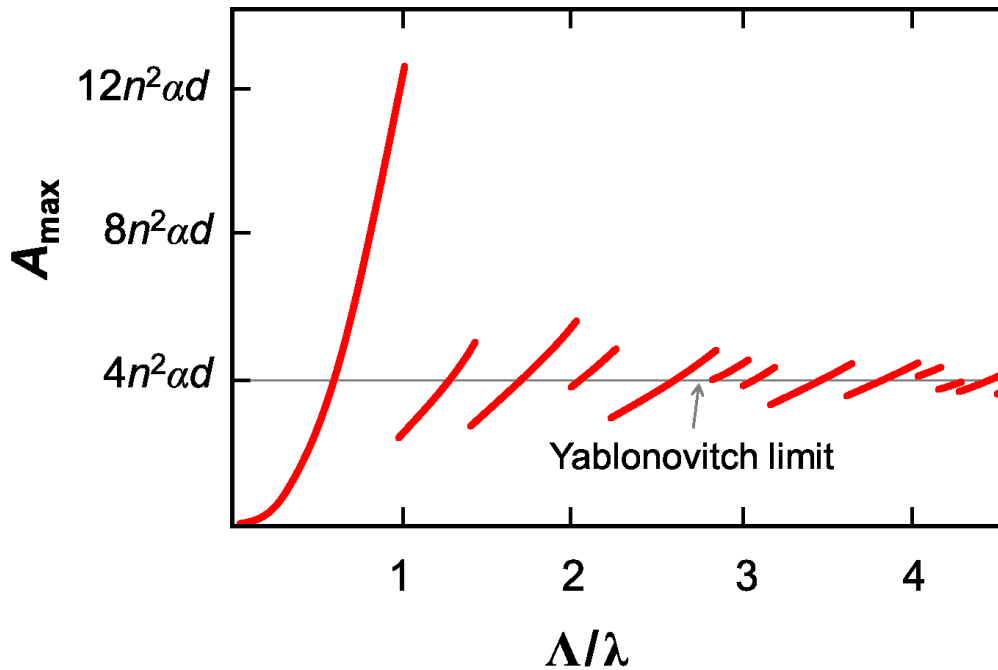


Figure 3-4 Theoretical limit of absorption (A_{max}) of the photovoltaic device with grating of periodicity (Λ)[7].

3.2 Practical implementations of light trapping

In the 1970s, the multiple-pass thin film photovoltaic device has been proposed as the first solar cell employing light trapping techniques[48]. Since then, studies of light trapping for photovoltaics has grown, for example resulting in the so-called black silicon for which 22.1% of PCE was achieved[49,50]. For organic photovoltaic devices, photonic crystals [51,52], surface patterning[53,54], scattering layers[55–57] and external concentrators were proposed[58]. In this thesis, periodically patterned PET substrates[54,59], periodically nano-imprinted polymer electrodes[60] and transparent, scattering electrodes[57] were investigated. We here focus especially on the practical implementations of light trapping effects with a mechanical flexibility. Therefore periodic patterns and scattering effects on flexible substrates and electrode are mainly discussed in this section.

3.2.1 Periodically patterned grating

Following the development of producing periodically patterned structures on a rigid or a soft materials, several techniques for making structures on substrates and electrodes for organic devices have been investigated. Thereby many shapes of structures such as line, hexagonal grating[61], wrinkles[62], three-dimensional single layer[63] and multi layers[64,65] have been explored. However to understand light trapping by a complex structure is still not easy without simulation[66]. In this study, we mainly focus on the line structured grating for simplifying optical models.

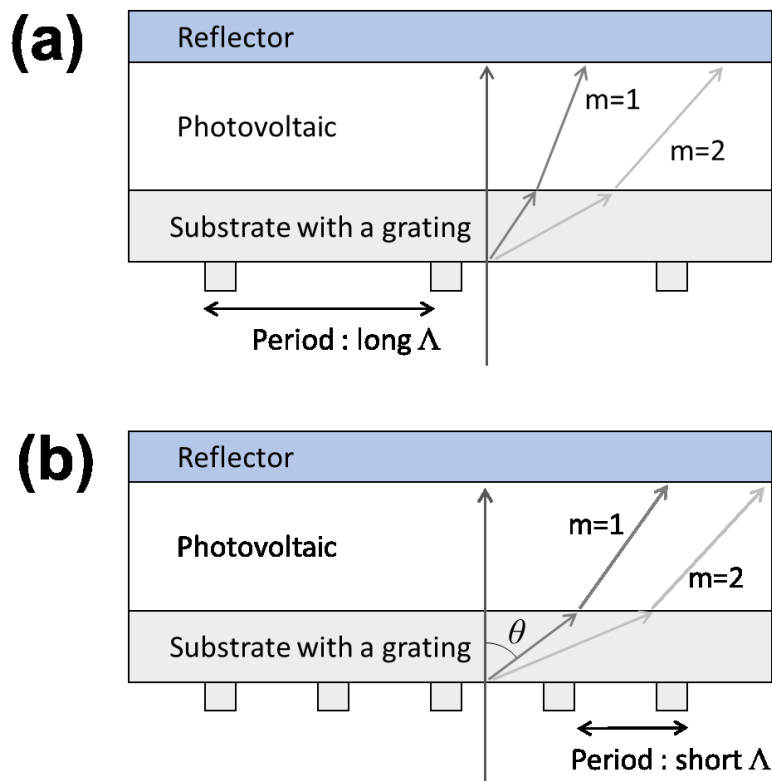


Figure 3-5 Schematic cross-section of a thin photovoltaic device with a diffracted light due to a grating of a long period (a) and a short period.

The period of the patterned structure (Λ) and the height of the structure are the most important factors that affect the absorption enhancement by light trapping. To estimate the path length increase, achievable by using a grating, the diffraction angle (θ_m) is an important factor which can determine light path in absorption layers and can be calculated as where m is an integer and λ is the wavelength:

$$m\lambda = \Lambda \sin\theta_m \quad (3 - 7)$$

Analyzing this simple equation, we note that shorter period (Λ) results in a higher diffraction angle (θ_m) as shown in Figure 3-5. Moreover a theoretical limitation of absorption by Yu, et al. shows also shorter Λ can provide higher maximum absorption limitation at the range of $\Lambda / \lambda > 1$. In our study, we have investigated OPV devices which incorporate grating structures with three different periods ($\Lambda = 1.0, 1.8, 2.6 \mu\text{m}$) and we found that indeed the shorter period has a higher light trapping efficiency. The range of maximum absorptions of a visible light (400nm - 800nm) for each three different periods are highlighted in Figure 3-6 and regime I ($\Lambda = 1.0 \mu\text{m}$) has relatively higher A_{max} than the others. Besides the period (Λ), the height of the grating structure is also very important for the light trapping, as shown in Figure 3-7. $1.6 \mu\text{m}$ height structures with a Λ of 1.8 and $2.6 \mu\text{m}$ diffract over 70 % of the incident light at the wavelength of 405 nm and over 50 % for the wavelength of 640 nm. However $0.5 \mu\text{m}$ height with a Λ of $1.0 \mu\text{m}$ diffracts only 25 % for the wavelength of 640 nm. This notes higher structures provide more light trapping effect to the devices. More details are given in chapter 5.1.

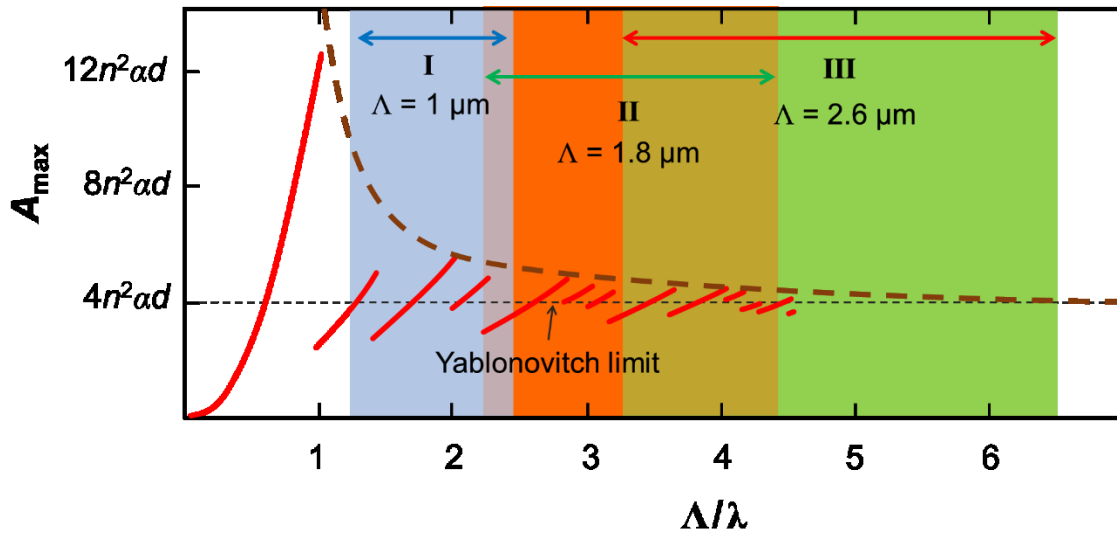


Figure 3-6 Theoretical limit of absorption (A_{max}) of the photovoltaic device and regimes for the periodicities(Λ) of $1.0 \mu\text{m}$, $1.8 \mu\text{m}$ and $2.6 \mu\text{m}$ (from 400nm to 800nm).

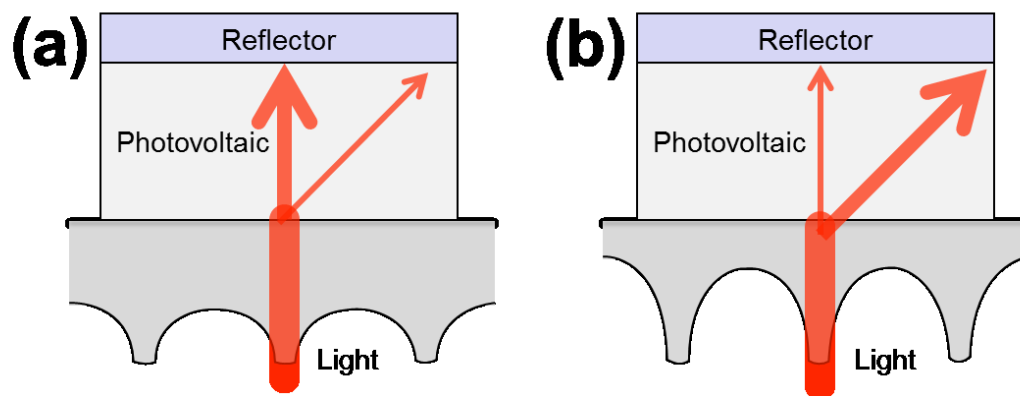


Figure 3-7 Schematics of light diffraction by patterned substrate with high (a) and low (b) height of structure.

3.2.2 Scattering layer

In parallel to the development of techniques for producing periodic patterns, random scattering structures, fabricated using chemical etching[67] and nano-particles[68], have been developed. As compared to the gratings, these methods have the advantage of an easier fabrication process. For an optimum light trapping effect, the size and the concentration of particles should be optimized. The size of particles correlates with the wavelength at which the maximum scattering takes place as shown in Figure 3-8(a). TiO₂ nano-particles with a diameter of 50, 100, 250 nm are used as scattering particles and the haze peaks at wavelengths of 380, 340, 570 nm respectively (Figure 3-8(b)). Although 250 nm particles have a good haze in the visible absorption region (300nm-800nm), it cannot be the best choice for scattering particles since the total transmittance of the scattering layer is low. The second important factor for light scattering are the nano-particles is also important factor for scattering. As shown in Figure 3-9(a), where 100 nm TiO₂ nano-particles are used, we can see that higher concentrations result in more scattering. However, a higher scattering results in less transmittance. Moreover a high concentration of nano-particles result in a rough surface, which makes it difficult to build organic devices on top of this layer. Thereby, to find optimized conditions for OPV performance enhancement, the size and the concentration of the nano-particles should be well considered with respect to optical and structural points. To quantify the scattering effect, the scattering coefficient (μ_s) is used. It is estimated using

$$\frac{T_{direct}}{T_{total}} = e^{-\mu_s d} \quad (3 - 8)$$

where d is the thickness of scattering layer, T_{direct} is directly transmitted transmittance and T_{total} is total transmittance measured with the Ulbricht sphere. We can estimate the optimized concentration for scattering by the value of the scattering coefficient (μ_s). [55] As shown in Figure 3-9(b) even scattering layer with a 3.0 wt% has twice more scattering particles than 1.5 wt%, the scattering coefficient is only 1.5 times higher. In other words, not all particles are effective proportional to the use of particles. In this case the optimized concentration should be located between 1.5 wt% and 3.0 wt%.

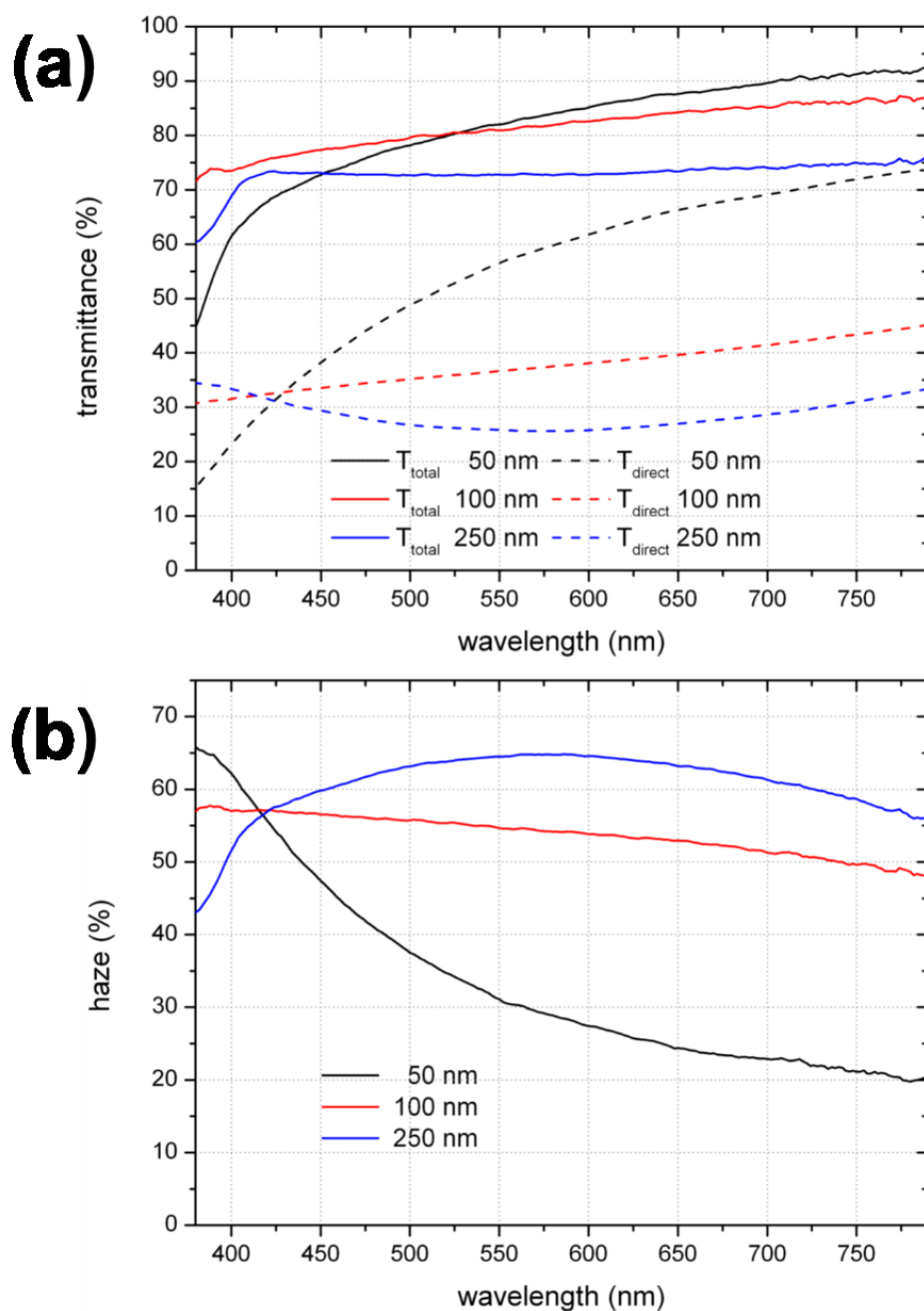


Figure 3-8 Transmittance (a) and haze (b) depending on particle size. For identical concentration, particles with 100 and 250 nm size have about equal scattering ability, while particles with 50 nm size only come into play in the blue wavelength range. All layers are fabricated with a particle concentration of 30 g/l[69].

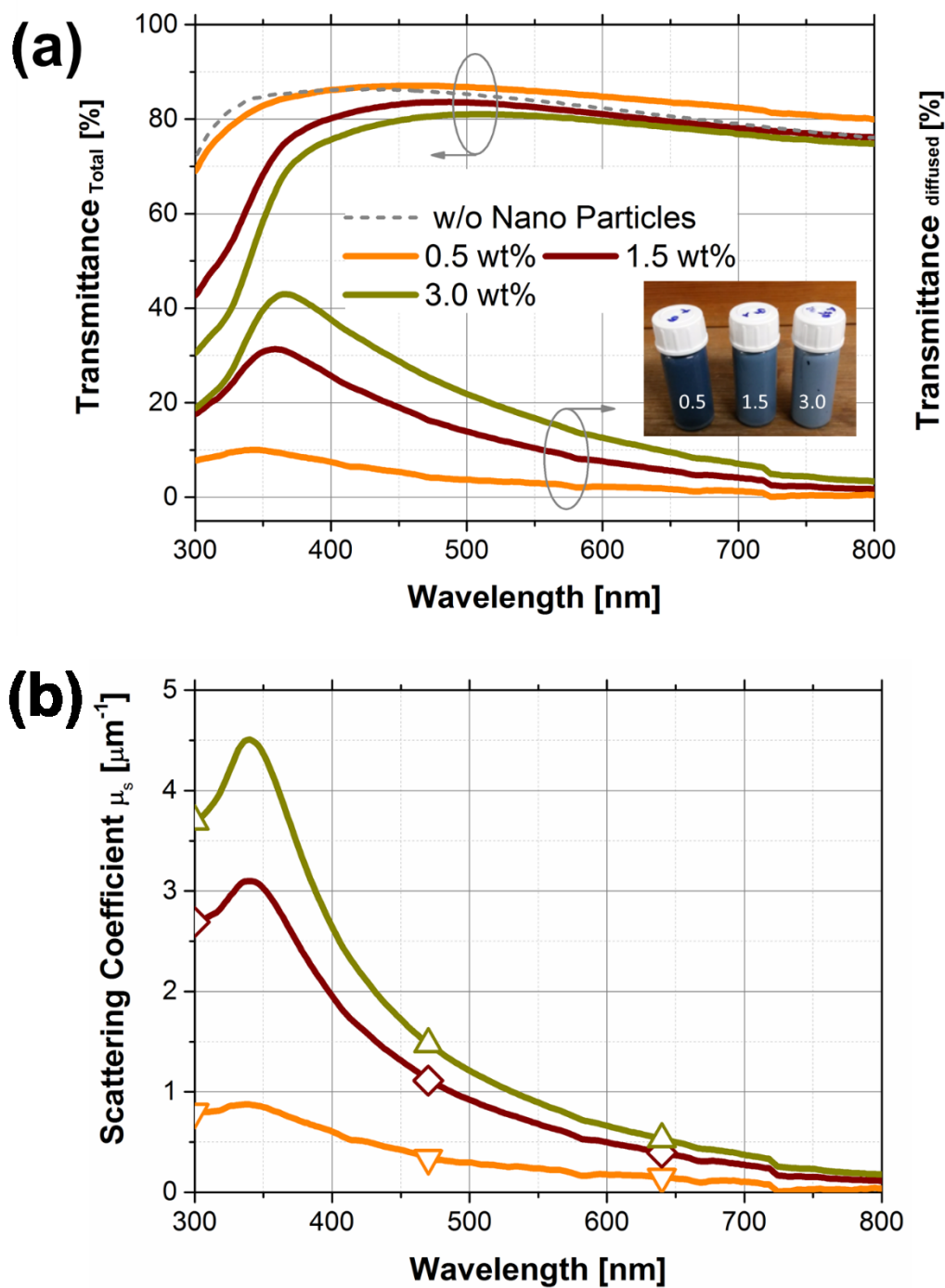


Figure 3-9 Optical properties of PEDOT:PSS layer embedded with NPs. Total and diffuse (total-direct) transmittance of NP:P with three different TiO₂ concentrations (a) and scattering coefficients of three different TiO₂ concentrations (b).

4. Experimental

4.1 Materials

The materials used in this study are shown in Table 4-1 with the values of the HOMO and LUMO energies and chemical formula. As acceptor material C₆₀ is used and DCV5T-Me as electron donor. A C₆₀ is a molecule consisting of only carbon in the form of a hollow sphere. It is also called buckyball and is currently the most widely used acceptor material for small molecule OPVs. DCV5T-Me is a donor material first introduced by Körner et al.[70]. BF-DPB and BPAPF are used as hole transport layers (HTL). BPAPF is highly transparent and doped with NDP9 (Novaled AG). BF-DPB is an alternative HTL, but it cannot be used to directly contact for DCV5T-Me due to its lower IP (5.2 eV). A C₆₀ layer is used as an electron transport layer (ETL) doped with the n-dopant W₂(hpp)₄ (Novaled AG). C₆₀ shows considerable absorption only at wavelengths shorter than 495 nm, although the (symmetry forbidden) optical gap is 1.7 eV in thin films. To reduce the parasitic absorption of doped C₆₀ and MH250 are introduced and used with the n-dopant, W₂(hpp)₄ (Novaled AG). MH250 has an optical gap of 3.0 eV and are as transparent as BPAPF. Full names of each materials are shown below.

DCV5T-Me 2,2'-((3'',4''-dimethyl-[2,2':5',2'':5'',2''':5''',2''''-quinquethiophene]-5,5''''-diyl)-bis(methanylylidene))dimalononitrile

BF-DPB N,N'-((Diphenyl-N,N'-bis)9,9,-dimethylfluoren-2-yl)-benzidine

BPAPF 9,9-bis[4-(N,N-bis-biphenyl-4-yl-amino)phenyl]-9H-fluorene

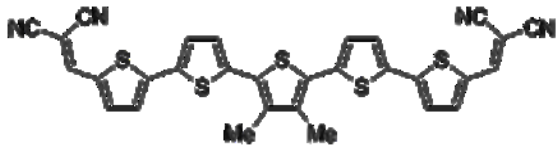

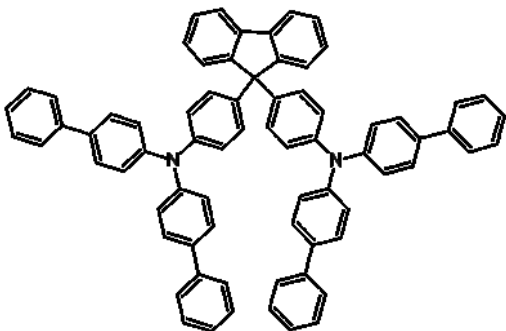
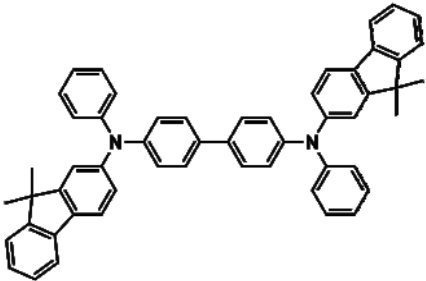
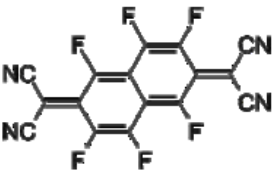
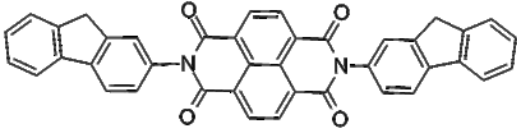

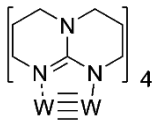
F₆-TCNNQ 2,2'-(perfluoronaphthalene-2,6-diylidene)dimalononitrile

NDP9 Novaled p-dopant 9

MH250 N,N-Bis(fluoren-2-yl)-naphthalenetetracarboxylic diimide

W₂(hpp)₄ Tetrakis(1,3,4,6,7,8-hexahydro-2H-pyrimido[1,2-a]pyrimidinato)ditungsten (II)

Table 4-1 Organic materials used for solar cell preparation.

	Material	HOMO [eV]	LUMO [eV]	Material	HOMO [eV]	LUMO [eV]
Absorber						
	DCV5T-Me	5.6	3.7	C ₆₀	6.4	4.0
HTL						
	BPAPF	5.6	2.2	BF-DPB	5.2	2.3
p-dopant				not published		
	F ₆ -TCNNQ	7.5	3.4	NDP9		
ETL						
	MH250	6.5	3.7	C ₆₀	6.4	4.0
n-dopant						
	W ₂ (hpp) ₄	2.7				

4.2 Sample preparation

4.2.1 Preparation of electrodes (PEDOT:PSS)

Highly conductive PEDOT:PSS (Clevios PH1000, Heraeus, Germany) mixed with 6 vol. % ethylene glycol is prepared as solution (Figure 4-1). Substrates, containing an AlO_x barrier layer of which the details are discussed below, are pre-treated with oxygen plasma for 15 minutes just before film preparation. After plasma treatment, the PEDOT:PSS solution is filtered with a $0.45\ \mu\text{m}$ syringe filter (polytetrafluoroethylene (PTFE)) and spin coated on the substrates with a spin speed of 1000 rpm for 30 seconds. Subsequently, samples are annealed on a hot plate at $120\ ^\circ\text{C}$ for more than 30 minutes.

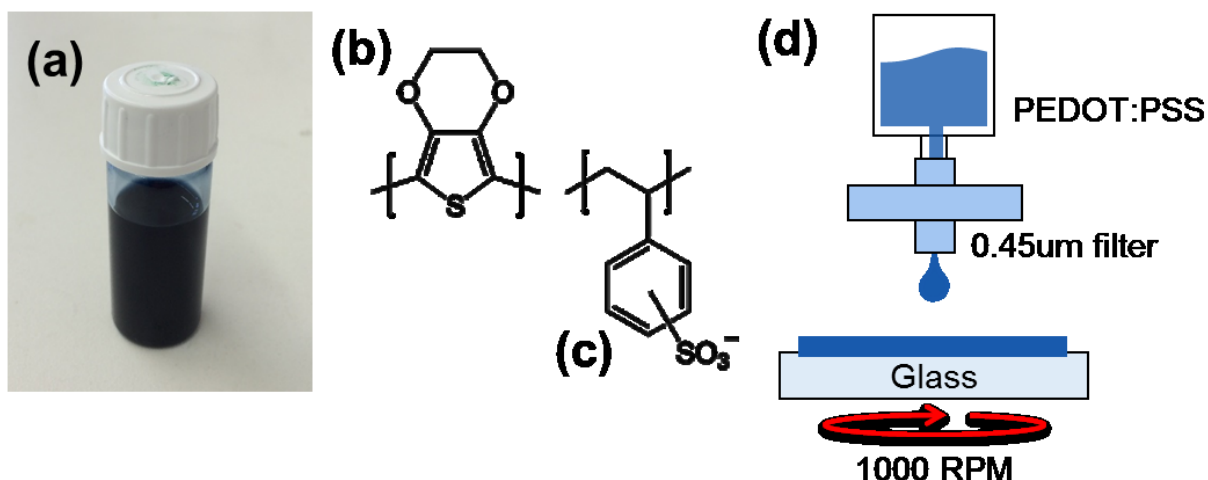


Figure 4-1 Photograph of PEDOT:PSS solution mixed with 6 vol. % ethylene glycol (a), structural formulas of PEDOT (b) and PSS (c) and a schematic representation of the spin coating process (d).

4.2.2 Preparation of OPV devices

After the preparation of PEDOT:PSS electrodes on substrates, the electrodes are structured using laser ablation with a Nd:YAG laser (ACI Laser) resulting in half covered substrates with PEDOT:PSS, as shown in Figure 4-2. The subsequent organic layers comprising the rest of the solar cell stack are deposited in the middle of the substrates. The photovoltaic device is completed with a top Al electrode. Each substrate contains four devices with identical area.

Small molecular OPV devices are fabricated by a thermal co-evaporation system in a vacuum chamber (K. J. Lesker, U. K.) at a base pressure around 10^{-8} mbar, as described in Figure 4-3[71]. The organic layers that consist solar cells on the 120 nm PEDOT:PSS transparent anode are

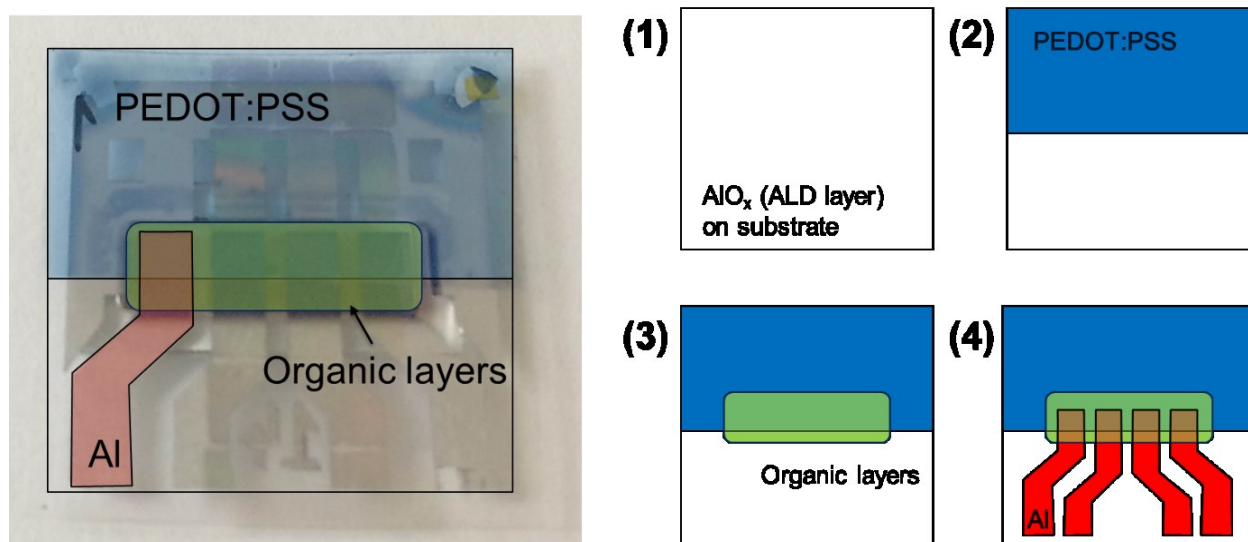


Figure 4-2 Schematic structure of the organic solar cells (left) and their layout on the substrates (right): (1) an AlO_x layer is deposited as an encapsulation (oxygen and moisture barrier) layer on the substrate using an ALD system, (2) half coated transparent PEDOT:PSS bottom electrode, (3) organic layers deposited by an evaporation system and (4) 4 - fingers structured Al top electrode.

- 30 nm MH250 transparent ETL material, doped by 7 wt. % $W_2(hpp)_4$
- 15nm C_{60} fullerene as an electron transport layer
- 40 nm of mixed DCV5T-Me and fullerene C_{60} (ratio of 2:1) as an absorber layer, deposited at a substrate temperature of 90 °C
- 5 nm BPAPF as a hole transporting layer
- 35 nm of BPAPF and 10 nm of BF-DPB transparent matrix materials doped with 10 wt. % NDP9 (Novaled AG)
- 120 nm Al cathode.

For preparing the bottom encapsulation, a 20nm thick AlO_x thin film is deposited by plasma enhanced atomic layer deposition (ALD) in a Sentech SI reactor (SENTECH Instruments GmbH, Berlin, Germany) on PET substrates. At 100 °C electrode temperature, 220 cycles are done using

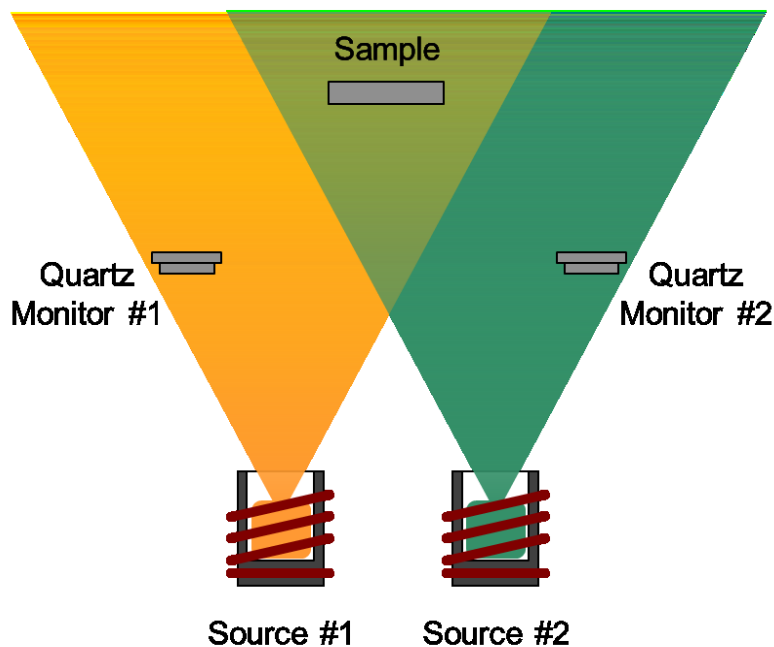


Figure 4-3 Schematic representation of the thermal co-evaporation system. The growth rate of each material is measured by quartz monitors for precisely determining the mixing ratio.

electronic grade trimethylaluminium (TMA) and atomic oxygen from the plasma as precursors. In between precursor pulses, the chamber is purged with 99.9999% chemically pure nitrogen gas. For the top encapsulation, an equivalent thin-film is deposited on 125 µm planarised Teonex PEN (Dupont Teijin Films Ltd.,UK). In a glovebox, this barrier film is directly laminated onto the OPV devices using a special moisture barrier adhesive film (tesa SE, Germany)[72], which contains a latent getter, protecting the photo-active layers from lateral oxygen and water diffusion.

4.3 Sample Characterization

- OPV Characterization method

Current voltage curves are acquired under simulated AM 1.5G sunlight (16S-150 V.3, Solar Light Co., USA) using a Keithley 2400 source measuring unit (SMU). Spectral mismatch is taken into account. The illumination intensity is kept at (100 ± 1) mW/cm² monitored by a silicon reference diode. The EQE, used to calculate the mismatch factor is measured using a lock-in amplifier (Signal Recovery SR 7265) with the device under monochromatic illumination (Oriel Xe Arc-Lamp Apex Illuminator combined with Cornerstone 260 1/4 m monochromator, Newport, USA). Since the sun simulator spectrum, $\Phi_{sim}(\lambda)$ of the measurement system is different from the standardized AM1.5G sun spectrum ($\Phi_{AM1.5G}(\lambda)$). The mismatch factor, M (Equation 4-1) is required to correct the illumination intensity of the measurement system with that of AM1.5G. The spectral response of the samples, $SR_{OPV}(\lambda)$ is obtained by the EQE and $SR_{ref}(\lambda)$ of the silicon reference solar cell ('S1337-33BQ', Hamamatsu, Japan), is calibrated by Fraunhofer Institute for Solar Energy Systems (ISE, Germany). It yields a current $I_{ref}^{AM1.5G}$ of 0.78mA at 100mW/cm² AM1.5G illumination intensity.

$$M = \frac{\int SR_{osc}(\lambda) \cdot \Phi_{sim}(\lambda) d\lambda}{\int SR_{osc}(\lambda) \cdot \Phi_{AM1.5G}(\lambda) d\lambda} \cdot \frac{\int SR_{ref}(\lambda) \cdot \Phi_{AM1.5G}(\lambda) d\lambda}{\int SR_{ref}(\lambda) \cdot \Phi_{sim}(\lambda) d\lambda} \quad (4 - 1)$$

Moreover, for a precise determination of the photocurrent density, the exact size of all pixels are measured by optical microscopy.

- UV-VIS-NIR spectroscopy

To investigate optical properties of light trapping substrates and electrode, total and direct transmittance measurements are carried out with an integrating sphere at a SolidSpec-3700 two beam spectrometer (Shimadzu, Japan).

- Atomic force microscopy (AFM)

The topography of light trapping substrates and electrodes are acquired by using a Combiscope AFM (AIST-NT, Netherlands) in standard tapping mode. TAP-AI-G tips (BudgetSensors, Bulgaria) with 300 kHz resonance frequency are used. After acquiring the AFM images, they were evaluated with the software Gwyddion.

- Scanning electron microscopy (SEM)

The micro structures of samples are investigated by SEM (Zeiss GSM 982 Gemini, Germany) operated by Susanne Goldberg (Physical Chemistry, TU Dresden). Less than 2 nm of gold was sputtered onto the samples before SEM analysis for removing noise due to sample charging.

- Goniometer

Optical measurements are performed with Ocean Optics Maya2000 Pro spectrometer and goniometer (after fixing samples a white light source detector was rotated around the samples as shown in Figure 4-4). An Osram halogen lamp (Xenophot 64610 HLX) is used as white light source and light was collected with a fiber and guided to the spectrometer[73]

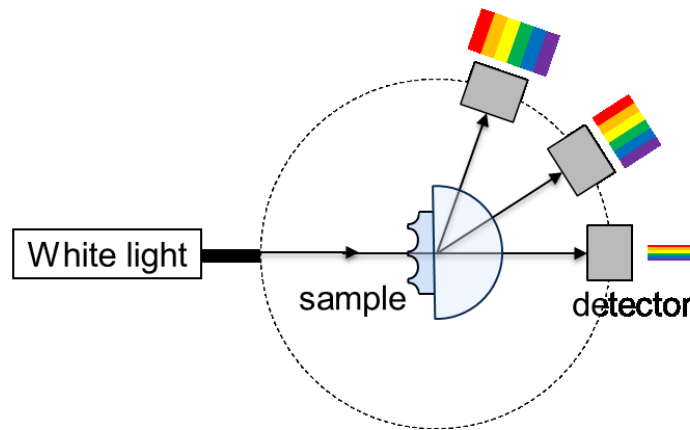


Figure 4-4 A schematic of the goniometer.

- Optical microscopy

In order to check a dispersion of nano-particles in PEDOT:PSS, microscopic images are taken by optical microscope (Eclipse, Nikon, Japan). Moreover the size of each pixels in the devices is measured.

- Profilometer

The height of samples was measured by a surface profilometer (Dektak 150, Veeco, USA). A stylus radius of 25 μm and scan length 20 mm were used. After acquiring profile data, a leveling was performed for estimating the height of samples.

- Bending test

In order to check a flexibility of OPVs, bending tests with various bending radii (Figure 4-5(a)) are manually performed (Figure 4-5(b,c)). For checking a correlation between the performance and number of bending cycles, the PCE of each devices was measured before and just after bending.

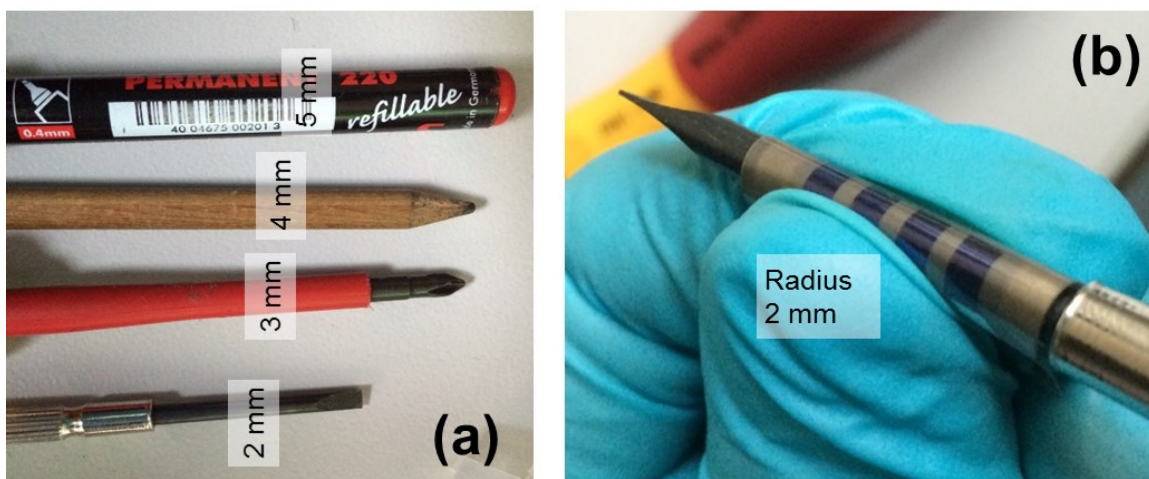


Figure 4-5 Photographs of screws and pens for providing constant bending radius (a) and device bent at a 2 mm radius (b).

5. Light trapping substrates

Flexible substrates are an essential element for the production of flexible devices. Moreover, unlike rigid glasses, flexible substrates such as PET and PDMS allow additional processing. For glass, elaborate equipment such as reactive ion etching (RIE) is required to fabricate light trapping structures on its surface. However micro- or macro-scale structures can be easily constructed on polymer substrates by laser ablation techniques. In this chapter, periodic structures are fabricated on PET films and used as light trapping substrates. To this end, also commercial display films are tested.

5.1 Motivation

Small molecule based organic photovoltaics (OPV) are a promising candidate for solar energy conversion due to their scalability, flexibility and low cost. However, the thin absorber layer thickness required for efficient charge carrier extraction limits the photovoltaic efficiency. To overcome this drawback, light trapping can be an effective method to enhance photon harvesting. In the last years, photonic crystals[74,75], surface patterning[53,54,76–78] and scattering layers[55–57] have been studied for an enhanced light harvesting in solar cells. To fabricate periodic light trapping elements on various substrates such as transparent conducting oxide[79], glass[10,80] and polyethylene terephthalate (PET)[61], several techniques have been developed, leading to remarkable improvements in photovoltaic performance. Studies on light trapping in

flexible organic devices have been shown in the literature[4,5]. Yu et al. have investigated the correlation between OPV performance and the period of patterned structures based on Yablonovitch limit[15-18]. However, a universal design rule for the height of the patterned structure is still missing.

In this chapter, we structure PET substrates with direct laser interference patterning (DLIP), which is a powerful and scalable one step technique for patterning micro-structures on polymer[81,82] and thin metal films[83] without any chemical treatment. Several conditions of periods and heights are examined to optimize and understand the light trapping properties of the patterned PET substrates. Novel approaches for structuring the surface of substrates are still difficult to apply to large areas uniformly. Moreover the application of light trapping substrates to large scale OPV module production requires a well-developed and low cost supply chain. In this respect, attractive substrates are the macro scale patterned display films used as back light scattering units in liquid crystal display (LCD)[11]. Such display films have the advantage of a proven, commercial upscaling. They can be easily produced in large formats of several meters width. We therefore also test, in addition to laser-structured PET substrates, these commercialized substrates. With the transition to flexible substrates, the production of light trapping structures on them poses a new challenge and new approaches are needed to improve their performance.

5.2 Patterned PET substrates by laser structuring

Micro-structured organic photovoltaic (OPV) devices on PET substrates are produced using DLIP. Below, we show that the performance of organic solar cells on these substrates is improved by a factor of 1.16 and a power conversion efficiency (PCE) of 7.7 % is achieved. We show that shorter spatial periods of the pattern allow for a stronger light trapping effect in solar cells, as they lead to longer light paths. Moreover, since the patterned structures are located on the outside of the fully encapsulated OPV devices, there are no problems with roughness-induced shunts.

5.2.1 Patterned PET films as substrates

PET substrates (Melinex ST504) from Dupont Tejin (125 μm thick) are cleaned with isopropanol and deionized water in an ultrasonic bath. A high-power pulsed Nd:YAG laser (Quanta Ray, Spectra Physics) emitting a linearly polarized beam is used for structuring these substrates. The

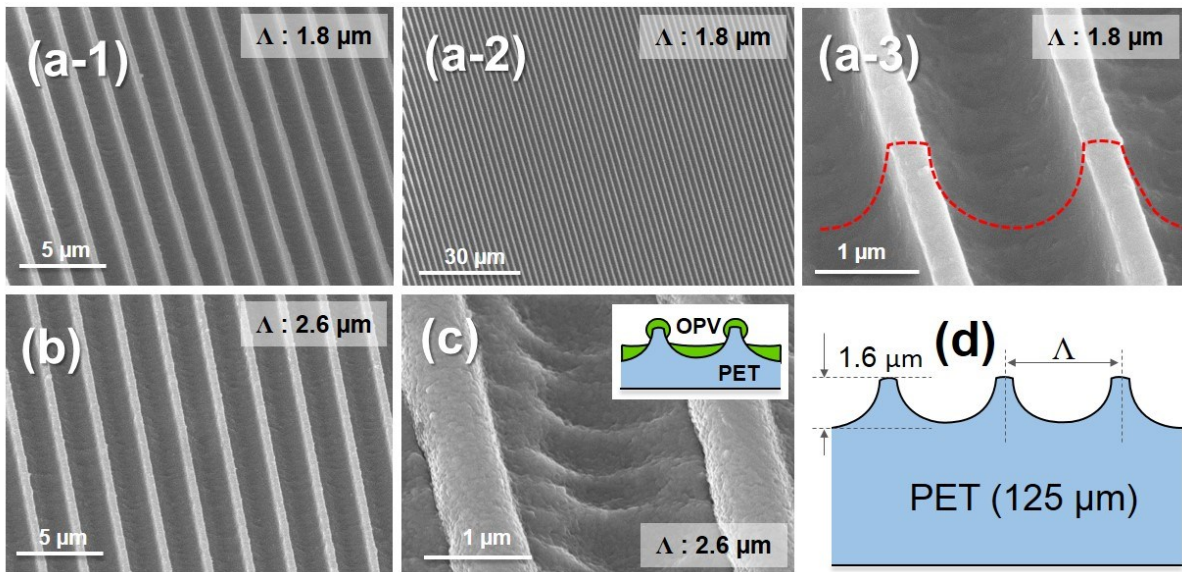


Figure 5-1 The micro-structure of patterned PET film with different periods. SEM images of line structure with $1.8 \mu\text{m}$ period (a), $2.6 \mu\text{m}$ period without organic layers (b), with organic layers on the patterned PET substrate including a schematic (c) and a schematic of the patterned film (d).

fundamental wavelength of the Nd:YAG laser is 1064 nm, from which shorter wavelengths (532, 355, and 266 nm) can be obtained by higher harmonic generation. The fourth harmonic wavelength of 266 nm is used to irradiate the samples with pulses lasting 10 ns at a repetition rate of 10 Hz. The scheme of the experimental setup for the laser interference patterning has been already introduced elsewhere[83–86].

5.2.2 Optical properties of the patterned PET substrates

Using DLIP, we fabricate two line structures (U-shaped) with a period of 1.8 μm and 2.6 μm on the PET substrates, as shown in the SEM images in Figure 5-1(a-c). Organic devices are fabricated on both sides of the PET substrates using solution processed PEDOT:PSS as the bottom anode. Due to a poor coverage of the organic layers on the sharp edge of the line structure (Figure 5-1(c)), devices on the patterned side have a low fill factor, low PCE and poor reproducibility. However, the devices built on the planar side of the patterned PET outperform the unstructured PET references. The line pattern leads to a diffraction of light into guided modes, which in turn increase the light path length in the absorber layer. The increase of the optical light path depends on the angle of diffraction, with a higher diffraction angle leading to a longer path. To estimate the path length increase, the diffraction angle (θ_m) is calculated by equation 3-7

$$m \lambda = \Lambda \sin\theta_m \quad (3 - 7)$$

where m is the integer representing the propagation-mode, λ is the wavelength of the incident light and Λ is the period of the patterned PET. Figure 5-2(a) shows the angular distribution of diffracted light for two different substrates with different periods, determined by using equation 3-7. In this plot, a large angle on the Y-axis also means a longer light path in the OPVs. The increased light path by diffraction can be calculated by a simple trigonometric function. For example, a diffraction angle of 30° allows for an increase of the light path by a factor of 1.15. A shorter period Λ (1000 nm) leads to higher angles (over 30°) for lower order (1st - 3rd) diffractions. We can thus expect a longer light path as compared to that of the OPV on a planar substrate. For longer Λ (2600 nm), diffraction curves are also visible at higher angles. However, the light intensities of higher order curves ($> 4^{\text{th}}$ order), shown on the Y-axis over 30° , are weak, as shown in Figure 5-

2(b-c). Most of the light diffracts in small angles, meaning that the light path enhancement is not as effective as for lower Λ . Table 5-1 shows the experimentally measured intensities of direct and diffracted light. A blue (405 nm) and a red (640 nm) laser are used for measuring the precise fraction of diffracted-to-incident light with a photodiode. Over 79% (blue) and 50% (red) of the light are detected at lower (1st - 3rd) order diffraction as shown in Figure 5-3. From the comparison between the calculated dispersion curves and the measured curves (Figure 5-2) combined with the measured intensity of the diffracted light (Figure 5-3), we conclude that most diffraction occurs at lower orders (1st - 3rd). A shorter Λ will thus provide a longer light path due to diffraction at higher angles. The DLIP technique, used for producing the periodic structure on PET substrates, can create patterns with Λ values as low as 550 nm. However, a feature depth of only 500 nm can be reached for the shortest period shown here ($\Lambda = 1000$ nm), which only diffracts less than 25 % of the red light (640 nm laser). This amount of diffraction is insufficient for providing an efficient light trapping effect as compared to 1.6 μm deep structures which diffract 50 % of the light. Using a fixed depth of 1.6 μm , we now compare structured PET substrates with periods (Λ) of 1.8 μm and 2.6 μm .

Table 5-1 Normalized intensities of direct and diffracted light by blue and red laser.

Ratio	Blue (405 nm)					Red (640 nm)				
	Zero order	Diffracted light				Zero order	Diffracted light			
		1 st	2 nd	3 rd	4 th		1 st	2 nd	3 rd	4 th
1.8 μm	0.21	0.79				0.47	0.53			
		0.39	0.23	0.12	0.05		0.31	0.13	0.09	-
2.6 μm	0.31	0.69				0.56	0.44			
		0.32	0.16	0.12	0.09		0.19	0.11	0.11	0.04

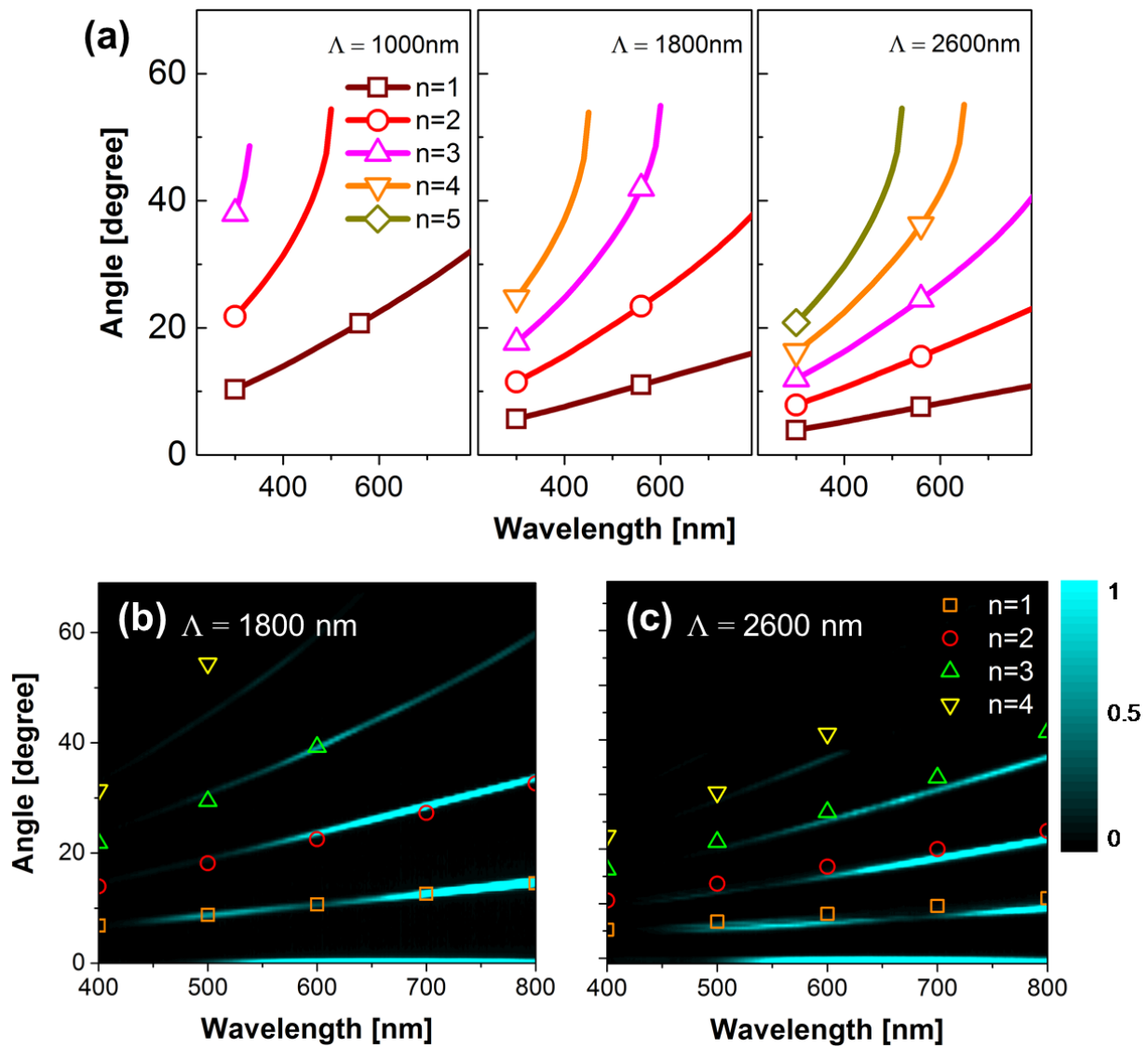


Figure 5-2 Calculated and measured light diffraction angles. Calculated angular distribution of diffracted light for the different periods of patterned PET of 1000 nm, 1800nm and 2600 nm (a) and measured angular distribution of diffracted light using goniometer set-up (samples and light source are fixed and only detector is moving) with $\Lambda = 2600$ nm (b) and $\Lambda = 1800$ nm (c).

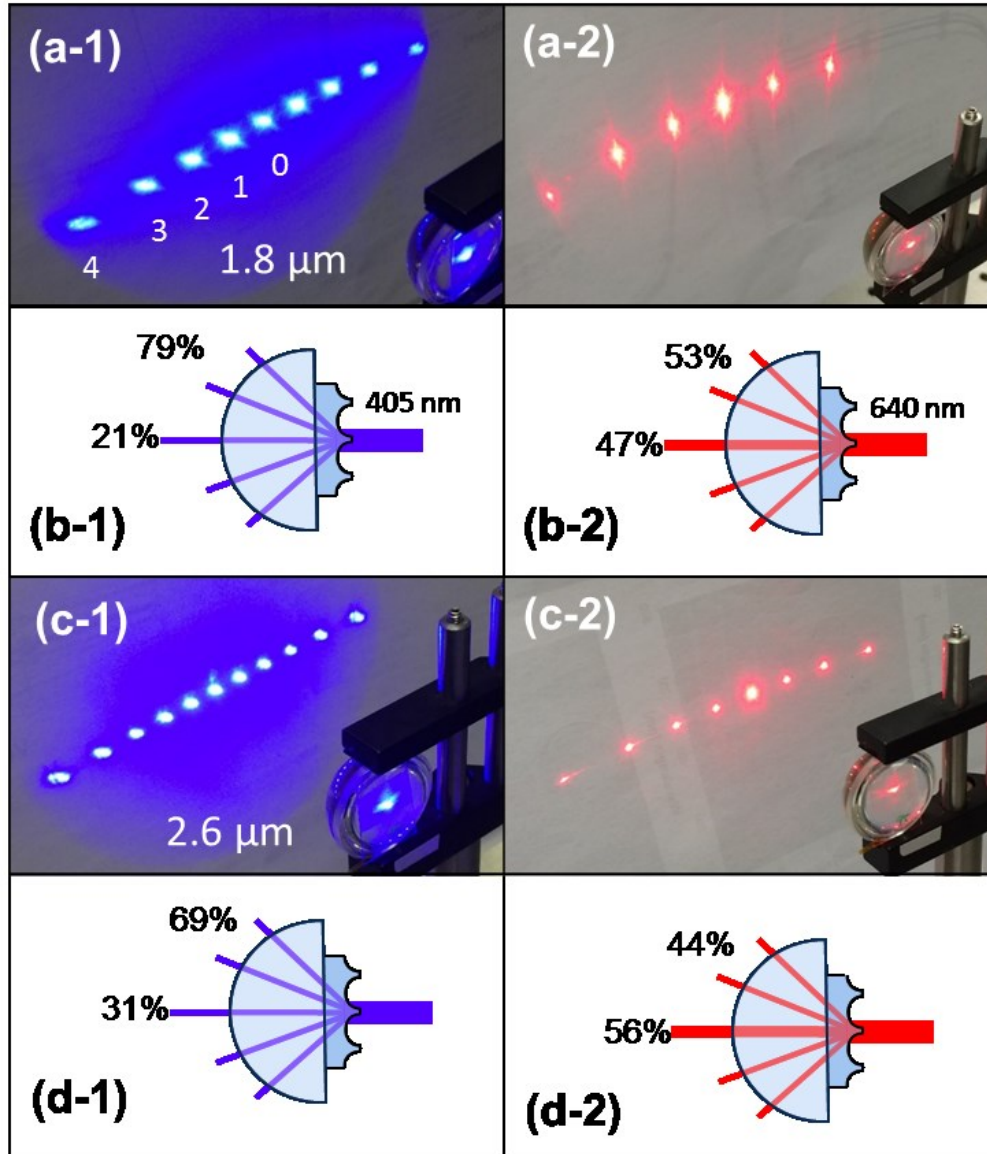


Figure 5-3 Diffraction patterns of $\lambda = 1800\text{nm}$ (a) and its ratios of direct transmitted and diffracted light (b) with blue and red light and those of $\lambda = 2600\text{nm}$ (c,d).

5.2.3 Photovoltaic characteristics of devices

We construct the solar cell on planar PET substrate as reference and obtain a J_{sc} of 11.29 mA/cm^2 , which suggests that the reference cell has an internal quantum efficiency as high as 91%. Figure 5-4(a) and Table 5-2 show current density-voltage (J-V) characteristics and key parameters of devices built on both planar and patterned substrates. The reference device shows a PCE of 6.62 %, while cells on the $1.8 \text{ }\mu\text{m}$ line patterned PET substrate yield 7.7%. The J_{sc} enhancement to 13.30 mA/cm^2 is the main reason for a PCE increase by a factor of 1.16. V_{oc} and FF are similar to the reference cell, which is expected, since the devices are built on the planar side of the patterned PET substrate. The PCE for the solar cell constructed on the substrate with $\Lambda = 2.6 \text{ }\mu\text{m}$ is 7.39 % (enhanced by a factor of 1.11). As assumed, we achieve a higher PCE enhancement by using the PET substrate with lower Λ . To elucidate the enhancement, the external quantum efficiency (EQE) spectrum and total reflection of the devices are measured and the results are shown in Figure 5-4(c, d). For both patterned devices, the EQE increases, especially in the longer wavelength range (from 650 nm to 750 nm), up to 25 %. When plotting the EQE ratio between the devices on the patterned and planar substrates, we find a similar shape (Figure 5-4(c-1)) as for the curve showing the reduction of reflection losses (Δ reflection spectra (Figure 5-4(d-1))). This indicates that the enhanced absorption is indeed due to a light path increase. Considering the electrode materials PEDOT:PSS and Al, parasitic losses are predicted to be rather high in the wavelength regime between 400 and 700 nm. We therefore expect a more pronounced enhancement using a more transparent front electrode, and a more reflective back electrode, such as Ag [87] which is

Table 5-2 Performance characteristics of OPV devices on display film and planar PET

Substrate	V_{oc} [V]	J_{sc} [mA/cm^2]	FF [%]	η [%]
Λ 1.8 μm line	0.94	13.30	61.37	7.70 ± 0.1
Λ 2.6 μm line	0.94	12.98	60.89	7.39 ± 0.0
Planar PET	0.94	11.29	61.69	6.62 ± 0.3

chemically not as stable as Al in the presented devices. To further demonstrate fully flexible OPVs including light trapping elements, devices are produced with 20 nm thick, flexible AlO_x moisture barrier layers for the bending tests in ambient air. The moisture barrier layers each exhibit a water vapor transmission rate (WVTR) of 2×10^{-5} g/m² day[72]. Degradation of OPVs with this encapsulation was previously investigated and the AlO_x layers still showed similar WVTR values without cracking after 300 bending cycles at a bending radius of 15 mm[88]. To check the stability of the solar cells on the PET substrates, a bending test is performed under ambient conditions. The devices remained working after bending with 10 mm radius without any degradation, similar to a previous study[54]. However, bending at a 5 mm radius (over 10 cycles) decreases the PCE by 20% as shown in Figure 5-4(b). This result proves a reasonably good bending stability of the solar cell constructed on the structured PET substrates. A 10 mm bending radius would be sufficient to use these substrates in a roll-to-roll process.

5.2.4 Summary

In summary, we have constructed OPV devices on patterned PET substrates and achieved a PCE of 7.7%. We have also shown that a shorter period of the pattern allows for a stronger light trapping effects in solar cells, as it leads to a longer light path. OPV devices can be easily built on the proposed light trapping substrates, without having to consider rough or a sharp surfaces, since the planar side of the PET substrates are used. This study shows that additional enhancement of solar cell performance can be achieved through the use of a simple laser patterning process.

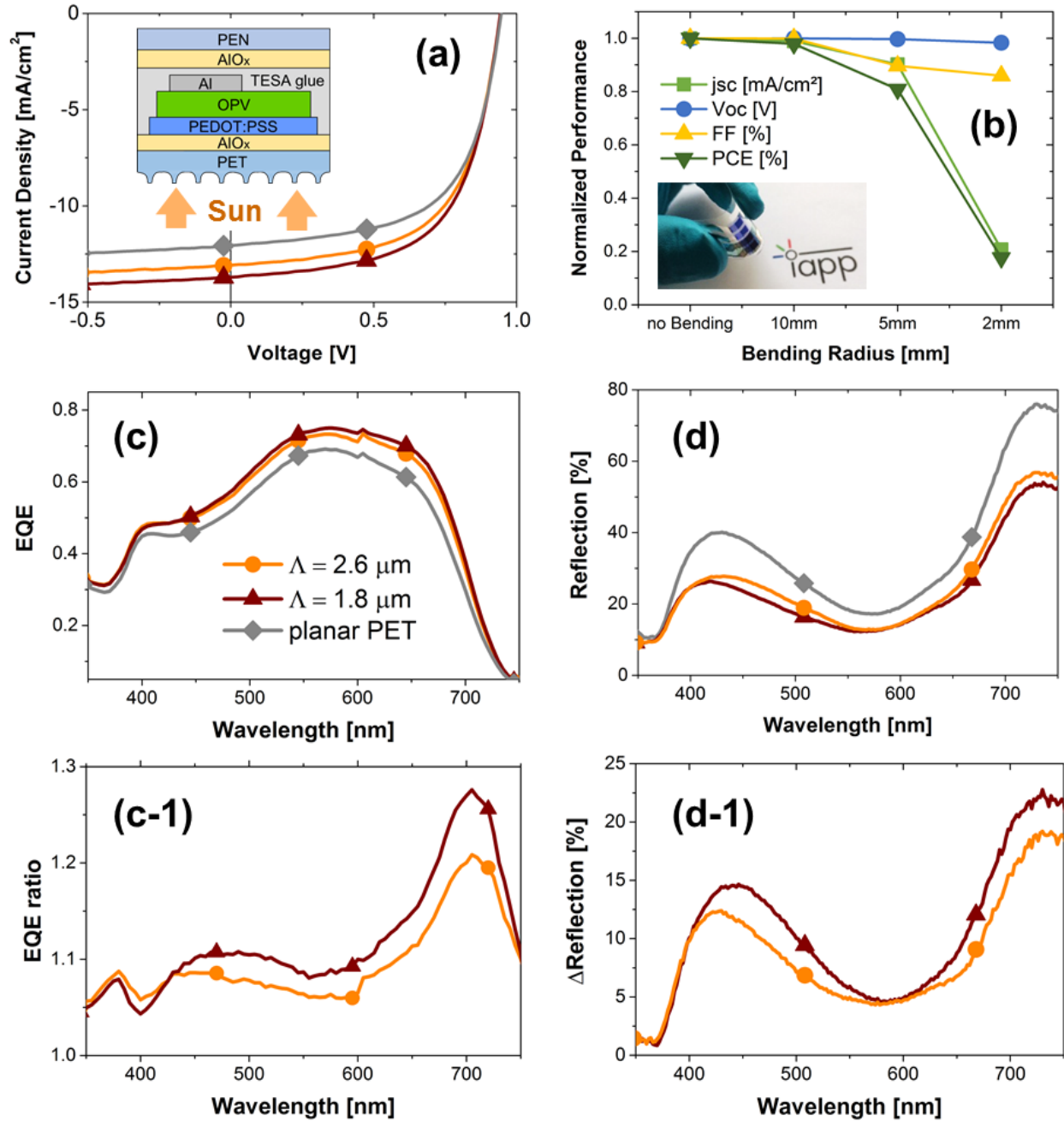


Figure 5-4 Properties of OPV devices on light trapping substrates. *J-V* curves with an inset of a device schematic (a), Normalized performance parameters after 10 cycles of bending with different radiuses (b), EQE (c) and ratio between EQE of devices on patterned PET substrates and unpatterned references (c-1), total reflection spectra (d) and Δ reflection spectra, a measure of decreased reflections in OPV devices with patterned PET substrates compared to the reference (d-1).

5.3 Display film for LCD as substrate

Several techniques for producing periodic structures on OPV substrates are still difficult to uniformly apply to large areas. The application of light trapping substrates in industrial production of large scale OPV modules requires a well-developed and low cost supply chain. In this respect, an attractive substrate is micro scale patterned display film, originally developed for liquid crystal displays (LCD). This film has been used as back light scattering unit in LCD[89] and can be easily produced in large formats of several meters width. These kinds of cheap, textured plastic substrates have previously been investigated as back reflector for thin film silicon solar cells[90,91]. For polymer solar cells, substrates incorporating micro-prism arrays enabled a light absorption enhancement by 44%[92]. However in these previous two studies, devices are built on the grating side and any beneficial optical effects could be counter-balanced by deteriorated electrical properties due to that the devices are built onto a rough surface. Therefore, in the study presented here, we also fabricate devices on the more planar side of the substrate.

5.3.1 Display films as substrates

Figure 5-5 shows SEM images of the micro-structure of both sides of the display film and the OPV layers. The prisms on one side of the substrates have a height of 24 μm and a width of 48 μm . On the other side of the substrate, there is a light scattering layer containing acryl based particles with diameters from 1 μm to 3 μm . Due to the relatively large prism structures, spin-coated PEDOT:PSS does not cover the top of the prisms, resulting in short-circuiting of the photovoltaic devices. However, on top of the scattering layer on the other side it is possible to obtain working devices, when covering the substrate with a smoothening polymer electrode. Before and after deposition of the organic layers, the surface topology of the scattering layer looks similar as shown in Figures 5-5(b,c). Scattering particles with different sizes are randomly distributed as shown in Figure 5-5(b). The surface has an RMS value of 253 nm before deposition of the organic layers and 239 nm after deposition (Table 5-3). Although the roughness is significant, particles are now smoothly covered by 120 nm of polymer electrode and there are no sharp edges as shown in Figures 5-5(d).

Table 5-3 The roughness of each surface measured by atomic force microscopy.

Substrate	Ra [μm]	RMS [μm]	Note
Bare display film	0.169	0.253	All area in Fig. 2(b) including particles
OPV on display film	0.149	0.239	All area in Fig. 2(c) including particles
Planar PET	0.003	0.002	

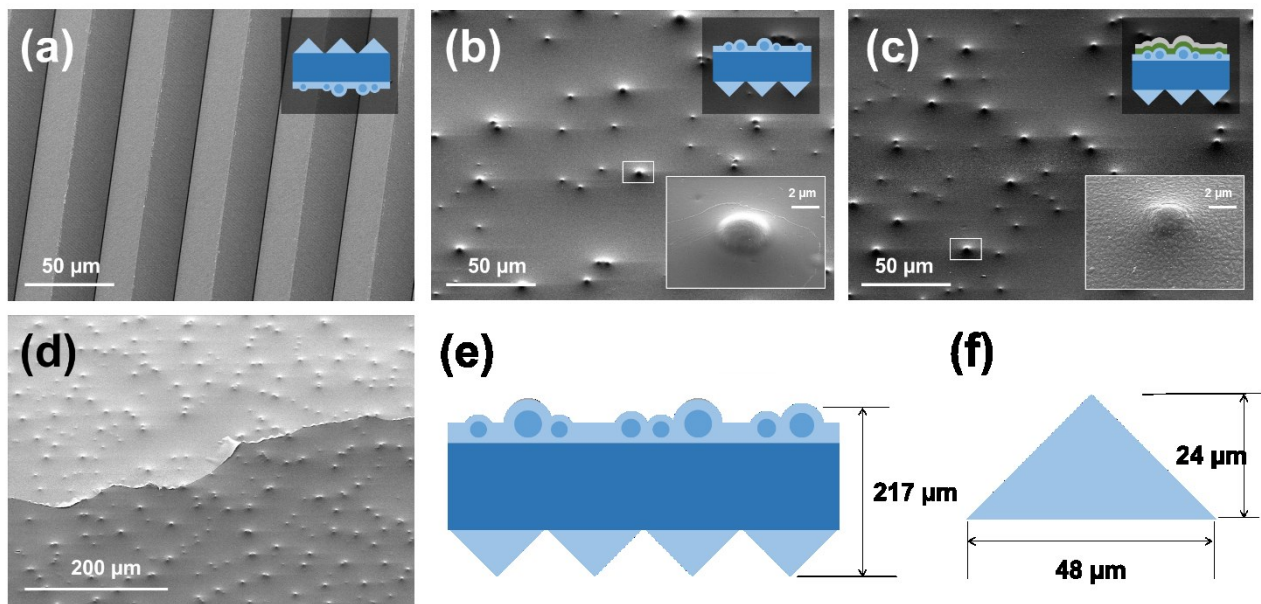


Figure 5-5 SEM images of prism structure (a), scattering particle on display film (b), organic layers on scattering side (c), half-peeled organic layers on scattering side (d). Schematics of display film (e) and prism structure (f)

5.3.2 Optical properties of the display films

The transmission spectrum of the display film depends on the illumination side, as shown in Figure 5-6. When measured with the incident light beam on the prism side (a-direction in Figure 5-6(a)) almost 80% of the light in the visible region is transmitted. However, when illuminated from the other side, only 5% is transmitted (b-direction in Figure 5-6(a)) and more than 65% is reflected. Since PET is not significantly absorbing in this regime, the sum of total transmittance and total reflectance should be approximately 100%. However, in this case 15% of the light is not detected by the UV-vis spectrometer, because this fraction is trapped in the display film. Moreover, the light direction changes. Figure 5-6(b) shows the angular distribution of light measured by a goniometer. Light is scattered at an angle between 30° and 35°. This is a consequence of the 45° prism angle. This provides an increased light path in the absorber layers of the OPV device. The scattering at a certain angle is visualized in Figures 5-6(c-d) using a white light source and normal desk lamp. This is characteristic of LCD backlight films, designed to enable large area uniform light sources.

5.3.3 Photovoltaic characteristics of devices

OPV devices are built on the scattering side of the display film. A reference device is fabricated on a planar PET substrate. Figure 5-7 and Table 5-4 show current density-voltage (J-V) characteristics of the devices. The reference device shows a power conversion efficiency (PCE) of 6.6 % with a short-circuit current density (J_{sc}) of 11.3 mA/cm² and a fill factor (FF) of 61.7 %. 7.5 % of PCE is achieved by the device on the scattering side of display film with an enhanced J_{sc} of 13.0 mA/cm² and FF of 60.1 %. The PCE is enhanced by a factor of 1.13 using the display film. The increase in photocurrent stems from the dispersion of the light at an angle of around 32 degrees, increasing the path length of the light in the device. To elucidate on the J_{sc} enhancement, the EQE spectrum is measured, which exhibits increases up to 20% from 400 nm to 750 nm wavelength, but for shorter values (from 300 to 400 nm) it decreases as the reflectance of display film drops around 400 nm. As a result, OPVs on display film show higher performance than OPVs on glass substrates using a PEDOT:PSS electrode (7.1 %). However, due to rough surface, the V_{oc} decreases slightly and the larger effective surface increases the fill factor, as previously observed by Müller-Meskamp et al. [61].

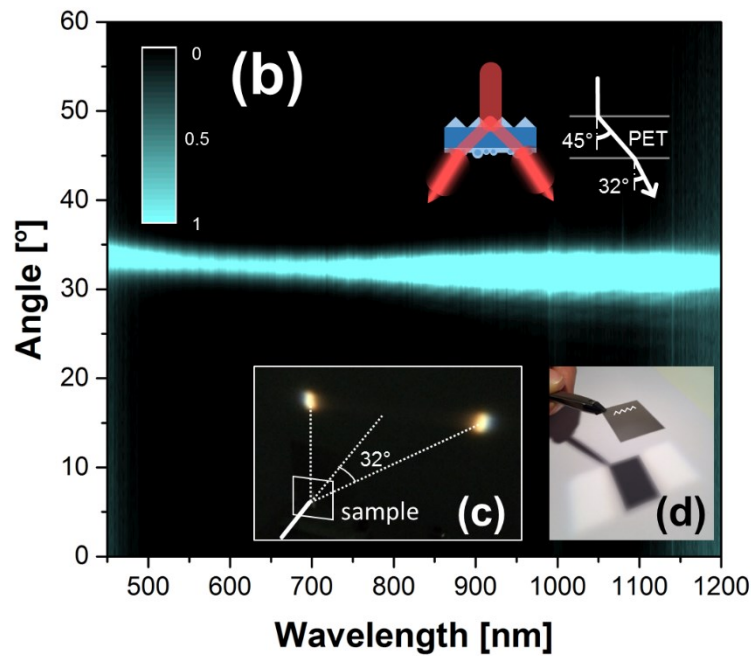
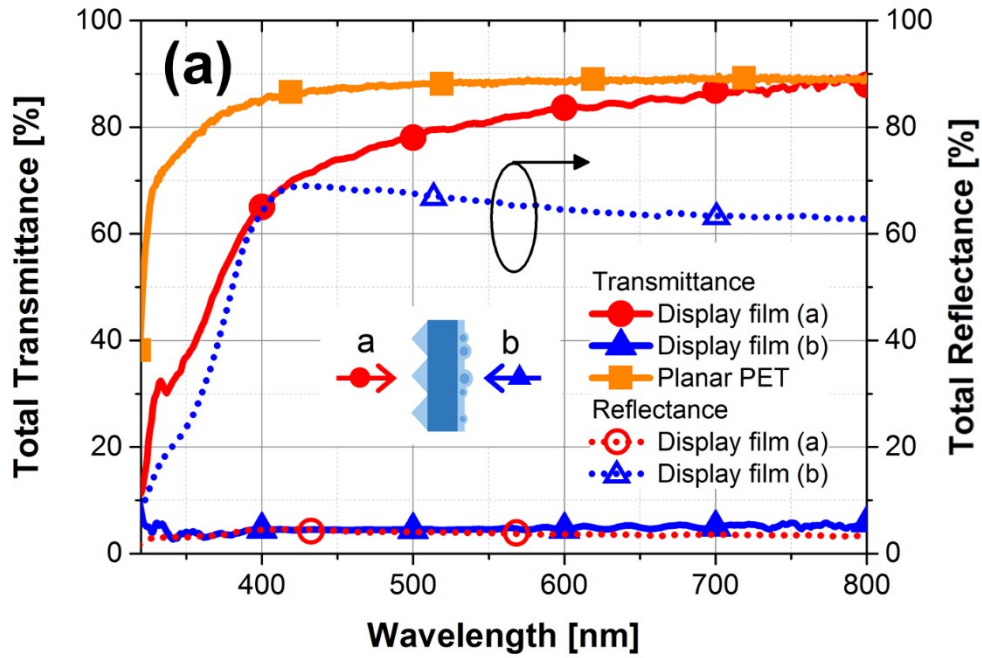


Figure 5-6 Optical properties of the display film. (a) Total transmittance and reflection spectra, (b) Angular distribution of transmitted white light and (c) photographs of dispersed light from directed white light and (d) normal stand light.

Table 5-4 Photovoltaic performance parameters of OPV devices on display film and planar PET (more than 4 samples are measured for each conditions).

Substrate	Open circuit voltage V_{oc} [V]	Short circuit current density J_{sc} [mA/cm ²]	Fill factor [%]	Power conversion efficiency η [%]
Display film	0.94	13.1	60.1	7.5 ±0.1
Planar PET	0.94	11.3	61.7	6.6 ±0.3
Glass	0.96	12.9	57.8	7.1 ±0.1

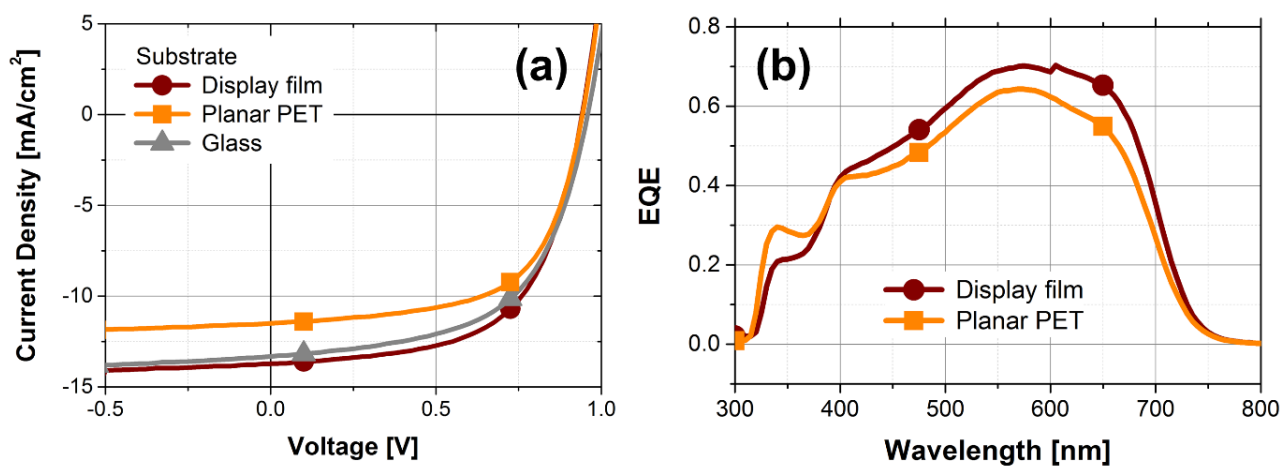


Figure 5-7 Performance characteristics of OPV devices on display film and planar PET. (a) J-V curves with schematic of OPV device and (b) EQE spectra.

5.3.4 Summary

In summary, we demonstrate fully flexible encapsulated OPV using a commercial display film with excellent industrial scalability as substrate. The OPV device on display film shows 7.48 % of PCE, which is enhanced by a factor of 1.13 as compared to a reference device fabricated on planar PET. These results indicate that the use of standard optical display films is a cheap, simple and efficient way to increase the photocurrent and overall efficiency of organic photovoltaic devices.

6. Light trapping electrodes

Next to suitable substrates, flexible electrodes are key for realizing flexible organic electronic devices. Conventional ITO electrodes are brittle making and therefore not suitable. To overcome this, polymer electrodes, especially PEDOT:PSS, have been investigated for over 4 decades, since the discovery of Shirakawa et al. that polyacetylene can reach high electrical conductivity. Polymer electrodes can be easily handled and manipulated due to their soft nature and solution based preparation process. In this chapter, two new electrode architectures to enhance light trapping in flexible devices are investigated: a scattering electrode obtained by mixing polymer with nano-particles and a nano-patterned PEDOT:PSS electrode imprinted by PDMS a mold.

6.1 Motivation

In order to overcome insufficient incoupling or extraction of light in optoelectronic devices, two strategies are often utilized: integration of periodically textured structures[53,54,61,74] or randomly distributed textures[93–95]. Even though theory predicts that light harvesting by periodic structures can be better than that of random structures[96,97], devices with random structure still show enhanced performance, and are less wavelength sensitive. Scattering layers constituting randomly distributed NPs have been implemented into OLEDs and OPVs[56,98,99] because of their superior merits in terms of cost and easy processing. In previous studies, the

scattering layers were often made by mixing NPs, with a high refractive index, into a transparent polymer matrix such as propylene glycol-monomethyl-ether acetate (PGMEA)[55] or polystyrene (PS)[100]. For flexible organic opto-electronic devices, the ITO electrode needs to be replaced with a flexible, highly conductive, and transparent conductive film.[101,102]. In this respect, electrodes based on poly(3,4-ethylenedioxythiophene) polystyrene sulfonate (PEDOT:PSS) solutions are very interesting, since they can be mixed with TiO₂ NPs, resulting in a thin film which functions both as electrode and scattering layer. Moreover, PEDOT:PSS can be imprinted and structured as patterned PET substrates. Previous work has reported on imprinted PEDOT:PSS as HTL[103], with the scale of the structures in the 60 nm height and 70nm width range. However, in this chapter we investigate and discuss nano-imprinted PEDOT:PSS, structured at the scale of a smaller 40 nm height and wider 750nm width as transparent electrodes.

6.2 TiO₂ nano-particles embedded in PEDOT:PSS

The performance of organic optoelectronic devices can be improved by employing a suitable optical cavity design beyond the standard plane layer approach, e.g. by the inclusion of periodically or randomly textured structures which increase light incoupling or extraction. One of the simplest approaches is to add an additional layer containing light scattering particles into the device stack. Solution processed poly(3,4-ethylenedioxythiophene):poly(styrenesulfonate) (PEDOT:PSS) thin

Table 6-1 Weight and volume ratio of NPs in PEDOT:PSS obtained by measurement and simulation.

Weight ratio in solution (experimental)	-	0.5 wt%	1.5 wt%	3.0 wt%
	normalized	1	3	6
Volume ratio in thin film (by Mie theory simulation)	-	4.4%	13.6%	18.3%
	normalized	1	3.25	4.5

films are promising for replacing the brittle and expensive indium tin oxide (ITO) transparent

electrode. We use a blend of 100 nm TiO₂ scattering particles in PEDOT:PSS solution to fabricate transparent electrode films which also function as a scattering layer. When utilized in an organic photovoltaic (OPV) device, a power conversion efficiency of 7.92% is achieved, which is an 8.6% relative improvement compared to a device with a neat PEDOT:PSS electrode without the nanoparticles (NPs). This improvement is caused by an increase in short-circuit current due to an improved photon harvesting in the 320 nm – 700 nm spectral wavelength range.

6.2.1 Preparation of light scattering electrodes

To fabricate TiO₂ embedded PEDOT:PSS electrodes, three different amounts (0.5 wt %, 1.5 wt %, 3.0 wt %) of TiO₂ NPs (Anatase, mean diameter 100nm, M K Impex Corp., Canada) were dispersed in 10 ml each of highly conductive PEDOT:PSS which has 1.1 wt % of solid content in water[104] (Clevios PH1000, Heraeus, Germany) solutions mixed with 6 vol % ethylene glycol.. In order to prepare well dispersed NPs in PEDOT:PSS solution, 100 mg of ZrO₂ milling particles (mean diameter 100 μm, ZetaBeads® plus 0.1, NETZSCH-Feinmahltechnik GmbH, Germany) were added to the mixture. Physical vibration, stirring, and milling by a planetary rotary mixer for more than 3 hours resulted in a homogenous dispersion of NPs in the PEDOT:PSS solution. Subsequently, the solution was filtered (pore size 0.45 μm) to remove the ZrO₂ milling particles and agglomerated TiO₂ NPs. It turned out to be difficult to prepare films homogeneous films on glass without the use of milling particles. Moreover, the solution could not be filtered well due to agglomerated TiO₂ particles. TiO₂ nano-particles embedded PEDOT:PSS (NP:P) solutions were spun on glass substrates at 2500 rpm for 30 seconds and cured on a hotplate at 120 °C for 15 minutes. Subsequently, an additional neat PEDOT:PSS layer was spun on top of the scattering layer at 1000 rpm for 30 seconds followed by a curing step to remove residual water in the layers. NP:P electrodes were optically characterized using a Shimadzu MPC3100 Spectrophotometer. A Nikon Microscope was used to check homogeneous dispersion of NPs on the substrate and an AFM (AIST-NT Combiscope, USA) was used to characterize the surface morphology. The layer thickness was measured by a Dektak stylus profilometer. The scattering coefficients for each NP:P concentration are simulated by open source software (<http://omlc.ogi.edu/software/mie/>) using a refractive index of 2.87 ($\lambda=430$ nm) for TiO₂ NPs and 1.50 ($\lambda=430$ nm) for PEDOT:PSS.

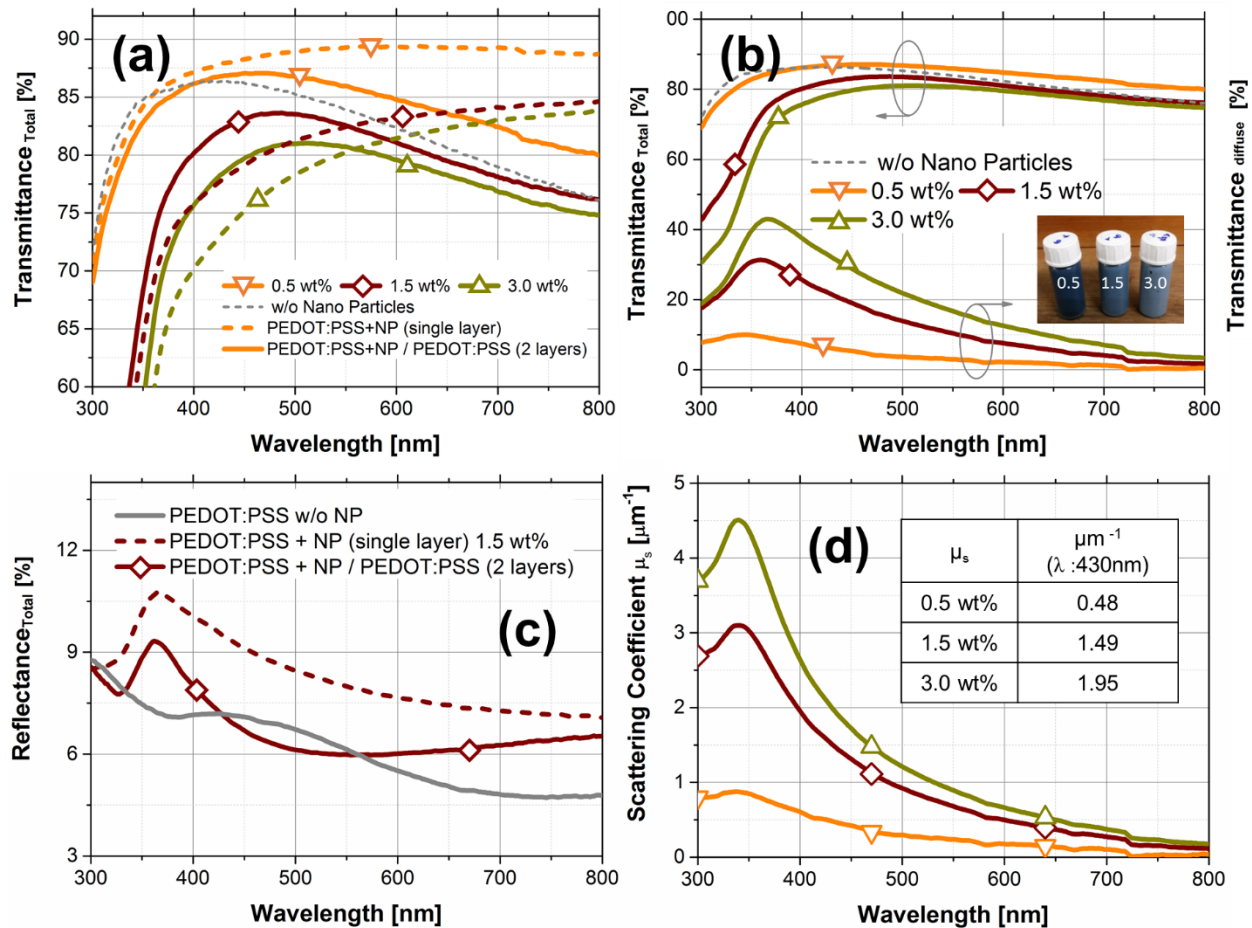


Figure 6-1 Optical properties of PEDOT:PSS layer embedded with NPs with and without a 2nd PEDOT:PSS layer. (a) Total transmittance of layers with different TiO_2 concentrations, (b) total and diffuse (total - direct) transmittance of NP:P with three different TiO_2 concentrations, (c) total reflectance of neat PEDOT:PSS and NP:P with and without second PEDOT:PSS layer and (d) scattering coefficients of three different TiO_2 concentrations.

6.2.2 Characterization of scattering effect in devices

A single layer of PEDOT:PSS with embedded TiO₂ NPs has higher transmittance between 500 and 800 nm than a neat PEDOT:PSS layer (figure 6-1(a)). This indicates the presence of only a small amount of PEDOT:PSS within the film. This causes the sheet resistance of this layer to be too high for it to function as an electrode in OPV devices. By adding a second PEDOT:PSS layer, as shown schematically in figure 6-2, the sheet resistance drops from 285.3 Ω/□ to 121.6 Ω/□, close to the value of neat PEDOT:PSS (101.0 Ω/□). However, the overall transmittance decreases. To better understand the correlation between the scattering effect and NP concentration, the scattering coefficient (μ_s) is estimated from

$$\frac{T_{direct}}{T_{total}} = e^{-\mu_s d} \quad (6 - 1)$$

where d is the thickness of NP:P layer. By carrying out simulation and experiment, volume ratios between TiO₂ NPs and PEDOT:PSS are estimated and shown in Table 6-1. The estimated volume ratios of NP in PEDOT:PSS correlate with the initial content of NP in the PEDOT:PSS solution. However, at the NP concentration of 3 wt%, there is a deviation, most likely due to a decreased

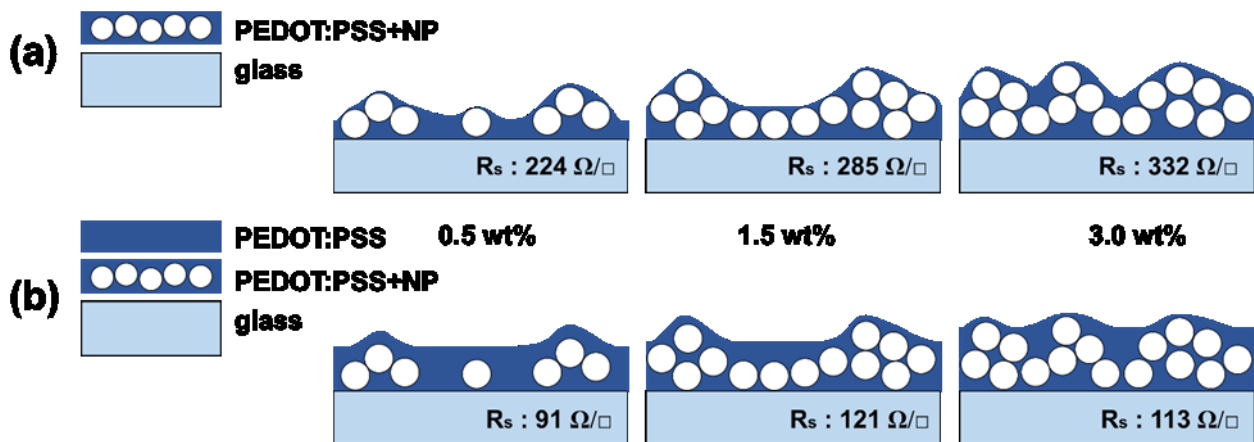


Figure 6-2 Schematics of layers on glass and sheet resistance of each sample: without (a) and with (b) second PEDOT:PSS layer.

active scattering volume. The simulation also indicates that almost all NPs at the concentration of 1.5 wt % are working as scattering volume, while at 3 wt% a small fraction of the NPs does not contribute to light scattering. Microscope pictures (Figure 6-3, 6-4) show that TiO₂ NPs are uniformly dispersed within the PEDOT:PSS. The thickness and roughness of the NP:P films increases with an increasing concentration of TiO₂, as shown in Figure 6-4. The large difference in the refractive indexes of TiO₂ (2.72, λ : 500nm) and PEDOT:PSS (1.47, λ : 500nm) results in strong scattering. Figure 6-1(b) shows total and diffuse ($T_{\text{total}} - T_{\text{direct}}$) transmittance of each of the NP:P thin films.

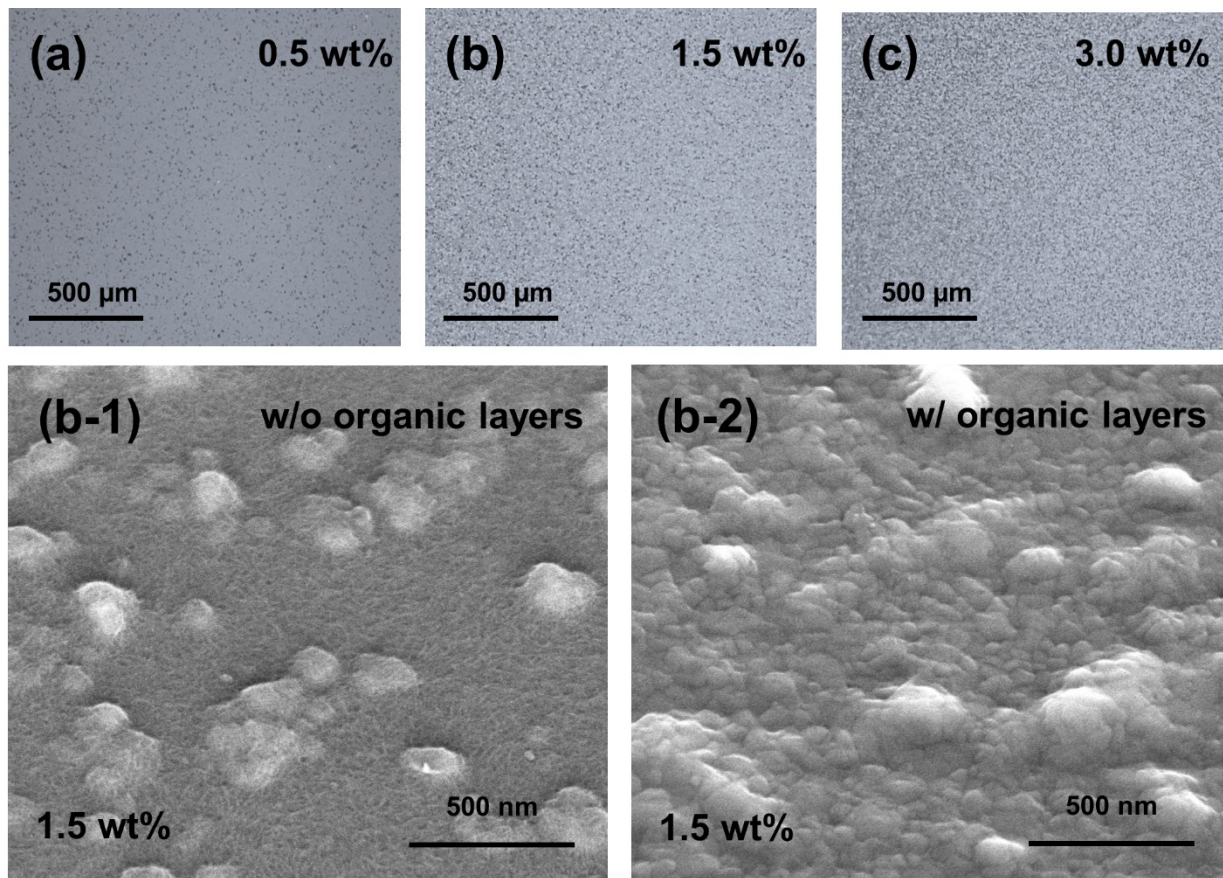


Figure 6-3 Optical microscopy and AFM images of (a) 0.5 wt %, (b) 1.5 wt % and (c) 3.0 wt % TiO₂ NPs embedded PEDOT:PSS layer which were spun on glass substrates at 2500 rpm for 30 seconds and SEM images of 1.5 wt % NP:P (b-1) without and (b-2) with organic layers.

An increased amount of embedded NPs results in an increased diffuse transmittance due to omnidirectional scattering. Surprisingly, the 0.5 wt % NP:P shows a higher transmittance than the neat PEDOT:PSS. This effect was not investigated further and is probably caused by a beneficial arrangement of the transparent, high refractive index particles within the PEDOT:PSS microstructure, which consists of PEDOT:PSS gel-like micro-particles or lamella in a PSS matrix[105,106]. In addition to the increased path-length of light in the forward direction, the embedded NPs can also contribute to an increase in reflection which in turn reduces the amount of light reaching the active region of the OPV. To investigate this effect, reflection measurements of neat PEDOT:PSS layer, and NP:P with and without the second PEDOTT:PSS layer were carried out. The NP:P without second PEDOT:PSS layer has higher reflectance than the neat PEDOT:PSS film. However, NP:P with a second PEDOT:PSS layer has similar values of reflectance than the neat PEDOT:PSS layer, except at wavelengths around 350nm, as shown in figure 6-1(c).

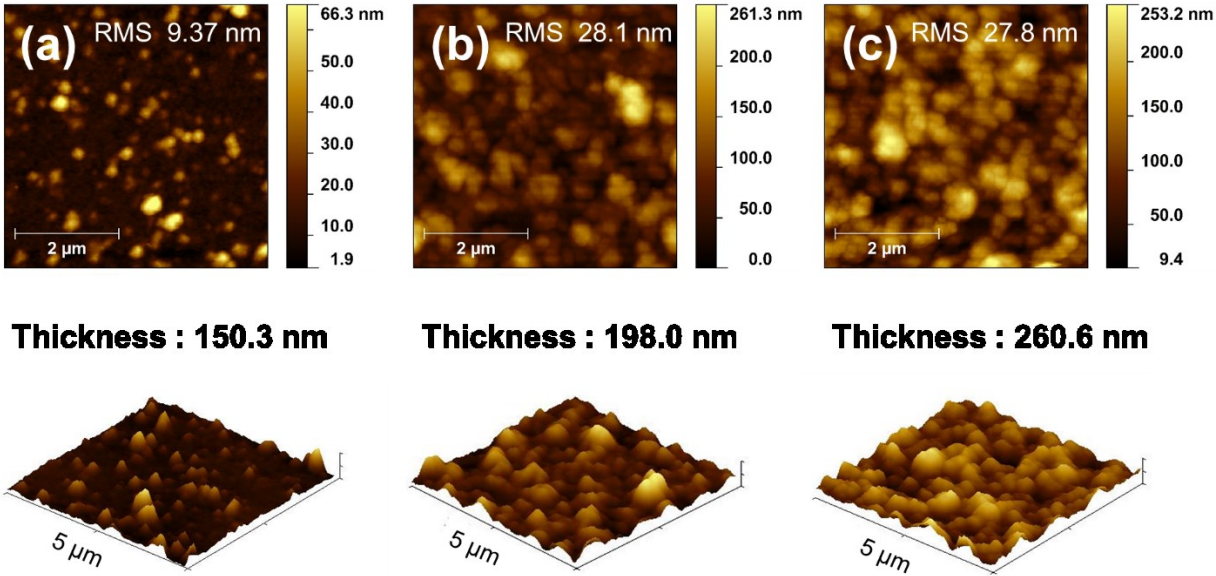


Figure 6-4 AFM images of (a) 0.5 wt %, (b) 1.5 wt % and (c) 3.0 wt % TiO₂ NPs embedded PEDOT:PSS layer with the values of RMS and thickness.

To investigate the performance of the developed electrodes in solar cells, OPV devices are built on the 1.5 wt % TiO₂ NPs embedded PEDOT:PSS and on neat PEDOT:PSS electrodes as reference. OPVs with 1.5 wt % NP:P electrode are found to be optimal, with the subsequently deposited photovoltaic absorber layers (~100nm) covering the rough electrode surfaces well, as shown in figure 6-3(b-1, b-2). The 3.0 wt % of TiO₂ based electrode resulted in short-circuited devices. Figure 6-5 and Table 6-2 show current density-voltage (J-V) characteristics of the devices. The reference device shows a power conversion efficiency (PCE) of 7.29 % with a short-circuit current density (J_{sc}) of 12.38 mA/cm² and a fill factor (FF) of 61.5 %. An efficiency of 7.92 % is achieved by the device on the 1.5 wt % NP:P electrode with an enhanced J_{sc} of 13.78 mA/cm² and FF of 60.0 %. The PCE is enhanced by a factor of 1.08 simply by using NPs embedded into the PEDOT:PSS electrode, mainly due to a J_{sc} increase. A slight decrease in FF is also observed probably caused by the increased electrode roughness, and slightly higher sheet resistance value. The standard deviation of PCE for devices on NP:P is 0.2 %, which is bigger than that of normal devices (0.0 %) due to randomly distributed NPs. Figure 6-5(b) shows the increase of the EQE by the scattering effect in the wavelength regime from 360nm to 660nm. This increase in EQE correlates well with the increase in the diffuse transmittance spectrum. The ratio of the EQEs of the NP:P and reference device is compared to the diffuse transmittance spectrum

Substrate	V _{oc} [V]	J _{sc} [mA/cm ²]	FF [%]	η [%]
PEDOT:PSS with TiO₂	0.96 ± 0.0	13.78 ± 0.3	60.0 ± 1.1	7.92 ± 0.2
PEDOT:PSS	0.96 ± 0.0	12.38 ± 0.2	61.5 ± 1.1	7.29 ± 0.0

Table 6-2 OPV device performance parameters for NP:P and PEDOT:PSS electrode. (8 devices are measured for each condition)

in Figure 6-5(c-d). Both curves have a similar shape for wavelengths down to 380 nm. However, the EQE ratio drops in the wavelength range from 300nm to 380nm, which is the peak of the diffuse transmittance. The total transmittance also decreases in the same range, i.e. this drop of the EQE enhancement ratio is influenced by the total transmittance. We thus conclude from these EQE and optical measurements that the enhanced performance of the OPV devices is mainly due to the scattering effect caused by the NP:P electrode.

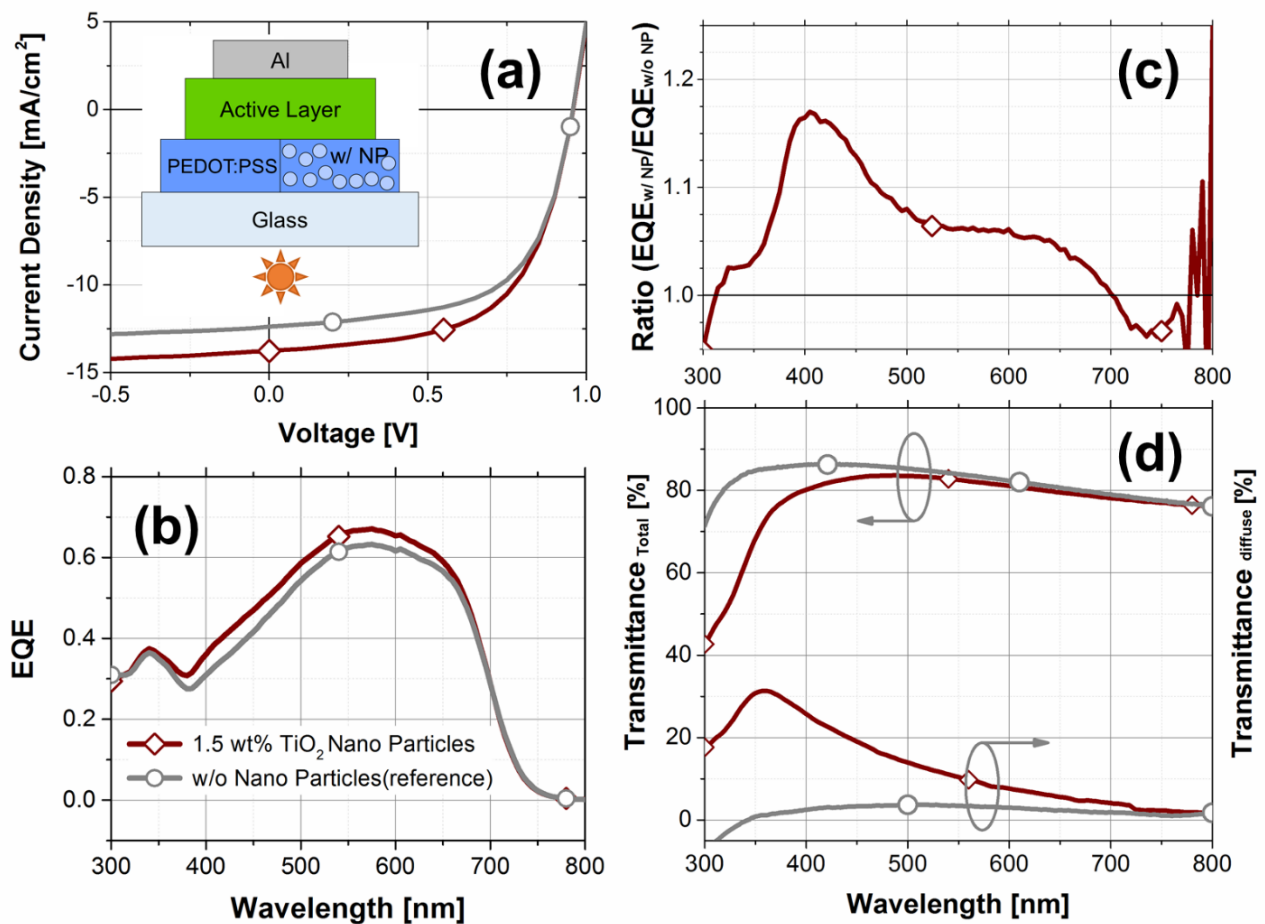


Figure 6-5 Photovoltaic performance of OPV devices on NP:P and PEDOT:PSS electrode (a) *J-V* curves with a scheme of the OPV device architecture and (b) EQE spectra. (c) Ratio between EQE of NP:P device and that of reference device, (d) Total and diffuse transmittance of 1.5 wt% NP:P.

6.2.3 Summary

OPV devices using PEDOT:PSS electrodes with embedded NPs show a PCE of 7.92 %, which is enhanced by a factor of 1.08 as compared to normal, neat PEDOT:PSS devices. In this work, we thus introduce an easily processable and low cost ITO-free transparent electrode which also acts as a scattering volume for increased incoupling of light for OPV devices. With the added advantage of mechanical flexibility and low material cost of PEDOT:PSS and TiO₂ NPs, such electrodes can be easily incorporated into flexible devices with improved performances.

6.3 Nano imprinted PEDOT:PSS

As discussed in chapter 5, periodically patterned structures can provide light trapping enhancements in photovoltaics. Here, we demonstrate nano-scale structured PEDOT:PSS electrodes obtained by a nano-imprinting system. Since the deposition of PEDOT:PSS is solution based forming a film of soft material, it can be structured during a subsequent annealing process. Polydimethylsiloxane (PDMS) stamps with controlled wrinkles at a scale of 120 nm are prepared by an air plasma technique[107–109] and used as mold for imprinting. The effect of nano-imprinted PEDOT:PSS layers has been investigated previously for polymer solar cells where an increase in photocurrent was observed due to a decrease in hole drift length[103]. In our case, PEDOT:PSS is used as transparent electrodes and light trapping effects are expected.

6.3.1 Preparations for nano-imprinted PEDOT:PSS

PDMS molds are prepared by Leibniz-institut für polymerforschung Dresden(IPF)[107]. PDMS elastomer samples are stretched by a uniaxial strain stage after fixing by two clamps. Plasma oxidation is applied on the strained films, resulting in a line patterned structure on the PMDS samples, after the release of the strain, as shown in Figure 6-6.

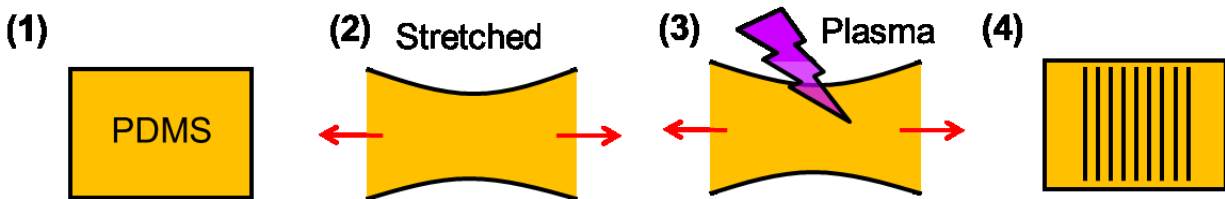


Figure 6-6 Formation of wrinkles on PDMS elastomer.

In order to imprint nano-structures from PDMS molds to the PEDOT:PSS electrodes, a self-made nano-imprinting system made by P.-A. Will[110] has been used. It provides a uniform pressure of 1 bar on the samples. The most important parameter for making structures is to find a proper resting

time, attaching and pressing the PDMS masks on PEDOT:PSS layer. We found that, for a normal PEDOT:PSS layer, after 15 mins annealing, it is impossible to transfer structures from a stamp to PEDOT:PSS without applying additional heat and pressure. In a previous study, imprinting is done by applying 2 bar of pressure in elevated temperature of 100 °C[103]. For that case, rigid Si molds were used; however, in our experiment soft PDMS molds are used and high pressure is not possible. To achieve a nano-imprinted structure on PEDOT:PSS, different annealing times are tested and a comparatively low temperature of 40 °C for 5 minutes in air has been chosen. As-spun PEDOT:PSS on glasses are placed in the imprinting system with the PDMS stamp and subsequently, samples are placed in the oven at the temperature of 100°C for 30 minutes as described in Figure 6-7.

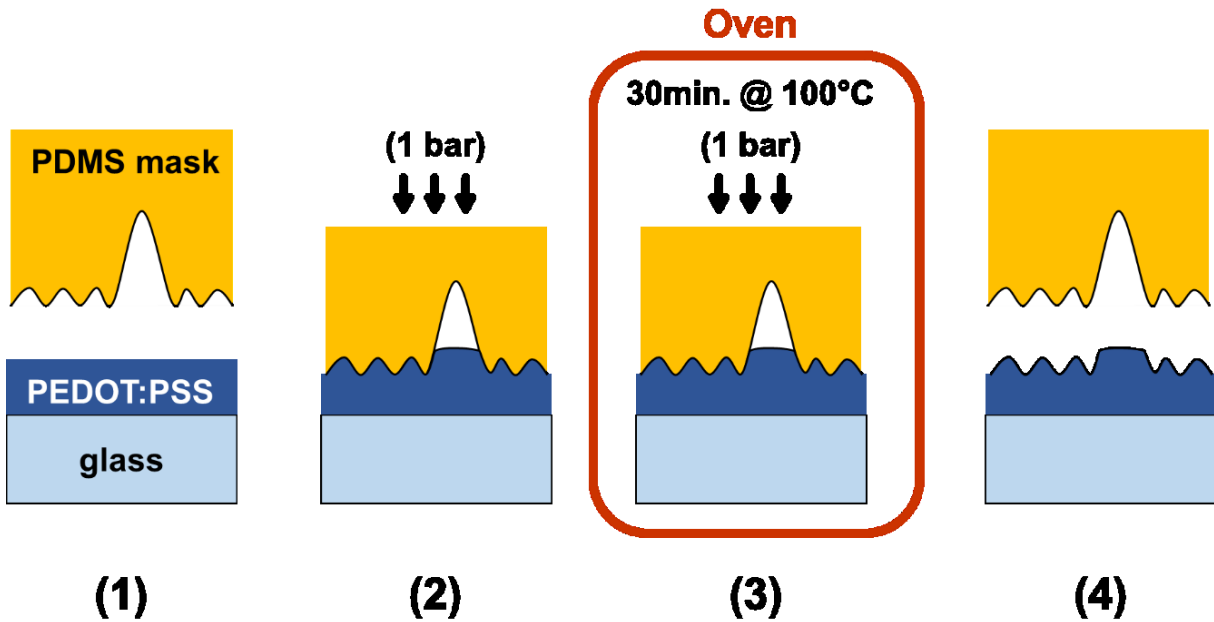


Figure 6-7 Schematics of the nano-imprinting on PEDOT:PSS. (1) As-spun PEDOT:PSS on glass, (2) imprinting PDMS mask on PEDOT:PSS, (3) keeping a sample in the oven (4) and completed patterned PEDOT:PSS.

6.3.2 Characterization of a nano-imprinted PEDOT:PSS

The morphologies of the PDMS mask and imprinted PEDOT:PSS are shown in Figure 6-8 and the height of structure imprinted by the nano-imprinting machine is around 40 nm. The period of the structures is 750 nm. The conductivity of the nano-imprinted electrode is as same as that of a planar PEDOT:PSS electrode. The two large horizontal lines, perpendicular to line structures in Figure 6-8(b) are the result of unavoidable cracks in the PDMS stamp (Figure 6-8(a)) used for imprinting. The size of the line resulting from the crack is relatively large as compared to the desired line structures. These cracks can be critical when used as substrates due to their large size.

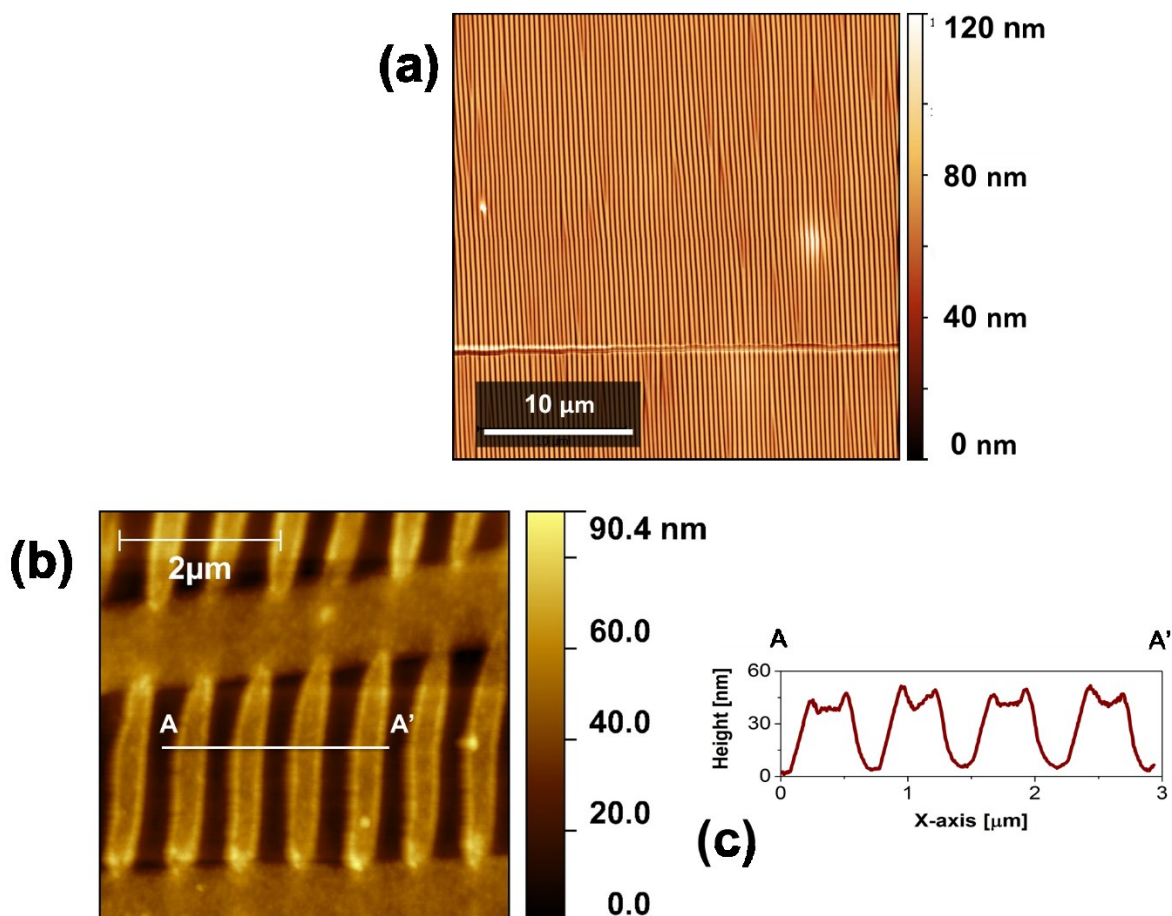


Figure 6-8 AFM images of PDMS stamp (a), imprinted PEDOT:PSS (b) and its profile (c).

However, when imprinted to PEDOT:PSS, the size of structures transferred from the cracks is not as big as the original one (described in Figure 6-8). Therefore, PDMS stamps with large cracks do not hinder their use for imprinting PEDOT:PSS film. Total and diffuse transmittance spectra are measured by a UV-vis spectrometer and are shown in Figure 6-9(a). We found that, unfortunately,

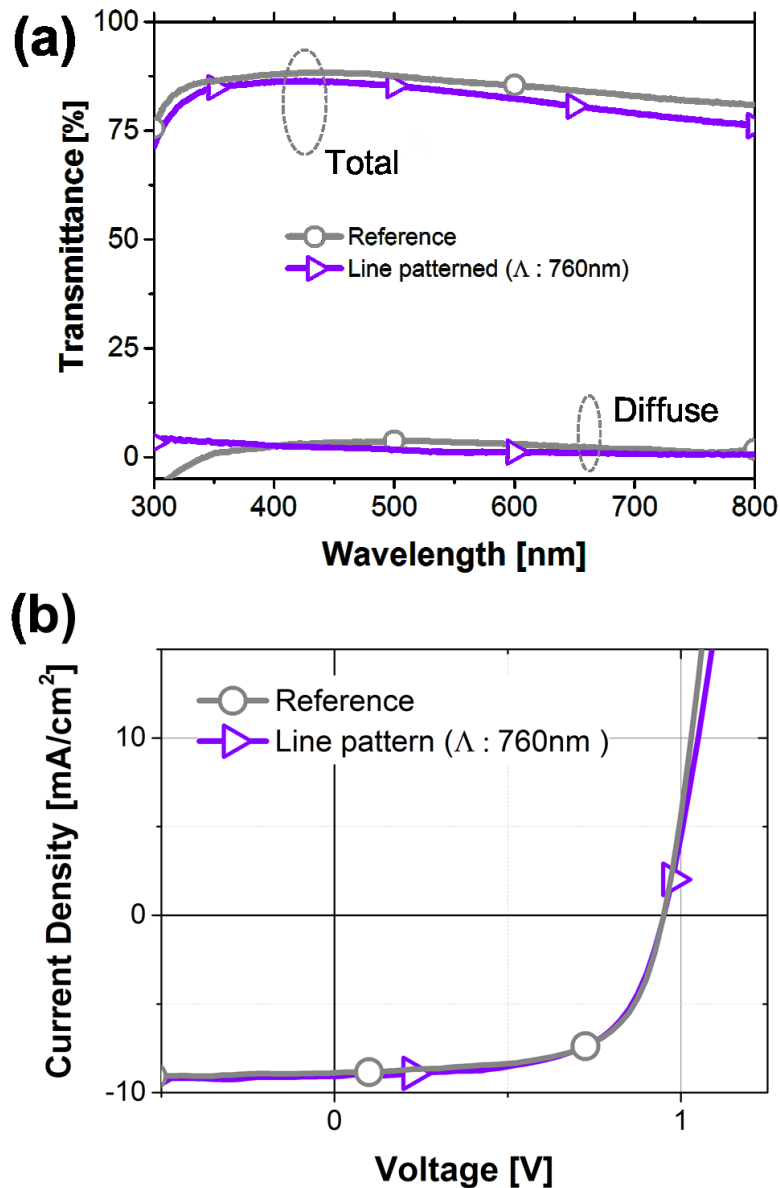


Figure 6-9 Total and diffuse transmittance of planar and nano-imprinted PEDOT:PSS (a) and photovoltaic performance of OPV devices on each PEDOT:PSS (b).

this nano-imprinting method does not change the optical properties of the PEDOT:PSS layer and, therefore, will not provide any light trapping effect to the photovoltaic devices (Figure 6-9(b)) similarly to what is observed for patterned PET substrates discussed in Chapter 5. The relatively small height of the patterned structures of the films obtained in this work is insufficient to make any significant scattering into the photoactive layer of the OPV device. As an experiment, we could only manage to imprint structures of 750 nm period with height of 40 nm. A finite element method (FEM) simulation, numerically solving Maxwell's equation[111,112] is performed. These calculations indeed show that no enhancement is expected if structures of 40 nm having a period ranging from 200nm to 1000nm, incorporated in the OPV device as shown in Figure 6-10.

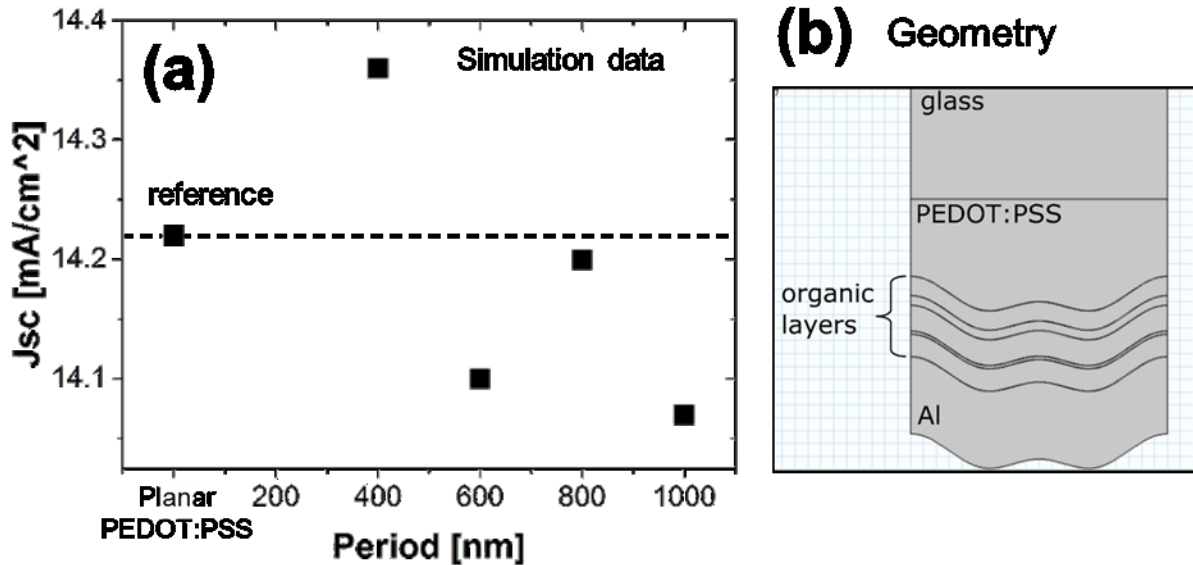


Figure 6-10 Calculated short circuit current densities of OPV devices on nano-imprinted PEDOT:PSS with different periods.

6.3.3 Summary

As introduced in Chapter 5, periodic structures with a proper height provide light trapping effects to organic photovoltaic devices. Nano-imprinting is one of the promising technique for fabricating

large scale nanostructure and attempted to transfer structures of a PDMS stamp to PEDOT:PSS because of its solution based process. However nano-imprinted PEDOT:PSS with a structure height of 40 nm does not provide sufficient light trapping effects due to relatively smaller dimensions of the structures. Patterned PEDOT:PSS with a height of 40 nm and different periods are calculated but no enhancement could be observed. In other words, future studies, aiming to produce higher structures are needed.

7. Conclusions and Outlook

7.1 Conclusions

In this thesis, flexible polymer electrodes and substrates are implemented into organic photovoltaic (OPV) devices. Moreover, light trapping effects are incorporated for enhancing light absorption and the overall photovoltaic performance.

In order to realize flexible OPVs, indium tin oxide electrodes and glass substrates are too brittle. Therefore, PEDOT:PSS is exploited in this thesis as flexible electrode, while polyethylene terephthalate (PET), coated with an AlO_x barrier layer is used as flexible substrate. PEDOT:PSS electrodes are prepared by a solution based process allowing an easy addition of light trapping effects. In this thesis, PEDOT:PSS electrodes and light scattering layers are combined in a single light trapping electrode by blending 100 nm TiO_2 particles in a PEDOT:PSS solution. When utilized in an OPV as electrode, a power conversion efficiency of 7.92% is achieved, which is an 8.6% relative improvement compared to a device with a neat PEDOT:PSS electrode without the nano-particles. This improvement is caused by an increase in short-circuit current due to an improved photon harvesting in the 320 nm–700 nm spectral wavelength range.

Furthermore, the light trapping properties of periodic structures imprinted into substrates and electrodes have been investigated. The fabrication of periodic structures on glass substrates is briefly explored, but abandoned due to processing difficulties: almost 13 hours are required to fabricate micro-structures of 1 m^2 area on glass. In contrast, such structures can be implemented into PET in 1 minute. In this study, line structured PET substrates with the periods of 1.8 and 2.6 μm are fabricated using the direct laser interference patterning (DLIP) technique. OPVs are built on each substrate and the performance is improved by a factor of 1.16 as compared to devices on unstructured PET. This resulted in a power conversion efficiency of 7.70%. We find that a

shorter spatial period of the pattern allows for a stronger light trapping effect, as it leads to a longer light path.

Next, optical display films commercialized to liquid crystal display are introduced as light trapping substrates for OPVs. Display films have prism structures on one side and the other side scattering particles are embedded within an anti-reflection layer. This structure allows over 80% of light to pass through the films from the prism side, but almost no light can pass through in the opposite direction. With these unique properties, OPVs are built on the scattering side and shows, a power conversion efficiency of 7.48%, which is a factor of 1.13 higher as compared to a device fabricated on a planar PET (6.62%). Therefore, the use of standard optical display films is a cheap, simple and efficient way to increase the photocurrent and overall efficiency of OPVs.

In addition, we investigate nano-imprinted PEDOT:PSS as a light trapping electrode. The polymer electrode is printed using a PDMS stamp with a structure height over 100 nm. However, only 40 nm height can be transferred to the PEDOT:PSS. OPVs on these nano-imprinted electrodes show similar performance as those fabricated on unstructured PEDOT:PSS. With a 40 nm height, FEM simulations are calculated with different periods and indeed show that no enhancement is expected. In order to get improvement, the structures should be heightened to at least 80 nm.

Finally, thin atomic layer deposited (ALD) AlO_x as top and bottom encapsulation is used for fully flexible devices. The encapsulated devices are sufficiently flexible to withstand a bending with a 10 mm radius for more than 50 cycles at ambient condition. This flexibility is sufficient to use these materials for a roll-to-roll process and to be applied to flexible electronic devices.

In short, small molecule OPVs with various light trapping effects, for instance display films, laser patterned PET films, nano-particles embedded PEDOT:PSS electrodes and nano-imprinted PEDOT:PSS electrode have been explored in this thesis. All these approaches can be implemented into flexible devices. We believe that the research done provides a meaningful milestone in the development of flexible OPVs with enhanced light absorption.

7.2 Outlook

Three dimensional structures

In this thesis, only 2-dimensional line structures are fabricated and investigated as light trapping substrates, for simplicity. However, using direct laser interference (DLIP), 3-dimensional structures, for example, hexagonal, rectangular, dot and hole structures, can be fabricated. Various structures for exploring an optimized light trapping condition for OPVs should be investigated.

Large area devices

Most OPVs in this thesis are produced with PEDOT:PSS electrodes, which have around $100 \Omega/\square$ of sheet resistance. This is insufficient to be used as large area electrode. In comparison, ITO has a sheet resistance of $25 \Omega/\square$. To explore more conductive and flexible materials for electrodes, silver nanowire (AgNW) and PEDOT:PSS based electrodes are investigated and less than $17 \Omega/\square$ is achieved[113]. With the highly conductive electrodes, two potential approaches could be undertaken for producing large area devices.

1. Nano-particles in PEDOT:PSS solution can be spin-coated on AgNW electrodes. With the scattering particles, light trapping effects can be achieved. Moreover 90 nm diameter of AgNWs and 100 nm TiO_2 nano-particles can provide relatively smooth surface since the TiO_2 particles fill the voids between AgNWs.
2. In our previous study, AgNWs with PEDOT:PSS electrodes are coated on PET substrates and shows high flexibility together with high conductivity. Hybrid electrodes can directly be applied to the patterned PET substrates to produce large area solar cells with light trapping effects.

Environmental durability

Due to a relatively large size of the structures (over 1.5 μm) as compared to 100 nm of organic layers, the patterns are located on the outside of solar cell. In other words, structures are exposed to an ambient environment. Micro-structures are very sensitive to tiny external forces, and easily destroyed. In order to provide a robust durability to patterned PET, several approaches can be examined.

1. Filling a space around the micro-structures by materials which have a refractive index far different from that of PET.
2. Fabricating debossed structures which are more suitable for providing environmental durability, departing from embossed structures in this study.

Nano-imprinting PEDOT:PSS

Before imprinting nano-structures on PEDOT:PSS, it should not be totally dried. To find an the optimum viscosity of PEDOT:PSS by adjusting an annealing temperature or a time, several attempts have been undertaken. However with the optimized conditions up to now, the realization of structures with a high aspect ratio is difficult. More studies are required to optimize the nano-imprinting of PEDOT:PSS.

OLED

As well as light trapping (in-coupling) for solar cells, organic light emitting diodes (OLED) require light out-coupling techniques for extracting internally confined light to outside of devices. All approaches in this thesis, scattering, micro and nano structured electrodes and substrates can be directly used for OLED. With Paul-Aton Will, Yuan Liu and Yungui Li in OLED group, we have tried to build OLED using our methods. However, conductive polymer, PEDOT:PSS used as electrodes in our study, is still electrically insufficient to be used as anode for OLED. Further examination will be taken place with them.

8. Appendix

Bibliography

- [1] Ben Knight, “Merkel shuts down seven nuclear reactors,” *Reuters*. (2011). <http://www.dw.com/en/merkel-shuts-down-seven-nuclear-reactors/a-14912184> (accessed October 10, 2016).
- [2] S. Böll, “Bundesländer wollen Benzin- und Dieselaautos ab 2030 verbieten,” *SPIEGEL ONLINE*. (2016). <http://www.spiegel.de/auto/aktuell/bundeslaender-wollen-benzin-und-dieselaautos-ab-2030-verbieten-a-1115671.html> (accessed October 8, 2016).
- [3] GEA Writing Team, *Global Energy Assessment*, Cambridge University Press, Cambridge, UK and New York, NY, USA and the International Institute for Applied Systems Analysis, Laxenburg, Austria, 2012. doi:<http://dx.doi.org/10.1017/CBO9780511793677>.
- [4] United Nations, *World Energy Assessment: Energy and the Challenge of Sustainability*, Bureau for Development Policy, United Nations Development Programme, New York, 2000. http://www.undp.org/content/undp/en/home/librarypage/environment-energy/sustainable_energy/world_energy_assessmentenergyandthechallengeofsustainability.html.
- [5] Alan Chodos, “This Month in Physics History,” (2009). <https://www.aps.org/publications/apsnews/200904/physicshistory.cfm> (accessed October 8, 2016).
- [6] F. Dimroth, M. Grave, P. Beutel, U. Fiedeler, C. Karcher, T.N.D. Tibbits, E. Oliva, G. Siefert, M. Schachtner, A. Wekkeli, A.W. Bett, R. Krause, M. Piccin, N. Blanc, C. Drazek, E. Guiot, B. Ghyselen, T. Salvetat, A. Tauzin, T. Signamarcheix, A. Dobrich, T. Hannappel, K. Schwarzbürg, “Wafer bonded four-junction GaInP/GaAs//GaInAsP/GaInAs concentrator solar cells with 44.7% efficiency,” *Progress in Photovoltaics: Research and Applications*. **22** (2014) 277–282. doi:10.1002/pip.2475.
- [7] Heliatek, “Heliatek sets new Organic Photovoltaic world record efficiency of 13.2% - Heliatek – The future is light,” (2016). <http://www.heliatek.com/en/press/press-releases/details/heliatek-sets-new-organic-photovoltaic-world-record-efficiency-of-13-2> (accessed October 9, 2016).
- [8] “Heliatek raises €80 million - Heliatek – The future is light,” (2016). <http://www.heliatek.com/en/press/press-releases/details/heliatek-raises-80-million> (accessed September 21, 2016).
- [9] A.F. Lasagni, T. Roch, J. Berger, T. Kunze, V. Lang, E. Beyer, To use or not to use (direct laser interference patterning), that is the question, in: U. Klotzbach, K. Washio, C.B. Arnold (Eds.), *International Society for Optics and Photonics*, 2015: p. 935115. doi:10.1117/12.2081976.
- [10] K. Chakanga, O. Siepman, O. Sergeev, S. Geißendörfer, K. von Maydell, C. Agert, “Laser textured substrates for light in-coupling in thin-film solar cells,” *Journal of Photonics for Energy*. **4** (2014) 044598. doi:10.1117/1.JPE.4.044598.

- [11] M. Schwoerer, H.C. Wolf, *Organic Molecular Solids*, Wiley-VCH Verlag GmbH, Weinheim, Germany, 2007. doi:10.1002/9783527618651.
- [12] W. Tress, *Organic Solar Cells: Theory, Experiment, and Device Simulation*, Springer International Publishing, Switzerland, 2014. doi:10.1007/978-3-319-10097-5_3.
- [13] A. Pochettino, “Sul comportamento foto-elettrico dell’antracene,” *Acad. Lincei Rend.* **15** (1906) 355.
- [14] P. Yam, “Plastics Get Wired,” *Scientific American.* **273** (1995) 82–87. doi:10.1038/scientificamerican0795-82.
- [15] G. Gustafsson, G.M. Treacy, Y. Cao, F. Klavetter, N. Colaneri, A.J. Heeger, “The ‘plastic’ led: A flexible light-emitting device using a polyaniline transparent electrode,” *Synthetic Metals.* **57** (1993) 4123–4127. doi:10.1016/0379-6779(93)90568-H.
- [16] D.R. Gamota, P. Brazis, K. Kalyanasundaram, J. Zhang, *Printed organic and molecular electronics*, Springer US, New York, 2004. doi:10.1007/978-1-4419-9074-7.
- [17] T. Sekitani, T. Yokota, K. Kuribara, M. Kaltenbrunner, T. Fukushima, Y. Inoue, M. Sekino, T. Isoyama, Y. Abe, H. Onodera, T. Someya, “Ultraflexible organic amplifier with biocompatible gel electrodes,” *Nature Communications.* **7** (2016) 11425. doi:10.1038/ncomms11425.
- [18] M. Irimia-Vladu, P.A. Troshin, M. Reisinger, L. Shmygleva, Y. Kanbur, G. Schwabegger, M. Bodea, R. Schwödiauer, A. Mumyatov, J.W. Fergus, V.F. Razumov, H. Sitter, N.S. Sariciftci, S. Bauer, “Biocompatible and Biodegradable Materials for Organic Field-Effect Transistors,” *Advanced Functional Materials.* **20** (2010) 4069–4076. doi:10.1002/adfm.201001031.
- [19] M. Irimia-Vladu, E.D. Głowacki, G. Voss, S. Bauer, N.S. Sariciftci, “Green and biodegradable electronics,” *Materials Today.* **15** (2012) 340–346. doi:10.1016/S1369-7021(12)70139-6.
- [20] M. Pope, C.E. Swenberg, *Electronic processes in organic crystals and polymers*, 2nd ed., Oxford University Press, New York, 1999.
- [21] B.P. Rand, H. Richter, *Organic solar cells: fundamentals, devices, and upscaling*, CRC Press, Taylor & Francis Group, Boca Raton, Florida, 2014.
- [22] C. Deibel, V. Dyakonov, “Polymer–fullerene bulk heterojunction solar cells,” *Reports on Progress in Physics.* **73** (2010) 096401. doi:10.1088/0034-4885/73/9/096401.
- [23] W. Brütting, C. Adachi, R.J.D. Holmes, *Physics of organic semiconductors*, 2nd ed., Wiley-VCH, 2012. <http://eu.wiley.com/WileyCDA/WileyTitle/productCd-3527410538.html> (accessed September 26, 2016).
- [24] T. Stübinger, W. Brütting, “Exciton diffusion and optical interference in organic donor–acceptor photovoltaic cells,” *Journal of Applied Physics.* **90** (2001) 3632. doi:10.1063/1.1394920.
- [25] B. Kippelen, J.-L. Brédas, “Organic photovoltaics,” *Energy & Environmental Science.* **2** (2009) 251. doi:10.1039/b812502n.
- [26] N. Karl, “Charge carrier transport in organic semiconductors,” *Synthetic Metals.* **133** (2003) 649–657. doi:10.1016/S0379-6779(02)00398-3.
- [27] J.-I. Park, J.W. Chung, J.-Y. Kim, J. Lee, J.Y. Jung, B. Koo, B.-L. Lee, S.W. Lee, Y.W. Jin, S.Y. Lee, “Dibenzothiopheno[6,5-*b*:6',5'-*f*]thieno[3,2-*b*]thiophene (DBTTT): High-Performance Small-Molecule Organic Semiconductor for Field-Effect Transistors,” *Journal of the American Chemical Society.* **137** (2015) 12175–12178. doi:10.1021/jacs.5b01108.
- [28] I. Kang, H.-J. Yun, D.S. Chung, S.-K. Kwon, Y.-H. Kim, “Record High Hole Mobility in Polymer Semiconductors via Side-Chain Engineering,” *Journal of the American Chemical*

- Society*. **135** (2013) 14896–14899. doi:10.1021/ja405112s.
- [29] “Electrical properties of Silicon (Si),” (2016). <http://www.ioffe.ru/SVA/NSM/Semicond/Si/electric.html> (accessed November 8, 2016).
- [30] I.I. Fishchuk, A.K. Kadashchuk, J. Genoe, M. Ullah, H. Sitter, T.B. Singh, N.S. Sariciftci, H. Bässler, “Temperature dependence of the charge carrier mobility in disordered organic semiconductors at large carrier concentrations,” *Physical Review B*. **81** (2010) 045202. doi:10.1103/PhysRevB.81.045202.
- [31] D.M. Chapin, C.S. Fuller, G.L. Pearson, “A New Silicon p-n Junction Photocell for Converting Solar Radiation into Electrical Power,” *Journal of Applied Physics*. **25** (1954) 676. doi:10.1063/1.1721711.
- [32] C.W. Tang, “Two-layer organic photovoltaic cell,” *Applied Physics Letters*. **48** (1986) 183. doi:10.1063/1.96937.
- [33] G. Yu, J. Gao, J.C. Hummelen, F. Wudl, A.J. Heeger, “Polymer Photovoltaic Cells: Enhanced Efficiencies via a Network of Internal Donor-Acceptor Heterojunctions,” *Science*. **270** (1995).
- [34] P. Peumans, A. Yakimov, S.R. Forrest, “Small molecular weight organic thin-film photodetectors and solar cells,” *Journal of Applied Physics*. **93** (2003) 3693. doi:10.1063/1.1534621.
- [35] T.M. Clarke, J.R. Durrant, “Charge Photogeneration in Organic Solar Cells,” *Chemical Reviews*. **110** (2010) 6736–6767. doi:10.1021/cr900271s.
- [36] G. He, M. Pfeiffer, K. Leo, M. Hofmann, J. Birnstock, R. Pudzich, J. Salbeck, “High-efficiency and low-voltage p-i-n electrophosphorescent organic light-emitting diodes with double-emission layers,” *Applied Physics Letters*. **85** (2004) 3911. doi:10.1063/1.1812378.
- [37] J. Blochwitz, M. Pfeiffer, T. Fritz, K. Leo, “Low voltage organic light emitting diodes featuring doped phthalocyanine as hole transport material,” *Applied Physics Letters*. **73** (1998) 729. doi:10.1063/1.121982.
- [38] B. Maennig, J. Drechsel, D. Gebeyehu, P. Simon, F. Kozłowski, A. Werner, F. Li, S. Grundmann, S. Sonntag, M. Koch, K. Leo, M. Pfeiffer, H. Hoppe, D. Meissner, N.S. Sariciftci, I. Riedel, V. Dyakonov, J. Parisi, “Organic p-i-n solar cells,” *Applied Physics A*. **79** (2004) 1–14. doi:10.1007/s00339-003-2494-9.
- [39] M. Pfeiffer, A. Beyer, B. Plönnigs, A. Nollau, T. Fritz, K. Leo, D. Schlettwein, S. Hiller, D. Wöhrle, “Controlled p-doping of pigment layers by cosublimation: Basic mechanisms and implications for their use in organic photovoltaic cells,” *Solar Energy Materials and Solar Cells*. **63** (2000) 83–99. doi:10.1016/S0927-0248(00)00022-2.
- [40] M. Hiramoto, H. Fujiwara, M. Yokoyama, “Three-layered organic solar cell with a photoactive interlayer of codeposited pigments,” *Applied Physics Letters*. **58** (1991) 1062. doi:10.1063/1.104423.
- [41] P. Peumans, S. Uchida, S.R. Forrest, “Efficient bulk heterojunction photovoltaic cells using small-molecular-weight organic thin films,” *Nature*. **425** (2003) 158–162. doi:10.1038/nature01949.
- [42] T. Tiedje, E. Yablonovitch, G.D. Cody, B.G. Brooks, “Limiting efficiency of silicon solar cells,” *IEEE Transactions on Electron Devices*. **31** (1984) 711–716. doi:10.1109/T-ED.1984.21594.
- [43] M.A. Green, “Lambertian light trapping in textured solar cells and light-emitting diodes: analytical solutions,” *Progress in Photovoltaics: Research and Applications*. **10** (2002) 235–241. doi:10.1002/pip.404.
- [44] A. Luque, G.L. Araújo, *Solar cells and optics for photovoltaic concentration*, CRC Press,

Bristol, England; Philadelphia, 1989.

- [45] E. Yablonovitch, G.D. Cody, "Intensity Enhancement in Textured Optical Sheets for Solar Cells," *IEEE Transactions on Electron Devices*. **29** (1982) 300–305.
- [46] Z. Yu, A. Raman, S. Fan, "Fundamental limit of nanophotonic light trapping in solar cells," *Proceedings of the National Academy of Sciences*. **107** (2010) 17491–17496. doi:10.1073/pnas.1008296107.
- [47] Z. Yu, A. Raman, S. Fan, "Fundamental limit of light trapping in grating structures," *Optics Express*. **18** (2010) A366. doi:10.1364/OE.18.00A366.
- [48] D. Redfield, "Multiple-pass thin-film silicon solar cell," *Applied Physics Letters*. **25** (1974) 647. doi:10.1063/1.1655344.
- [49] H. Savin, P. Repo, G. von Gastrow, P. Ortega, E. Calle, M. Garín, R. Alcubilla, "Black silicon solar cells with interdigitated back-contacts achieve 22.1% efficiency," *Nature Nanotechnology*. **10** (2015) 624–628. doi:10.1038/nnano.2015.89.
- [50] H.-C. Yuan, V.E. Yost, M.R. Page, P. Stradins, D.L. Meier, H.M. Branz, "Efficient black silicon solar cell with a density-graded nanoporous surface: Optical properties, performance limitations, and design rules," *Applied Physics Letters*. **95** (2009) 123501. doi:10.1063/1.3231438.
- [51] V.E. Ferry, M. a Verschuuren, H.B.T. Li, E. Verhagen, R.J. Walters, R.E.I. Schropp, H. a Atwater, A. Polman, "Light trapping in plasmonic solar cells," *Optics Express*. **18** (2010) 237–245. <http://www.ncbi.nlm.nih.gov/pubmed/20588593>.
- [52] S. John, "Why trap light?," *Nature Materials*. **11** (2012) 997–999. doi:10.1038/nmat3503.
- [53] C. López-López, S. Colodrero, A. Jiménez-Solano, G. Lozano, R. Ortiz, M.E. Calvo, H. Míguez, "Multidirectional Light-Harvesting Enhancement in Dye Solar Cells by Surface Patterning," *Advanced Optical Materials*. **2** (2014) 879–884. doi:10.1002/adom.201400160.
- [54] Y. Park, F. Nehm, L. Müller-Meskamp, K. Vandewal, K. Leo, "Optical display film as flexible and light trapping substrate for organic photovoltaics," *Optics Express*. **24** (2016) A974. doi:10.1364/OE.24.00A974.
- [55] H.-W. Chang, J. Lee, S. Hofmann, Y. Hyun Kim, L. Müller-Meskamp, B. Lüssem, C.-C. Wu, K. Leo, M.C. Gather, "Nano-particle based scattering layers for optical efficiency enhancement of organic light-emitting diodes and organic solar cells," *Journal of Applied Physics*. **113** (2013) 204502. doi:10.1063/1.4807000.
- [56] Z. Tang, A. Elfving, J. Bergqvist, W. Tress, O. Inganäs, "Light Trapping with Dielectric Scatterers in Single- and Tandem-Junction Organic Solar Cells," *Advanced Energy Materials*. **3** (2013) 1606–1613. doi:10.1002/aenm.201300524.
- [57] Y. Park, L. Müller-Meskamp, K. Vandewal, K. Leo, "PEDOT:PSS with embedded TiO₂ nanoparticles as light trapping electrode for organic photovoltaics," *Applied Physics Letters*. **108** (2016) 253302. doi:10.1063/1.4954902.
- [58] C. Cho, S. Jeong, H.-J. Choi, N. Shin, B. Kim, E. Jeon, J.-Y. Lee, "Toward Perfect Light Trapping in Thin-Film Photovoltaic Cells: Full Utilization of the Dual Characteristics of Light," *Advanced Optical Materials*. **3** (2015) 1697–1702. doi:10.1002/adom.201500471.
- [59] Y. Park, J. Berger, Z. Tang, L. Müller-meskamp, "Flexible , light trapping substrates for organic photovoltaics," *Applied Physics Letters*. **109** (2016) 093301. doi:10.1063/1.4962206.
- [60] Y. Park, J. Berger, P. Will, M. Soldera, B. Glatz, L. Müller-, B. Aires, "Light trapping for flexible organic photovoltaics," *Proc. SPIE*. **9942** (2016) 994211. doi:10.1117/12.2229582.
- [61] L. Müller-Meskamp, Y.H. Kim, T. Roch, S. Hofmann, R. Scholz, S. Eckardt, K. Leo, A.F. Lasagni, "Efficiency Enhancement of Organic Solar Cells by Fabricating Periodic Surface

- Textures using Direct Laser Interference Patterning,” *Advanced Materials*. **24** (2012) 906–910. doi:10.1002/adma.201104331.
- [62] J.B. Kim, P. Kim, N.C. Pégard, S.J. Oh, C.R. Kagan, J.W. Fleischer, H.A. Stone, Y.-L. Loo, “Wrinkles and deep folds as photonic structures in photovoltaics,” *Nature Photonics*. **6** (2012) 327–332. doi:10.1038/nphoton.2012.70.
- [63] S. Wooh, H. Yoon, J.-H. Jung, Y.-G. Lee, J.H. Koh, B. Lee, Y.S. Kang, K. Char, “Efficient Light Harvesting with Micropatterned 3D Pyramidal Photoanodes in Dye-Sensitized Solar Cells,” *Advanced Materials*. **25** (2013) 3111–3116. doi:10.1002/adma.201300085.
- [64] J. Na, Y. Kim, C. Park, E. Kim, “Multi-layering of a nanopatterned TiO₂ layer for highly efficient solid-state solar cells,” *NPG Asia Materials*. **7** (2015) e217. doi:10.1038/am.2015.105.
- [65] E.C. Nelson, N.L. Dias, K.P. Bassett, S.N. Dunham, V. Verma, M. Miyake, P. Wiltzius, J.A. Rogers, J.J. Coleman, X. Li, P. V. Braun, “Epitaxial growth of three-dimensionally architected optoelectronic devices,” *Nature Materials*. **10** (2011) 676–681. doi:10.1038/nmat3071.
- [66] V.E. Ferry, J.N. Munday, H.A. Atwater, “Design Considerations for Plasmonic Photovoltaics,” *Advanced Materials*. **22** (2010) 4794–4808. doi:10.1002/adma.201000488.
- [67] R. Windisch, P. Heremans, A. Knobloch, P. Kiesel, G.H. Döhler, B. Dutta, G. Borghs, “Light-emitting diodes with 31% external quantum efficiency by outcoupling of lateral waveguide modes,” *Applied Physics Letters*. **74** (1999) 2256. doi:10.1063/1.123817.
- [68] T. Nakamura, N. Tsutsumi, N. Juni, H. Fujii, “Improvement of coupling-out efficiency in organic electroluminescent devices by addition of a diffusive layer,” *Journal of Applied Physics*. **96** (2004) 6016. doi:10.1063/1.1810196.
- [69] T. Schaefer, Investigation of Light Scattering Nanoparticles in Top-Emitting Organic Light-Emitting Diodes, Technische Universität Dresden, 2014.
- [70] C. Körner, Oligothiophene Materials for Organic Solar Cells, Technische Universität Dresden, 2012.
- [71] K. Walzer, B. Maennig, M. Pfeiffer, K. Leo, “Highly efficient organic devices based on electrically doped transport layers,” *Chemical Reviews*. **107** (2007) 1233–1271. doi:10.1021/cr050156n.
- [72] F. Nehm, H. Klumbies, C. Richter, A. Singh, U. Schroeder, T. Mikolajick, T. Mönch, C. Hoßbach, M. Albert, J.W. Bartha, K. Leo, L. Müller-Meskamp, “Breakdown and Protection of ALD Moisture Barrier Thin Films,” *ACS Applied Materials & Interfaces*. **7** (2015) 22121–22127. doi:10.1021/acsami.5b06891.
- [73] V. Fiehler, F. Patrovsky, L. Ortmann, S. Derenko, A. Hille, L.M. Eng, “Plasmonic Nanorod Antenna Array: Analysis in Reflection and Transmission,” *The Journal of Physical Chemistry C*. **120** (2016) 12178–12186. doi:10.1021/acs.jpcc.6b02419.
- [74] S. John, “Why trap light?,” *Nature Materials*. **11** (2012) 997–999. <http://www.nature.com/nmat/journal/v11/n12/full/nmat3503.html> (accessed April 20, 2016).
- [75] J.R. Tumbleston, D.-H. Ko, E.T. Samulski, R. Lopez, “Electrophotonic enhancement of bulk heterojunction organic solar cells through photonic crystal photoactive layer,” *Applied Physics Letters*. **94** (2009) 043305. doi:10.1063/1.3075053.
- [76] Y.-G. Bi, J. Feng, Y. Chen, Y.-S. Liu, X.-L. Zhang, Y.-F. Li, M. Xu, Y.-F. Liu, X.-C. Han, H.-B. Sun, “Dual-periodic-corrugation-induced broadband light absorption enhancement in organic solar cells,” *Organic Electronics*. **27** (2015) 167–172. doi:10.1016/j.orgel.2015.09.021.

- [77] Y.-F. Liu, J. Feng, D. Yin, H.-F. Cui, X.-L. Zhang, Y.-G. Bi, D.-D. Zhang, L.-S. Liu, A.-W. Li, J.-F. Song, Q.-D. Chen, H.-B. Sun, “Viewing-angle independence of white emission from microcavity top-emitting organic light-emitting devices with periodically and gradually changed cavity length,” *Organic Electronics*. **14** (2013) 1597–1601. doi:10.1016/j.orgel.2013.03.030.
- [78] Y. Jin, J. Feng, X.-L. Zhang, M. Xu, Y.-G. Bi, Q.-D. Chen, H.-Y. Wang, H.-B. Sun, “Surface-plasmon enhanced absorption in organic solar cells by employing a periodically corrugated metallic electrode,” *Applied Physics Letters*. **101** (2012) 163303. doi:10.1063/1.4761947.
- [79] J. Li, L. Zuo, H. Pan, H. Jiang, T. Liang, Y. Shi, “Texture design of electrodes for efficiency enhancement of organic solar cells,” *Journal of Materials Chemistry A*. **1** (2013) 2379–2386. doi:10.1039/C2TA00687A.
- [80] Y.M. Song, G.C. Park, E.K. Kang, C. Il Yeo, Y.T. Lee, “Antireflective grassy surface on glass substrates with self-masked dry etching,” *Nanoscale Research Letters*. **8** (2013) 505. doi:10.1186/1556-276X-8-505.
- [81] D.A. Acevedo, A.F. Lasagni, C.A. Barbero, F. Mücklich, “Simple Fabrication Method of Conductive Polymeric Arrays by Using Direct Laser Interference Micro-/Nanopatterning,” *Advanced Materials*. **19** (2007) 1272–1275. doi:10.1002/adma.200601693.
- [82] A.F. Lasagni, D.F. Acevedo, C.A. Barbero, F. Mücklich, “One-Step Production of Organized Surface Architectures on Polymeric Materials by Direct Laser Interference Patterning,” *Advanced Engineering Materials*. **9** (2007) 99–103. doi:10.1002/adem.200600171.
- [83] L. Müller-Meskamp, S. Schubert, T. Roch, S. Eckhardt, A.-F. Lasagni, K. Leo, “Transparent Conductive Metal Thin-Film Electrodes Structured by Direct Laser Interference Patterning,” *Advanced Engineering Materials*. **17** (2015) 1215–1219. doi:10.1002/adem.201400454.
- [84] A.F. Lasagni, T. Roch, D. Langheinrich, M. Bieda, A. Wetzig, “Large Area Direct Fabrication of periodic Arrays using Interference Patterning,” *Physics Procedia*. **12** (2011) 214–220. doi:10.1016/j.phpro.2011.03.125.
- [85] M. D’Alessandria, A. Lasagni, F. Mücklich, “Direct micro-patterning of aluminum substrates via laser interference metallurgy,” *Applied Surface Science*. **255** (2008) 3210–3216. doi:10.1016/j.apsusc.2008.09.018.
- [86] J. Berger, M. Grosse Holthaus, N. Pistillo, T. Roch, K. Rezwani, A.F. Lasagni, “Ultraviolet laser interference patterning of hydroxyapatite surfaces,” *Applied Surface Science*. **257** (2011) 3081–3087. doi:10.1016/j.apsusc.2010.10.120.
- [87] C. Cho, H. Kim, S. Jeong, S.-W. Baek, J.-W. Seo, D. Han, K. Kim, Y. Park, S. Yoo, J.-Y. Lee, “Random and V-groove texturing for efficient light trapping in organic photovoltaic cells,” *Solar Energy Materials and Solar Cells*. **115** (2013) 36–41. doi:10.1016/j.solmat.2013.03.014.
- [88] L. Bormann, F. Nehm, N. Weiß, V.C. Nikolis, F. Selzer, A. Eychmüller, L. Müller-Meskamp, K. Vandewal, K. Leo, “Degradation of Sexithiophene Cascade Organic Solar Cells,” *Advanced Energy Materials*. **6** (2016). doi:10.1002/aenm.201502432.
- [89] G.-J. Park, Y.-G. Kim, J.-H. Yi, J.-H. Kwon, J.-H. Park, S.-H. Kim, B.-K. Kim, J.-K. Shin, H.-S. Soh, “Enhancement of the Optical Performance by Optimization of Optical Sheets in Direct-illumination LCD Backlight,” *Journal of the Optical Society of Korea*. **13** (2009) 152–157.
- [90] F.-J. Haug, T. Söderström, M. Python, V. Terrazzoni-Daudrix, X. Niquille, C. Ballif, “Development of micromorph tandem solar cells on flexible low-cost plastic substrates,”

- Solar Energy Materials and Solar Cells.* **93** (2009) 884–887. doi:10.1016/j.solmat.2008.10.018.
- [91] J. Escarré, F. Villar, M. Fonrodona, D. Soler, J.M. Asensi, J. Bertomeu, J. Andreu, “Optical analysis of textured plastic substrates to be used in thin silicon solar cells,” *Solar Energy Materials and Solar Cells.* **87** (2005) 333–341. doi:10.1016/j.solmat.2004.07.031.
- [92] M. Niggemann, M. Glatthaar, P. Lewer, C. Müller, J. Wagner, A. Gombert, “Functional microprism substrate for organic solar cells,” *Thin Solid Films.* **511** (2006) 628–633. doi:10.1016/j.tsf.2005.12.011.
- [93] A.J. Smith, C. Wang, D. Guo, C. Sun, J. Huang, “ARTICLE Repurposing Blu-ray movie discs as quasi-random nanoimprinting templates for photon management,” *Nature Communications.* **5** (2014). doi:10.1038/ncomms6517.
- [94] S. Wiesendanger, M. Zilk, T. Pertsch, F. Lederer, C. Rockstuhl, “A path to implement optimized randomly textured surfaces for solar cells,” *Applied Physics Letters.* **103** (2013) 131115. doi:10.1063/1.4823554.
- [95] C. Rockstuhl, F. Lederer, K. Bittkau, T. Beckers, R. Carius, “The impact of intermediate reflectors on light absorption in tandem solar cells with randomly textured surfaces,” *Applied Physics Letters.* **94** (2009) 211101. doi:10.1063/1.3142421.
- [96] M. Niggemann, M. Riede, A. Gombert, K. Leo, “Light trapping in organic solar cells,” *Physica Status Solidi (a).* **205** (2008) 2862–2874. doi:10.1002/pssa.200880461.
- [97] C. Battaglia, C.-M. Hsu, K. Söderström, J. Escarré, F.-J. Haug, M. Charrière, M. Boccard, M. Despeisse, D.T.L. Alexander, M. Cantoni, Y. Cui, C. Ballif, “Light Trapping in Solar Cells: Can Periodic Beat Random?,” *ACS Nano.* **6** (2012) 2790–2797. doi:10.1021/nn300287j.
- [98] J. Lee, Y.Y. Kwon, E.-H. Choi, J. Park, H. Yoon, H. Kim, “Enhancement of light-extraction efficiency of organic light-emitting diodes using silica nanoparticles embedded in TiO₂ matrices,” *Optics Express.* **22 Suppl 3** (2014) A705–14. <http://www.ncbi.nlm.nih.gov/pubmed/24922378> (accessed April 25, 2016).
- [99] H.-W. Chang, Y.H. Kim, J. Lee, S. Hofmann, B. Lüssem, L. Müller-Meskamp, M.C. Gather, K. Leo, C.-C. Wu, “Color-stable, ITO-free white organic light-emitting diodes with enhanced efficiency using solution-processed transparent electrodes and optical outcoupling layers,” *Organic Electronics.* **15** (2014) 1028–1034. doi:10.1016/j.orgel.2014.02.017.
- [100] C.-H. Shin, E.Y. Shin, M.-H. Kim, J.-H. Lee, Y. Choi, “Nanoparticle scattering layer for improving light extraction efficiency of organic light emitting diodes,” *Optics Express.* **23** (2015) A133. doi:10.1364/OE.23.00A133.
- [101] Y.H. Kim, J. Lee, S. Hofmann, M.C. Gather, L. Müller-Meskamp, K. Leo, “Achieving High Efficiency and Improved Stability in ITO-Free Transparent Organic Light-Emitting Diodes with Conductive Polymer Electrodes,” *Advanced Functional Materials.* **23** (2013) 3763–3769. doi:10.1002/adfm.201203449.
- [102] Y.H. Kim, C. Sachse, M.L. Machala, C. May, L. Müller-Meskamp, K. Leo, “Highly Conductive PEDOT:PSS Electrode with Optimized Solvent and Thermal Post-Treatment for ITO-Free Organic Solar Cells,” *Advanced Functional Materials.* **21** (2011) 1076–1081. doi:10.1002/adfm.201002290.
- [103] Y. Yang, K. Lee, K. Mielczarek, W. Hu, A. Zakhidov, “Nanoimprint of dehydrated PEDOT:PSS for organic photovoltaics,” *Nanotechnology.* **22** (2011). doi:10.1088/0957-4484/22/48/485301.
- [104] A. Elschner, S. Kirchmeyer, W. Lovenich, U. Merker, *PEDOT: principles and applications of an intrinsically conductive polymer*, CRC Press, 2010.

<https://books.google.de/books?hl=ko&lr=&id=e12gOPc4IWAC&oi=fnd&pg=PP1&dq=PEDOT:+Principles+and+Applications+of+an+Intrinsically+Conductive+Polymer&ots=BW9eOaiK5u&sig=M8gxwJZL17PFQJk-YBxbQee4fUw> (accessed April 27, 2016).

- [105] A.M. Nardes, M. Kemerink, R.A.J. Janssen, J.A.M. Bastiaansen, N.M.M. Kiggen, B.M.W. Langeveld, A.J.J.M. van Breemen, M.M. de Kok, “Microscopic Understanding of the Anisotropic Conductivity of PEDOT:PSS Thin Films,” *Advanced Materials*. **19** (2007) 1196–1200. doi:10.1002/adma.200602575.
- [106] A.M. Nardes, R.A.J. Janssen, M. Kemerink, “A Morphological Model for the Solvent-Enhanced Conductivity of PEDOT:PSS Thin Films,” *Advanced Functional Materials*. **18** (2008) 865–871. doi:10.1002/adfm.200700796.
- [107] M. Nania, O.K. Matar, J.T. Cabral, “Frontal vitrification of PDMS using air plasma and consequences for surface wrinkling,” *Soft Matter*. **11** (2015) 3067–3075. doi:10.1039/C4SM02840F.
- [108] C. Lu, H. Möhwald, A. Fery, “A lithography-free method for directed colloidal crystal assembly based on wrinkling,” *Soft Matter*. **3** (2007) 1530–1536. doi:10.1039/b712706e.
- [109] A. Schweikart, A. Fery, “Controlled wrinkling as a novel method for the fabrication of patterned surfaces,” *Microchimica Acta*. **165** (2009) 249–263. doi:10.1007/s00604-009-0153-3.
- [110] P.-A. Will, *Organische Leuchtdioden auf periodisch korrigierten Substraten und Elektroden*, Technische Universität Dresden, 2015.
- [111] M. Soldera, K. Taretto, “Optical Modeling of Organic Solar Cells Deposited on Substrates Structured by Direct Laser Interference Patterning,” *31st European Photovoltaic Solar Energy Conference and Exhibition*. (2015) 1118–1121. doi:10.4229/EUPVSEC20152015-3BV.5.13.
- [112] M. Soldera, K. Taretto, J. Berger, A.F. Lasagni, “Potential of Photocurrent Improvement in $\mu\text{c-Si:H}$ Solar Cells with TCO Substrates Structured by Direct Laser Interference Patterning,” *Advanced Engineering Materials*. **18** (2016) 1674–1682. doi:10.1002/adem.201600225.
- [113] Y. Park, L. Bormann, L. Müller-Meskamp, K. Vandewal, K. Leo, “Efficient flexible organic photovoltaics using silver nanowires and polymer based transparent electrodes,” *Organic Electronics*. **36** (2016) 68–72. doi:10.1016/j.orgel.2016.05.032.

Table of figures

Figure 1-1 Photographs of the first solar cell that could generate significant amounts of electricity at Bell Laboratories in 1954 (a) and solar panels in the Gansu Province in China in 2015 (b). Images from AT&T Archives and REUTERS/Carlos Barria/Files.	20
Figure 1-2 Photographs of a flexible organic solar cell from IAPP (a), a rollable solar charger (WAACS design & consultancy, Netherlands) (b), roll-to-roll process for large area (Heliatek, Germany) (c), light solar cells installed on a temporary building (Paranet-Deutschland GmbH, Germany) (d), a solar bag (element5 Daochu AG, Switzerland) (e) and a roof window with transparent solar cell for an automotive application (Heliatek & Webasto, Germany) (f)	21
Figure 2-1 Schematics of orbitals and bonds in a conjugated carbon ring. A single sp^2 hybridized carbon atom (a), σ bond between sp^2 orbitals (b) and delocalized π system and π bonds of a benzene molecule (c).....	25
Figure 2-2 Schematics of hybridized orbitals of a carbon atom (left) and energy levels of the benzene molecule (right).	25
Figure 2-3 Jablonski band diagram that shows various processes of radiative and non-radiative transitions in a molecule/molecular solid (reproduced from[20]).....	26
Figure 2-4 Schematics of a Frenkel exciton (left) and a charge transfer exciton (right).....	27
Figure 2-5 Schematic of hopping transport in a disordered organic semiconductor. Reproduced from[11].....	28
Figure 2-6 Schematic energy diagram of an organic donor-acceptor heterojunction between an anode and a cathode. Steps for converting light into electricity are illustrated: (1) absorption, (2) exciton migration, (3) charge separation, and (4) charge transport and extraction (a) and electronic state diagram which shows charge transfer, recombination and separation (b).....	30

Figure 2-7 Schematics of different heterojunction p-i-n concepts in organic photovoltaics: planar heterojunction (a), ideal bulk heterojunction (b) real bulk heterojunction (c).32

Figure 2-8 Current-voltage and power density curves of an organic solar cell with the characteristic parameters j_{sc} , V_{oc} , j_{MPP} , V_{MPP} and FF.33

Figure 2-9 Equivalent circuit description of an OPV34

Figure 2-10 Current-voltage curve with different parallel resistances (a) and series resistances (b).35

Figure 3-1 Trapped light and slightly diffused light on patterned (a) and planar (b) PET substrates with the red laser ($\lambda=640\text{nm}$).37

Figure 3-2 Schematic cross-section of a photovoltaic device with textured structure.38

Figure 3-3 Schematic cross-section of a thin photovoltaic device with a grating on the reflector.40

Figure 3-4 Theoretical limit of absorption (A_{max}) of the photovoltaic device with grating of periodicity (Λ)[7].41

Figure 3-5 Schematic cross-section of a thin photovoltaic device with a diffracted light due to a grating of a long period (a) and a short period.42

Figure 3-6 Theoretical limit of absorption (A_{max}) of the photovoltaic device and regimes for the periodicities(Λ) of $1.0\ \mu\text{m}$, $1.8\ \mu\text{m}$ and $2.6\ \mu\text{m}$ (from 400nm to 800nm).44

Figure 3-7 Schematics of light diffraction by patterned substrate with high (a) and low (b) height of structure.44

Figure 3-8 Transmittance (a) and haze (b) depending on particle size. For identical concentration, particles with 100 and 250 nm size have about equal scattering ability, while particles with 50 nm size only come into play in the blue wavelength range. All layers are fabricated with a particle concentration of 30 g/l[69]. 46

Figure 3-9 Optical properties of PEDOT:PSS layer embedded with NPs. Total and diffuse (total-direct) transmittance of NP:P with three different TiO₂ concentrations (a) and scattering coefficients of three different TiO₂ concentrations(b). 47

Figure 4-1 Photograph of PEDOT:PSS solution mixed with 6 vol. % ethylene glycol (a), structural formulas of PEDOT (b) and PSS (c) and a schematic representation of the spin coating process (d). 51

Figure 4-2 Schematic structure of the organic solar cells (left) and their layout on the substrates (right): (1) an AlO_x layer is deposited as an encapsulation (oxygen and moisture barrier) layer on the substrate using an ALD system, (2) half coated transparent PEDOT:PSS bottom electrode, (3) organic layers deposited by an evaporation system and (4) 4 - fingers structured Al top electrode. 52

Figure 4-3 Schematic representation of the thermal co-evaporation system. The growth rate of each material is measured by quartz monitors for precisely determining the mixing ratio. 53

Figure 4-4 A schematic of the goniometer. 56

Figure 4-5 Photographs of screws and pans for providing constant bending radius (a) and device bent at a 2 mm radius (b). 57

Figure 5-1 The micro-structure of patterned PET film with different periods. SEM images of line structure with 1.8 μm period (a), 2.6 μm period without organic layers (b), with organic layers on the patterned PET substrate including a schematic (c) and a schematic of the patterned film (d). 61

Figure 5-2 Calculated and measured light diffraction angles. Calculated angular distribution of diffracted light for the different periods of patterned PET of 1000 nm, 1800nm and 2600 nm (a) and measured angular distribution of diffracted light using goniometer set-up (samples and light source are fixed and only detector is moving) with $\Lambda = 2600$ nm (b) and $\Lambda = 1800$ nm (c). 64

Figure 5-3 Diffraction patterns of $\Lambda = 1800$ nm (a) and its ratios of direct transmitted and diffracted light (b) with blue and red light and those of $\Lambda = 2600$ nm (c,d)..... 65

Figure 5-4 Properties of OPV devices on light trapping substrates. J-V curves with an inset of a device schematic (a), Normalized performance parameters after 10 cycles of bending with different radiuses (b), EQE (c) and ratio between EQE of devices on patterned PET substrates and unpatterned references (c-1), total reflection spectra (d) and Δ reflection spectra, a measure of decreased reflections in OPV devices with patterned PET substrates compared to the reference (d-1)..... 68

Figure 5-5 SEM images of prism structure (a), scattering particle on display film (b), organic layers on scattering side (c), half-peeled organic layers on scattering side (d). Schematics of display film (e) and prism structure (f)..... 70

Figure 5-6 Optical properties of the display film. (a) Total transmittance and reflection spectra, (b) Angular distribution of transmitted white light and (c) photographs of dispersed light from directed white light and (d) normal stand light. 72

Figure 5-7 Performance characteristics of OPV devices on display film and planar PET. (a) J-V curves with schematic of OPV device and (b) EQE spectra. 73

Figure 6-1 Optical properties of PEDOT:PSS layer embedded with NPs with and without a 2nd PEDOT:PSS layer. (a) Total transmittance of layers with different TiO₂ concentrations, (b) total and diffuse (total - direct) transmittance of NP:P with three different TiO₂ concentrations, (c) total reflectance of neat PEDOT:PSS and NP:P with and without second PEDOT:PSS layer and (d) scattering coefficients of three different TiO₂ concentrations. 78

Figure 6-2 Schematics of layers on glass and sheet resistance of each sample: without (a) and with (b) second PEDOT:PSS layer..... 79

Figure 6-3 Optical microscopy and AFM images of (a) 0.5 wt %, (b) 1.5 wt % and (c) 3.0 wt % TiO₂ NPs embedded PEDOT:PSS layer which were spun on glass substrates at 2500 rpm for 30 seconds and SEM images of 1.5 wt % NP:P (b-1) without and (b-2) with organic layers. 80

Figure 6-4 AFM images of (a) 0.5 wt %, (b) 1.5 wt % and (c) 3.0 wt % TiO₂ NPs embedded PEDOT:PSS layer with the values of RMS and thickness..... 81

Figure 6-5 Photovoltaic performance of OPV devices on NP:P and PEDOT:PSS electrode (a) J-V curves with a scheme of the OPV device architecture and (b) EQE spectra. (c) Ratio between EQE of NP:P device and that of reference device, (d) Total and diffuse transmittance of 1.5 wt % NP:P. 83

Figure 6-6 Formation of wrinkles on PDMS elastomer. 85

Figure 6-7 Schematics of the nano-imprinting on PEDOT:PSS. (1) As-spun PEDOT:PSS on glass, (2) imprinting PDMS mask on PEDOT:PSS, (3) keeping a sample in the oven (4) and completed patterned PEDOT:PSS. 86

Figure 6-8 AFM images of PDMS stamp (a), imprinted PEDOT:PSS (b) and its profile (c)..... 87

Figure 6-9 Total and diffuse transmittance of planar and nano-imprinted PEDOT:PSS (a) and photovoltaic performance of OPV devices on each PEDOT:PSS (b)..... 88

Figure 6-10 Calculated short circuit current densities of OPV devices on nano-imprinted PEDOT:PSS with different periods..... 89

Table of tables

Table 4-1 Organic materials used for solar cell preparation.....	50
Table 5-1 Normalized intensities of direct and diffracted light by blue and red laser.	63
Table 5-2 Performance characteristics of OPV devices on display film and planar PET	66
Table 5-3 The roughness of each surface from Fig. 5-5.....	70
Table 5-4 Photovoltaic performance parameters of OPV devices on display film and planar PET (more than 4 samples are measured for each conditions).	73
Table 6-1 Weight and volume ratio of NPs in PEDOT:PSS obtained by measurement and simulation.	76
Table 6-2 OPV device performance parameters for NP:P and PEDOT:PSS electrode. (8 devices are measured for each condition)	82

Acknowledgement

First of all, I would like to thank Prof. Karl Leo, who is a head of IAPP and has been my supervisor for doctoral study. He gave me an opportunity to study at IAPP when I desired to study abroad instead of working at company. I have experienced the best environment for studying and doing science at here IAPP. I am grateful for the valuable advice and guidance of my research. I also thank Prof. Koen Vandewal, who is my advisor for last two years after my ex-group leader, Lars left IAPP. When I had many problems especially to build solar cells, he gave me courage and helped me focus on the optical interpretation. Without his fruitful advice, guidance and proof-reading of papers and thesis, I could not complete my study within this short time. I am also grateful to Dr. Lars Müller-Meskamp, who was my group leader. Although I didn't make good results when he was at IAPP, based on his advice and discussion, I could make results with Koen after his leaving. I want to thank Prof. Stefan Mannsfeld for the effort on the review of this thesis and advice for my rigorosum.

I would like to thank group (once I was a member of EnE, when I came here in 2013 and the name of group was changed to OrBas on May of 2016 after that, now I am belong to ODS) members, Dr. Ludwig Bormann for jumping into swimming pool together and helping preparation of PEDOT:PSS and AgNW, Dr. Frederik Nehm, for his organizing EnE activities and providing a beautiful barrier layer that can realize flexible OPVs. Dr. Dhriti Ghosh for proof-reading paper and thesis, Jakob Holfeld and Matthias Saalfrank for helping with a soft landing in my first year at IAPP, Jakob's potato salad is the best in Sachsen, Dr. Christian Körner for reviewing thesis, Racine Nassau for introducing real USA English, Toni Meyer for struggling on a tandem cell with me and Dr. Sylvio Schubert, Dr. Franz Selzer, Dr. Hannes Klumbies, Fan-Yu Chen, Felix Dollinger, David Knepe, Dr. Nelli Weiß and Luisa Sonntag. All you are always helpful and friendly to me.

I am also want to thank Dr. Martin Schwarze for playing football, having food, beer and many kinds of things together for whole my time at IAPP, Dr. Felix Holzmüller for a small talking at every morning and having food and beer together especially thanks for the sled for Seojean last winter and a translation of my abstract in German, Dr. Stefan Kraner for discussing our daughter's behavior and his PhD party, Dr. Kyung-Keun Lim and Jaebok Kim for just being a Korean as like me they are big supporters to me. I am also want to thank Jonas Kublitski, Johannes Benduhn and Vasileios Christos Nikolis as lunch-mates (11:20). I thank Andreas Mischok, Axel Fischer, Marcus Klinger, Ludwig Popp and Irma Slowik for the exciting San Diego travel. I also thank Dr. Ji-Ling Hou as a good 朋友 and Dr. Donato Spoltore and Enkhtur Erdenebileg as German classmates and Andreas Hofacker and all officemates of Bey 95. I would like to thank Jana Berger and Prof. Andrés

Lasagni of Fraunhofer IWS for providing patterned PET substrates. I am particularly grateful to Sven Kunze and Andreas Büst for keeping the equipment running, Tobias Günther, Andreas Wendel and Caroline Walde for preparing precious samples, Kai Schmidt and Peter Leumer for all IT support (especially thank for the installation of MS Windows for me) and of course the administrative staff of IAPP: Johanna Katzschner, Carla Schmidt, Dr. Angelika Wolf, Dr. Annette Polte, Dr. Christian Zschalig and Dr. Hartmut Fröb. Last but not least, I sincerely thank my wife **Minso** and my daughter **Seojean** and my second baby **Seoki** still in mom's womb. Without their sacrifice, dedication, effort and love, I could not complete my study and live here even one day. They are all of me.

Here, I would like to thank some people in Korean.

승식이형 그리고 고유리학생, 매일 매일 같이 술먹어 주고 고민 상담하고 성공 공부까지 챙겨줘서 고마워요, 두분이 없었으면 드레스덴 생활이 정말 소주 없이 회먹는 느낌이었을거예요. 두분 다 얼릉 박사하세요. 멋진 요리사이자 사업가이자 이제는 한의학자인 동범이형 그리고 독일 최고 센스쟁이 민경이 누나, 독일에서 엄마집에 가는 편안함을 느낄수 있게 항상 쓰비카우에서 반겨줘서 고마워요. 민소의 영원한 형님, 한국가서 크게되실 정근욱이 이놈아 나 먼저 박사한다, 한국 같이 가면 정애령박사님과 같이 자주 밥사줘. 15년만에 함께 유럽여행을 다시한 치훈아 니가 놀러와서 재미있었다. 더 늙기 전에 한번 더 놀러가자. 싱가포르 공부하시는 이종학박사놈아 좋은 놀러와서 나눈 많은 이야기 고맙다 너 왔다간지가 벌써 3년이더라 얼릉 교수하셔, 시집가신 이민진씨, 술 많이 먹어서 드레스덴 여행을 통째로 날려 먹었으니 나중에 우리 없을때 신랑님과 한번 다시 놀러오렴. 무엇보다도 제가 한국에서 멀리 떨어진 이곳 독일에서 공부를 할 수 있었던건, 어머니, 아버지, 장모님, 장인어른의 든든한 응원 덕분입니다. 겨우 6달 밖에 자라지 않은 손녀를 타국에 데리고와 귀한 손녀 에게 주고 싶은 사랑을 주기 힘들게 만들었고, 타국에 있어 매일 자식걱정을 하게 만들어서 죄송합니다. 이제부터 항상 최선을 다해 지난 3년동안 진 빚을 꼭 갚도록 하겠습니다. 정말정말 사랑하고 감사합니다. 나보다도 나를 더 걱정해 주는 우리형 그리고 형수, 형 놀러온건 인생 최고 여행이었어, 지금처럼 항상 날 걱정하고 챙겨줘, 그리고 처제 조민경 독일 처음 올때 도와주고 항상 응원해 줘서 고마워 한국가면 월급으로 밥 한번 사주고 서진이 맨날 놀아줘. 마지막으로, 조민소 그리고 박서진 따님아 너희 둘이 없었으면 진짜 난 이 타지에서 하루도 살지 못했을 거고 공부도 커녕 사람 구실도 못했을거야. 정말로 진심으로 사랑해 고마워. 그리고엄마 뱃속에 있는 씨기야 너도 존재만으로도 고맙다. 마지막으로 저의 모든 시작과 끝을 준비해 주시는 하나님께 이 모든 영광을 드립니다.

Yoonseok Park

Hermann-Krone-Bau, February 2017

Erklärung

Diese Dissertation wurde am Institut für Angewandte Physik/Photophysik der Fakultät Mathematik und Naturwissenschaften an der Technischen Universität Dresden unter wissenschaftlicher Betreuung von Prof. Dr. Karl Leo angefertigt.

Hiermit versichere ich, dass ich die vorliegende Arbeit ohne unzulässige Hilfe Dritter und ohne Benutzung anderer als der angegebenen Hilfsmittel angefertigt habe. Die aus fremden Quellen direkt oder indirekt übernommenen Gedanken sind als solche kenntlich gemacht. Die Arbeit wurde bisher weder im Inland noch im Ausland in gleicher oder ähnlicher Form einer anderen Prüfungsbehörde vorgelegt.

Weiterhin versichere ich, dass bisher keine Promotionsverfahren stattgefunden haben. Ich erkenne die Promotionsordnung der Fakultät Mathematik und Naturwissenschaften an der Technischen Universität Dresden vom 01.09.2013 an.

Dresden, den 21. November 2016

Yoonseok Park